

https://dspace.org/

Stimuli-Responsive Transfersome-Based Bio-Mimetic Gels for Intra-Articular Drug Delivery in Osteoarthritis

Motaung, Atang

2024
University of the Witwatersrand, Johannesburg
https://hdl.handle.net/10539/48044

Motaung, Atang . (2024). Stimuli-Responsive Transfersome-Based Bio-Mimetic Gels for Intra-Articular Drug Delivery in Osteoarthritis [Master`s dissertation, University of the Witwatersrand, Johannesburg]. WIReDSpace. https://hdl.handle.net/10539/48044

Downloaded from a DSpace repository. https://dspace.org/

Stimuli-Responsive Transfersome-Based Bio-Mimetic Gels for Intra-Articular Drug Delivery in Osteoarthritis

ATANG MOTAUNG

A dissertation Submitted to the Faculty of Health Sciences, University of the Witwatersrand, Johannesburg, in fulfilment of the requirements for the degree of

Master of Science in Medicine



Supervisors

Professor Yahya Essop Choonara

Dr Thankhoe Abram Rants'o

Department of Pharmacy and Pharmacology, Faculty of Health Sciences, University of the Witwatersrand, Johannesburg, South Africa

Department of Pharmacology and Toxicology, College of Pharmacy, University of Utah, Salt Lake City, UT, 84112, USA

Johannesburg

2024

DECLARATION

I, Atang Motaung, declare that this dissertation is my own work. It has been submitted for the Master of Science in Medicine degree in the Faculty of Health Sciences at the University of the Witwatersrand, Johannesburg. It has not been submitted before for any degree or examination at this or any other university.



_____

Signed on this 18th day of April 2025

ACKNOWLEDGEMENTS

This has been one of the most fulfilling experiences of my life. It has been a path of growth, resilience, and relentless determination—marked by sleepless nights, challenges that tested my limits, and moments of unwavering faith. However, this achievement is not mine alone; it is the culmination of the unwavering support, guidance, and love of many remarkable individuals who have stood by my side through it all.

To my mother, Mmakwena Motaung: words cannot fully express my gratitude for the sacrifices you have made to ensure I reached this milestone. Your boundless love, strength, and selflessness have been my greatest source of motivation. My father, Moeketsi Motaung: thank you for being my protector, my role model, and my guiding compass. Your wisdom, resilience, and unwavering belief in me have shaped the person I am today. If I can one day embody even half of the man that you are, I will consider myself truly blessed. To my little sister, Karabelo Motaung: I am nothing without you. Despite your young age, you inspire me in ways you may not even realize. Your love and belief in me have been the light that has kept me moving forward.

I would also like to extend my deepest gratitude to Mr. Banyatsang (Meneer): thank you for your generosity and hospitality during the course of my studies. From the very beginning, you welcomed me into your home, treating me like family despite knowing so little about me. Your kindness, generosity, and unwavering support will never be forgotten. My closest friends, Tshepo Tieho Mofokeng, and Banele Samson Ndlovu, thank you for your unwavering support and encouragement throughout this journey. To Dr Sifiso Makhathini: your guidance and efforts in the early stages of this project were invaluable. I sincerely hope our paths cross again in the future.

I would like to express my sincerest gratitude to Prof Choonara and Dr Rants'o for the exceptional supervision and the incredible opportunities you have provided me have been instrumental in shaping this journey. I hope that my dedication and hard work reflect the immense trust and effort you have invested in me. To the staff members of WADDP and my fellow colleagues, thank you for your assistance, patience, and camaraderie. I have grown so much since we first met, and I hope that I left a mark on your lives just as you have on mine.

Lastly, I'd like to thank myself. Thank you for always showing up every single day, working hard, believing in yourself, and persevering. You are truly your ancestors' wildest dreams!

DEDICATION

This dissertation is dedicated to my family: Moeketsi Charles Motaung, Mmakwena Suzan Motaung, and Karabelo Motaung. You are the cornerstone of my life, and I will spend the rest of my years trying to figure out how to thank you.

RESEARCH OUTPUTS

1. National Science week (2023)| **Exhibition**.

2. Motaung, A., Rants'o, TA., Choonara, Y.E., (2023) Stimuli-responsive transferosome-based bio-mimetic gels for intra-articular drug delivery in osteoarthritis**| SAYAS Annual Young Scientist Conference - Oral Presentation**.

3. Motaung, A., Rants'o, TA., Choonara, Y.E., (2023) Stimuli-responsive transferosome-based bio-mimetic gels for intra-articular drug delivery in osteoarthritis| **Annual Conference of Pharmaceutical Sciences - Oral Presentation**.

4. Motaung A., Rants'o, TA., Walvekar, P., Lulinski, P and Choonara, YE., (2025) Recent Advances in Intra-Articular Bioactive Delivery for the Treatment of Osteoarthritis| **Review submitted to *European Journal of Pharmaceutical Sciences*.**

5. Motaung, A., Rants'o, TA., Bhade, RV., Somandi, K., and Choonara, Y.E., (2025) The Design and Development of a Dexamethasone-Tranfersome-PF-127/HA Stimuli-responsive Hydrogel for Intra-articular Therapy in Osteoarthritis| **Full length Research Article submitted to *Arthritis and Rheumatology Journal*.**

TABLE OF CONTENTS

DECLARATION 2
ACKNOWLEDGEMENTS 3
DEDICATION 4
RESEARCH OUTPUTS 5
LIST OF FIGURES 9
LIST OF TABLES 13
LIST OF EQUATIONS 14
LIST OF ABBREVIATIONS 15
ABSTRACT 18
CHAPTER ONE 20
INTRODUCTION AND BACKGROUND 20
1.1. Background of Osteoarthritis Drug Delivery 20
1.2. Rationale and Motivation 22
1.3. Aims and objectives 24
1.4. Potential benefits of the study 24
1.5. Novelty of study 25
1.6. Synopsis of the dissertation 25
1.7. Concluding Remarks 25
1.8. References 26
CHAPTER TWO 29
Recent Advances in Intra-Articular Bioactive Delivery for the Treatment of Osteoarthritis 29
2.1. Introduction 29
2.1.1. Anatomy and Pathogenesis of OA 30
2.1.2. Articular Cartilage Degeneration 30
2.1.3. Subchondral Bone Remodelling 32
2.2. Current Approaches and Key Limitations of Current OA Therapies 33
2.3. Challenges in IA Delivery 50
2.4. Colloidal Systems for Targeted and Site-Specific OA Therapy 35
2.4.1. Micelles 44
2.4.2. Liposomes 45
2.4.3. Polymeric Nanoparticles 48
2.4.4. Inorganic Nanoparticles (INPs) 53
2.4.5. tNPs 60
2.5.6. Niosomes 63

2.5. Hydrogels in OA Therapy 64
2.6. Molecularly Imprinted Materials with Potential to Treat OA 69
2.7. Current Clinical Trials on Intra-Articular OA Therapy 73
2.8. Review Summary: Colloidal Systems in OA Treatment 77
2.9. Conclusion and Future Research Perspectives 78
2.10. References 79
CHAPTER THREE 99
The Design and Development of a Dexamethasone-Tranfersome-PF-127/HA Stimuli-responsive Hydrogel for Intra-articular Therapy in Osteoarthritis 99
3.1. Introduction 99
3.2. Methods and Materials 101
3.2.1. Materials 101
3.2.2. Methods 102
3.2.2.3. Wave Scan (Lambda Max) and Standard Curve of DEX 104
3.3. RESULTS 112
tNPs 112
3.3.1. Wave Scan (Lambda Max) and Standard Curve of DEX 112
3.3.2. Size and Morphology of tNPs 114
3.3.3. Degree of Deformability 116
3.3.4. FTIR: Analysis of Identification of Structural Characteristics and Functional Groups of the tNPs 116
3.3.5. TGA: Thermal Stability and Decomposition of tNPs 117
3.3.6. XRD: Analysis of the Crystallographic Structure of the tNPs 118
3.3.7. Physical Stability of DEX-Loaded tNPs 119
3.3.8. *In Vitro* DEX Release from tNPs 120
Preparation and Characterization of DEX-tNP-P127/HA Stimuli-Responsive Hydrogel (Composite) 121
3.3.9. BET Surface Area Analysis Measurements of DEX-tNP-P127/HA Hydrogel 121
Physiochemical Characterization of DEX-tNP-P127/HA Hydrogels 122
3.3.10. FTIR: Analysis of Identification of Structural Characteristics and Functional Groups of tNP-P127/HA Hydrogels 122
3.3.11. XRD: Analysis of the Crystallographic Structure of the tNP-P127/HA Hydrogels 124
3.3.12. TGA: Thermal Stability and Decomposition for tNP-PF-127/HA Hydrogels 125
3.3.13. Gelation Time and Syringeability Evaluation of tNP-P127/HA Hydrogels 126
3.3.14. *In Vitro* DEX Release Profile from HA/PF-127 Hydrogel 127
3.3.15. *In Vitro* Drug Release Using a Knee Joint Simulator 128

3.3.16. Rheological Characterization of DEX-tNP-PF-127/HA Hydrogels 129
3.3.17. *In Silico* Analysis, the DEX-tNP Complex 131
3.3.18. Cytocompatibility Studies 133
4. Discussion 136
5. References 143
CHAPTER FOUR 154
Conclusions, Limitations, and Future Recommendations 154
5.1. Conclusions 154
5.2. Limitations of the study 155
5.3. Future Recommendations 155
APPENDICES 156
1. SAYAS Annual Young Scientist Conference - Oral Presentation Abstract 1566
2. Annual Conference of Pharmaceutical Sciences - Oral Presentation Abstract 158
3. Graphical Abstract for Chapter Two 160

LIST OF FIGURES

Figure 1.1. Chemical structures of (a) HA and (b) DEX.

Figure 1.2. Schematic illustration of in situ forming hydrogel joint cavity administration. Incorporation of drug-loaded tNPs into HA/PF-127 *in situ* hydrogel. IA administration of the gel with drug-loaded tNPs and its transition from sol-to-gel in the joint. This diagram illustrates how smart drug delivery works.

Figure 2.1. A comparison between a normal joint and an OA-affected joint.

Figure 2.2. Effects of HA-Lipo-DIC/DEX in suppressing OA in the paws of mice (adapted from an open access article; Chang et al., Copy right @ 2021 Adapted under a Creative Commons Attribution (CC BY).

Figure 2.3. Effects of DEX-Liposomes on expression levels of (A) TNF-α, IL-1β, and IL-6 in the femoral head and the (B) Concentrations of TNF-α and IL-10 in the serum, reprinted from Teng *et al.,* Copyright © 2023. Reproduced with permission from The Journal of the American Chemical Society.

Figure 2.4. *In vitro* assessment of the anti-inflammatory effects of IgG/Bb@BRPL. The experimental groups include untreated RAW 264.7 macrophage cells (column 1), LPS-stimulated cells (column 2), free Bb treatment (column 3), BRPL treatment (column 4), Bb@BRPL treatment (column 5), BSA/Bb@BRPL treatment (column 6), and IgG/Bb@BRPL treatment (column 7) (Kou et al., 2022). Adapted with permission from Elsevier

Figure 2.5. *In vitro* release profile of Rh from Rh-PLGA-NPs@NH4 under different conditions: (A) phosphate buffer at pH 7.4, (B) phosphate buffer at pH 5.4, and (C) simulated fluid environment (SFE). Figure adapted from Hu et al. (2020) and distributed under the terms of the Creative Commons CC BY license

Figure 2.6. Effects of PEG-MnO2 NPs on expression of catabolic mediators (A) iNOS, (B) MMP-1, (C) MMP-13, (D) ADAMTS-5and (E) ADAMTS-4 in chondrocytes (Kumar et al., 2019). Reproduced with permission from Elsevier.

Figure 2.7. Structures of nanoparticles used as drug delivery systems in the treatment of OA (image adapted from the open-access article; Guo *et al*., 2022). Adapted under the terms of the Creative Commons Attribution License (CC BY).

Figure 2.8. Micro-CT scans showing the effect of the microspheres on bone and articular cartilage injury. (Adapted from an open-access article; Li et al., 2021, licensed under a Creative Commons Attribution 4.0 International License).

Figure 2.9. Schematic illustration of the concept and function of chondrocyte-specific genome editing by the synthesized hybrid exosomes (B) The effect of Cas9 sgMMP-13 on MMP-13, ACAN, and COL2 levels in chondrocytes of the knee joints in rats (adapted from an open-access article; Liang et al., 2022.) Reproduced under the terms of Creative Commons CC BY

Figure 2.10. The general structure of a transfersome.

Figure 2.11. Radiological study results and observation before (A) and after treatment of OA rabbits. Adapted with no changes from Rasheed et al., 2022 under licensed under a Creative Commons Attribution CC BY license

Figure 2.12. The general structure of a noisome.

Figure 2.13. Formulation process and principle of the GelMA@DMA-MPC microspheres in OA (Reprinted from an open-access article Han et al., 2021 rats. Reproduced under the terms of Creative Commons under the CC BY-NC-ND license.

Figure 2.14. The effect of cerium oxide-NPs on mRNA expressions of Col2, ACAN, Col10, MMP-13, ADAMTS-5, ADAMTS-9 genes in chondrocytes (Li et al., 2024). Figure adapted an open access article and reproduced with permission from Elsevier.

Figure 3.1. Schematic representation of Thin Film Hydration method employed for the preparation of DEX-loaded tNPs.

Figure 3.2. Schematic representation of the cold method employed for the preparation of HA/PF-127 hydrogel

Figure 3.3. Knee simulator setup developed for the in-vitro drug release studies (Indian Design Registration no 375583-001).

Figure 3.4. Wave scan showing lambda max of DEX.

Figure 3.5. Calibration curve for DEX quantification: the curve illustrates the relationship between DEX concentration and absorbance.

Figure 3.6. Morphology of the tNPs shown by SEM at a scale of 1 µm (a) and 200 nm (b) as well as TEM (200 nm) (c).

Figure 3.7. FTIR spectra of DEX (green), Blank-tNPs (red) and DEX-loaded tNPs (blue).

Figure 3.8. TGA thermogram of DEX, Blank-tNPsand DEX-loaded tNPs.

Figure 3.9. XRD diffractograms of DEX (blue),Blank-tNPs (red) and DEX-loaded tNPs (orange).

Figure 3.10. DEX-release profiles from tNPs (blue) versus free drug (orange).

Figure 3.11. Morphological characterization of the DEX-tNPs-P127/HA Stimuli-responsive hydrogel.

Figure 3.12. FTIR spectra of HA (orange), PF-127 (red), blank-tNPs-PF-127/HA hydrogel (blue) and DEX-tNPs-PF-127/HA hydrogel (green).

Figure 3.13. Proposed molecular interactions between PF-127 and HA.

Figure 3.14. XRD diffractograms of HA (pink), PF-127 (blue), blank-tNPs-PF-127/HA hydrogel (red) and DNA-tNPs-PF-127/HA hydrogel (green).

Figure 3.15. TGA thermograms of HA, PF-127, blank-tNPs-PF-127/HA hydrogel and DEX-tNPs-PF-127/HA hydrogel.

Figure 3.16. Inverted tube method depicting sol-gel transition (a) of composite and syringeability profile of the hydrogel (b).

Figure 4.17. *In vitro* release profile of DEX from the tNPs incorporated into PF-127/HA hydrogel at pH 7.4.

Figure 3.18. The DEX-release profile obtained using the knee joint simulator.

Figure 3.19. Rheograms presenting the temperature ramp (a), stress sweep (b), and frequency sweep (c) of DEX-tNPs-PF-127/HA.

Figure 3.20. Rheograms presenting the yield stress (a) and thixotropy (b) of DEX-tNPs-PF-127/HA.

Figure 3.21. The *in silico* simulation of DEX-tNP complex. A) shows the DEX-tNP complex in the buffered water model. B) shows the successful DEX-loading in the tNPs and, C) displays the established molecular interactions between DEX and transfersomal constituents (only two monomers closest to DEX selected).

Figure 3.22. Micrographs of 264.7 RAW macrophage cells before treatment at 20× for (a) 264.7 RAW macrophage cells post 72 hours of treatment at 20× (b) (scale: 1 cm = 100 µm).

Figure 3.23. Cell proliferation and viability of murine RAW 264.7 macrophages exposed to DEX, Blank-NPs, DEX-NPs, Blank-NPs hydrogel, and DEX-NPs hydrogel composites for 48 hours.

Figure 4.23. Standard curve representative for mouse IL-4 Instant ELISA.

Figure 4.24. Quantification of IL-4 Secretion by Raw Macrophages Post-Treatment with Various Formulations after 24 hours of incubation.

LIST OF TABLES

Table 2.1. Summary of recent (2019-2023) advances in OA drug delivery systems with potential intra-articular application.

Table 2.2. List of clinical trials for intra-articular drug delivery in OA from clinicaltrials.gov.

Table 3.1. Summary of components of tNPs as well as their functions.

Table 3.2. DLS characterization of the generated tNPs.

Table 3.3. Effect of storage conditions on DEX-loaded tNPs over three months at 4°C and 25°C.

Table 3.4. BET measurement results of tNPs-PF-127/HA composite.

LIST OF EQUATIONS

Equation 1. $\text{EE}= \frac{\text{Total amount of the drug added} - \text{Amount of the free drug}}{\text{Total amount of the drug added}} \times 100$

Equation 2. $\text{DL} = \frac{Weight\ of\ Dex\ in\ nanonaprticles}{weight\ of\ Nanoparticles} \times 100$

Equation 3. $\text{D} = J \times \left(\frac{rv}{rp}\right)$

Equation 4: $\text{Cell viability} = \frac{Atreatment - Apos.control}{Aneg.control - Apos.control} \times 100$

Equation 5. $y = 0{,}0253x + 0{,}006$

Equation 6: $\text{y} = 0{,}006\text{x} + 0{,}2812$

LIST OF ABBREVIATIONS

- 2-methacryloyloxyethyl phosphorylcholine - MPC
- A multifunctional gene vector, arginine, histidine, and phenylalanine-modified generation 5 polyamidoamine - G5-AHP
- Acid-activatable polymeric - ACP
- A Disintegrin and Metalloproteinase with Thrombospondin motifs Aggrecan - ACAN
- Brunauer-Emmett-Teller - BET
- Beta-lapachone - βLap
- Bone Marrow Stromal Cell - BMSC
- Bovine serum albumin - BSA
- Carboxymethyl chitosan-assisted - CMC
- Collagen type ll - COL2A
- Cyclooxygenase-2 - COX-2
- Dexamethasone - DEX
- Diclofenac - DIC
- Diacerein®- DIA
- Drug loading - DL
- Dimethyl dioctadecyl ammonium bromide - DDAB
- Disease-modifying OA drugs - DMOADs
- Dynamic light scattering - DLS
- Dopamine poly(N,N-dimethylacrylamide) - DMA
- Drug loading – DL
- European Medicines Agency - EMA
- Etoricoxib - ETX
- Extracellular matrix - ECM
- Edge activator - EA
- Eicosapentaenoic acid - EPA
- EE - entrapment efficacy
- Food and Drug Administration - FDA
- Fourier Transformation Infrared - FTIR
- Gold Nanoparticles - GNPs
- Lambda max -λ max
- Linear viscoelastic - LVE

- Resolvin D1 encapsulated liposomes - Lipo-RvD1
- Hertz - hz
- Hyaluronic acid - HA
- Hyaluronan-loaded liposomal dexamethasone–diclofenac NPs - HA-Lipo-DIC/DEX
- Hydrophilic lipophilic balance - HLB
- High-performance liquid chromatography - HPLC
- iNOS
- Inorganic NPs - INPsInterleukin-1 – IL-1
- Intra-articular - IA
- Kartogenin - KGN
- Osteoarthritis - OA
- Nanoparticles - NPs
- Nitric oxide synthase -NOS
- Nanometer - nm
- Nonsteroidal anti-inflammatory drugs – NSAIDS
- Manganese oxide - MnOx
- Manganese dioxide - MnO_2
- Matrix metalloproteinases - MMPs
- Mesenchymal stem cells - MSCs
- Mesoporous silica NPs - MSNs
- Methacrylate gelatin - GelMA
- MicroRNA-140 - miR-140
- Millivolts - Mv
- Molecularly imprinted hydrogels – MIPs
- Nonsteroidal anti-inflammatory drugs (NSAIDS),
- Phosphate-buffered saline - PBS
- Prostaglandin E_2 - PGE_2
- Pluronic f-127- PF-127
- Poloxamer 407 - P407
- Polydopamine - PDA
- Polydispersity index - PDI
- Poly (ε-caprolactone) (PCL
- Poly (lactide) - PLA
- Poly (lactide-co-glycolide) copolymers - PLGA
- Polymeric NPs - PNPs

- Poly vinyl alcohol - PVA
- Reactive oxygen species - ROS
- Resolvin D1 - RvD1
- Rhein - Rh
- Rh and ammonium bicarbonate - NH_4HCO_3
- Rh and ammonium bicarbonate (NH_4HCO_3) laden PLGA NPs - Rh-PLGA-NPs@NH_4
- Scanning Electron Morphology - SEM
- Secretory phospholipase A2 inhibitor (thioetheramide-PC)-loaded micellar NPs - ($sPLA_2i$-NPs)
- SRY-box transcription factor 9 - SOX9
- Super-activated platelet lysate - sPL
- Superparamagnetic iron oxide NPs - SPIONs
- Texture analyzer - TA
- Triamcinolone acetonide – TCA
- Transfersome nanoparticles- tNPs
- Transmission electron microscopy - TEM
- Transforming growth factor β - TGF-β
- Thermogravimetric analysis - TGA
- Three-dimensional - 3D
- Tumour necrosis factor-α (TNF-α)
- Ultra-violet visible (UV-vis) spectroscopy - UV-Vis spectroscopy
- Western Ontario and McMaster Universities Osteoarthritis Index-pain - WOMAC
- World Health Organization - WHO
- X-ray diffraction – XRD

ABSTRACT

Osteoarthritis (OA) is one of the most prevalent debilitating joint diseases affecting over 7.6% of the global population. This disease is primarily characterized by cartilage degeneration, leading to pain, inflammation, and stiffness in affected joints. Current commercial treatment options for OA are mainly symptomatic and palliative. These include the pain and inflammation medicines acetaminophen, nonsteroidal anti-inflammatory drugs (NSAIDs), glucocorticoids, and opioids. However, these are associated with limitations such as gastric ulceration and acute kidney injury with classical NSAIDs, increased risk of cardiovascular disease with cyclooxygenase-2 (COX-2) selective inhibitors and the need for repeated intra-articular (IA) injections with glucocorticoids which, apart from increasing the risk for exposure to infections, are not cost-effective and often results in low patient compliance. However, to mitigate some of these drawbacks, stimuli-responsive drug delivery systems, such as nanocomposites, offer a promising approach to effective and sustainable treatment of OA.

In this study, we investigated the use of dexamethasone (DEX)-loaded tNPs nanoparticles (tNPs) incorporated in a Pluronic F-127/hyaluronic acid (PF-127/HA) hydrogel to treat OA. DEX, a potent anti-inflammatory and immunosuppressive agent, has been used for treatment of various inflammatory disorders, including OA.

DEX-loaded transfersomes (tNPs) were synthesized using thin-film hydration and incorporated into a thermo-responsive hydrogel composed of Pluronic F-127 (PF-127) and hyaluronic acid (HA). The formulation was evaluated for morphology, particle size, zeta potential, encapsulation efficiency, physiochemical characteristics, rheological properties, syringeability and drug release. *In vitro* release studies were conducted using a knee joint simulator to mimic physiological conditions. Biocompatibility was assessed using RAW 264.7 macrophages via MTT and IL-4 quantification assays to determine cytotoxicity and anti-inflammatory potential.

From the microscopic analysis (Scanning electron and transmission electron microscopy), the DEX-loaded tNPs had a hydrodynamic size of 76.43 ± 0.48 nm depicting a smooth and spherical morphology. Moreover, these tNPs had a remarkable EE of 98 ± 0.31%. The DEX-loaded tNPs also demonstrated high stability with insignificant changes in size, size distribution, and zeta potential over a period of 3 months. The amount of force required to extrude the hydrogel from a standard 22-gauge needle was 24 N, suggesting the required ease of injection. The drug release kinetic profile of these tNPs showed approximately 90% DEX release after 72 hrs, which, however, improved to approximately 2 months (7 weeks)

upon incorporation into the hydrogel matrix. In a knee joint simulator, the *in vitro* DEX release was confirmed to be 2 months from this nanosystem.

The rheological analysis showed promising mechanical properties such as stress sweep, thixotropy, yield stress, and frequency sweep, signifying the suitability of the hydrogel for the IA administration in OA joints. Furthermore, cell culture studies showed that the nanocomposite was biocompatible with RAW 264.7 macrophage cells, maintaining cell viability above 70%. Interleukin-4 (IL-4) quantification revealed that Blank-tNPs hydrogel induced the highest anti-inflammatory response, while DEX encapsulation slightly reduced IL-4 secretion

Taken together, the results from this study suggest that the developed DEX-tNPs-P127/HA hydrogel exhibited ideal physicochemical, rheological, and drug release properties for sustained IA delivery in OA. The formulation holds promise as a novel IA therapy, reducing injection frequency while maintaining therapeutic efficacy. However, further in vivo studies are warranted.

CHAPTER ONE

INTRODUCTION AND BACKGROUND

1.1. The Background of Osteoarthritis Drug Delivery

Osteoarthritis (OA) is the most prevailing form of chronic degenerative joint disease, which significantly impacts the quality of life thus limiting daily activities (He *et al*., 2020). OA is most frequently observed amongst middle and older populations and can be sub-categorized into primary and secondary OA based on etiology. Primary OA, prevalent in individuals aged >55, is a result of the natural aging process and mechanical “wear and tear”, whereas secondary OA develops due to external factors such as joint injuries and underlying diseases. As a result, secondary OA is common amongst younger individuals (PIzzorno *et al.,* 2016). The primary risk factors associated with OA include gender, age, diet, obesity and genetic predisposition (Palazzo *et al*., 2016).

Although the exact pathogenic mechanism of OA is unclear, the disease is largely associated with the progressive breakdown of articular cartilage. Articular cartilage physiologically acts as a shock absorber that mediates frictionless joint motion, (Dieppe, 2011; Tong *et al*., 2022). Thus, joint pain is the most prominent symptom of OA, which often worsens with movement and is exacerbated after periods of inactivity, a phenomenon known as the "gelling effect" (Pujalte, 2013). Under normal physiological conditions, synthetic and degradative enzymes within the cartilage matrix are balanced; however, in OA, this equilibrium is disrupted, and shifts, favouring the synthesis of degradative enzyme, ultimately leading to a net degradation and loss of matrix constituents (Martell-Pelletier *et al*., 2008). The early stages of OA are characterized by cartilage softening, fissures, and a reduction in cartilage thickness (Kleemann *et al*., 2005). As the disease advances, synovial inflammation leads to the influx inflammatory fluids in the joint capsule, thereby causing swelling, stiffness, and severe pain (Glyn-Jones and Palmer, 2015).

Current commercial OA treatments aid symptomatic and palliative care rather than modifying disease progression (Valderrabano and Steiger, 2010). The treatment primarily focuses on improving the overall quality of patients’ lives by reducing pain, correcting deformities, and attempting to improve the functionality of the affected joints (Kloppenburg and Berenbaum, 2019). The standard pharmacotherapy used for OA includes acetaminophen, COX-2 selective inhibitors, NSAIDs, opioids, corticosteroids, and hyaluronic acid (HA) injections (Sinusas, 2012). The use of intra-articular (IA) corticosteroids can provide short-term (4-6 weeks) pain

relief and can also be injected in conjunction with local anaesthetics to provide immediate relief (Orchard, 2020). However, these injections are only limited to up to four annually due to potential joint damage and heightened risk of infection (Guermazi *et al.,* 2023). The IA administration of an anti-OA drug offers several advantages over the systemic route such as improved systemic adverse reaction profiles and bioavailability of therapeutics due to the direct targeting of the affected joint (Fajardo and Di Cesare, 2005).

Corticosteroids such as dexamethasone (DEX) exert their anti-inflammatory actions by down regulating pro-inflammatory transcription factors while upregulating anti-inflammatory transcription factors. At lower doses, corticosteroids provide anti-inflammatory benefits, whereas prolonged use at higher doses result in immunosuppressive effects (Yasir *et al*., 2018).

Despite these benefits, challenges associated with IA drug delivery remain. The complex composition of the joint and high viscosity of the synovial fluid, interfere with the drug diffusion, as a result, drugs are cleared from the synovial fluid at an accelerated rate. Additionally, the extracellular matrix (ECM) of cartilage consists of a dense network of proteoglycans and collagen fibers that hinder drug absorption (Li *et al*., 2021). Furthermore, cartilage ECM has a net negative charge (anionic) as a result of densely packed negatively charged molecules. This ananionic charge hinders the diffusion of anionic drugs into the cartilage, reducing their therapeutic effects (Li *et al*., 2021). The most effective way to increase the therapeutic efficacy of such drugs is by repeated injections. However, frequent injections heighten the risk of joint infections, joint structural damage, and impose a financial burden on patients.

To address these obstacles that are linked to conventional dosing methods, innovative delivery systems have been explored to enhance the retention, bioavailability, and targeting efficiency of the administered therapeutic agents. Nanotechnology-based strategies, including nanoparticle (NP) formulations, have emerged as a promising alternative (Li *et al.,* 2021). In this regard, NPs, typically ranging between 1-100 nm in size, have shown potential for improving OA therapy by optimizing drug delivery and retention in joint (Li *et al*., 2021).

NPs have been widely applied in drug delivery for various diseases, utilizing diverse administration routes to optimize pharmacokinetic properties of therapeutics (Yuan *et al*., 2019). These nanostructures have the potential to solve issues with current delivery systems, which include poor solubility, low drug retention time, and drug efficacy (Bonifacio *et al*., 2014). Furthermore, NPs are highly stable (long half-life) and can be engineered to integrate both hydrophobic and hydrophilic therapeutic agents thus increasing their solubility (Gelperina *et al*., 2005). Drugs can also reach their targets more effectively as they can be protected from proteolytic degradation. Specifically, nanostructures such as tNPs have gained attention in OA

treatment due to their high drug entrapment efficiencies and prolonged drug release profiles which make them ideal for the pharmacotherapy of OA (Rajan *et al*., 2011). By maintaining stable therapeutic drug concentrations over extended periods, tNPs enhance treatment outcomes while minimizing systemic toxicity and injection-associated complications (Rudnik-Jansen *et al.,* 2017). This, in turn, improves patient compliance and reduces overall treatment costs.

In addition to tNP-based delivery systems, incorporating HA into OA therapies can potentially provide a complementary therapeutic approach. HA is a naturally occurring glycosaminoglycan found in tissue and has numerous functions, including lubrication to reduce bone to bone friction, inflammation modulation, cartilage generation, and restoration of rheological properties, i.e., viscoelasticity in the synovial fluid (Gupta et al., 2019). In OA-affected joints, HA concentrations are significantly reduced compared to healthy joints thus compromising joint function and exacerbating inflammation (Li, et al., 2021). This suggests that exogenous HA can be administered to restore viscoelasticity and for viscosupplementation. Supplementing with exogenous HA can potentially enhance chondrocyte synthesis, provide chondrocyte protection, promote cartilage regeneration, and reduce pro-inflammatory mediator production. HA can also alleviate pain and improve joint mobility, making it a valuable adjunct in OA treatment (Gupta *et al.,* 2019).

Using the concepts from nanotechnology and stimuli-responsive hydrogel technology, this study aimed to design and develop a delivery system by encapsulating DEX, a model anti-inflammatory drug, into the nano-sized tNPs incorporated into a bio-mimetic hydrogel that has *in situ* gelling properties, for IA administration in OA. Among the materials explored for such advanced delivery systems, the polymer - Pluronic F-127 (PF-127), stands out due to its thermo-responsive properties. This non-ionic tri-block can transition from sol to gel at higher temperatures, making it particularly suitable for smart drug delivery applications as it has low toxicity, and high biocompatibility (Brandani and Stroeve, 2003; Singh-Joy and McLain, 2008).

1.2. Rationale and Motivation

Current pharmacological treatments and drug delivery systems targeting OA have inadequate therapeutic efficacy. Symptomatic pain management is used as a first-line treatment; however, poor drug bioavailability and associated adverse effects hinder their long-term application. Most analgesics are administered orally, undergo hepatic first-pass metabolism which reduces their concentrations that reach the site of action (Adebajo, 2012). The diminished drug concentrations result in poorer therapeutic outcomes while frequent dosing can further contribute to poor patient compliance. Acetaminophen, NSAIDs, and COX-2 inhibitors have been reported to subdue pain and improve joint function. However, NSAIDs heighten the risk

of gastrointestinal bleeding and renal impairment (Adebajo, 2012), whereas COX-2 inhibitors elevate the risk of cardiovascular diseases (Deeks *et al*., 2002) and opioids pose a risk of dependence (Evans and Cahill, 2016).

The IA route of administration offers several advantages over oral or systemic delivery. By evading first-pass metabolism, IA drug delivery improves the bioavailability of drugs and ensures direct access of treatment to the cavity of the affected joint. Corticosteroids such as DEX and bioactive agents such as hyaluronans are administered via IA injections; however, these agents undergo rapid elimination from the cavity as a result of the complex composition of the synovial cavity (Sinusas, 2012). To address these limitations, we hypothesized that delivery of anti-OA drugs using precision-engineered nano-constructs modified for a controlled and targeted manner, is a potential solution to enhance therapeutic outcomes.

Thus, in this study, we investigated the potential of combining DEX-loaded tNPs and PF-127/HA to formulate an injectable *in situ* thermo-responsive hydrogel for IA application in OA treatment. In this approach, anti-inflammatory effects of DEX is complemented by HA's ability to mediate chondrocyte synthesis and joint lubrication. Additionally, the bio-viscous hydrogel forms a lubrication layer between the joint surfaces to reduce friction and alleviate pain. The thermo-responsive polymer (PF-127) transitions from sol to gel at physiological temperature, facilitating localized and sustained drug release upon IA administration. An illustrative representation of the HA-based gel model investigated in this study is shown in Figure 1.1.

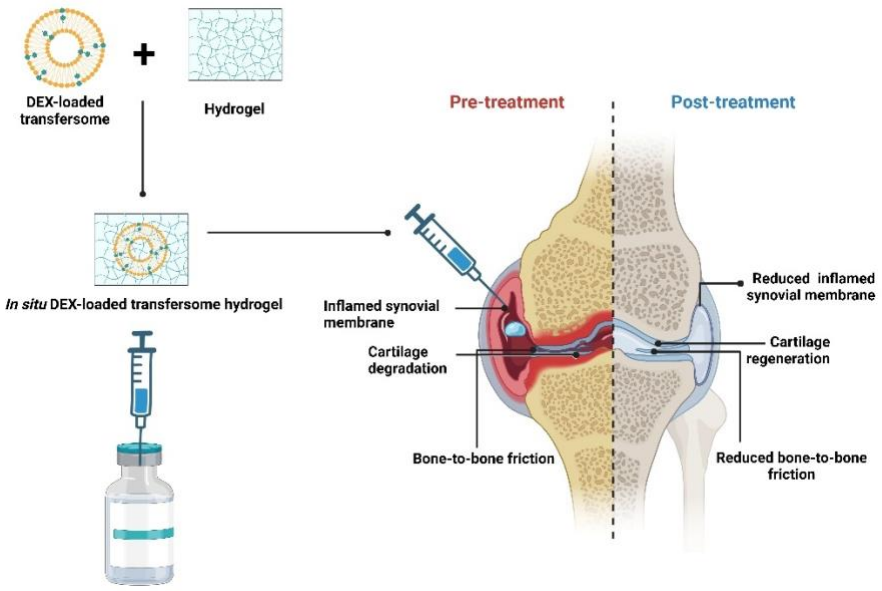


Figure 1. Schematic illustration of in situ forming hydrogel joint cavity administration. Incorporation of DEX-loaded tNPs into the PF-127/HA *in situ* hydrogel. IA administration of the gel and its transition from sol-to-gel in the joint.

This proposed nanosystem has the potential to increase the residence time and efficacy, improve the side effect profile of DEX, and provide a cationic environment to improve drug delivery. Figure 1.2 shows the chemical structures of HA (a) and DEX (b).

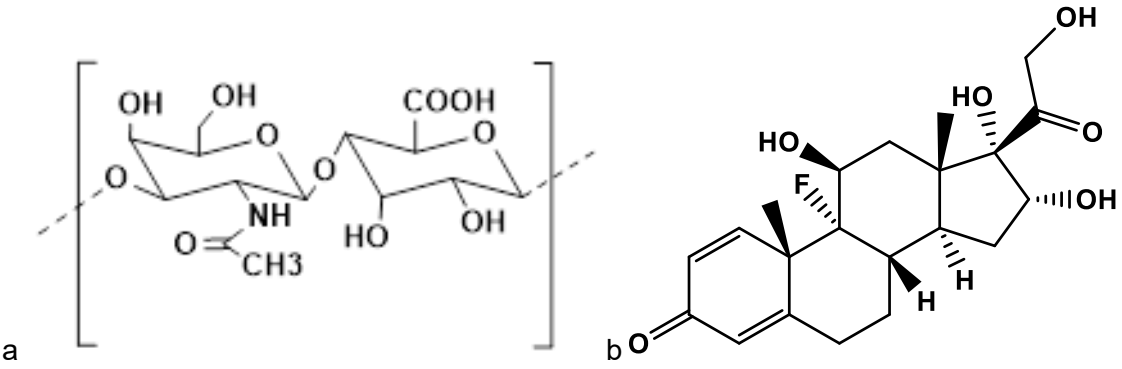


Figure 1.2. The chemical structures of (a) HA and (b) DEX.

1.3. Aims and Objectives

1.3.1. Aim

This study aimed to design and develop the DEX-loaded cationic nano-sized tNPs fixated within an HA-based colloidal hydrogel as an *in situ* thermo-responsive transitioning gel for the IA injection in the treatment of OA.

To achieve this aim, the following objectives were set:

1.3.2. Objectives

Objective 1: To synthesize the biocompatible and degradable DEX-loaded cationic nano-sized tNPs delivery system by thin film hydration and encapsulate these into PF-127/HA *in situ* to form an injectable hydrogel.

Objective 2: To characterize the tNPs and tNPs-PF-127/HA hydrogel by determining their size, morphology, surface charge, physicochemical properties, entrapment efficiency (EE), and DEX release kinetics.

Objective 3: To investigate *in vitro* cytotoxicity and anti-inflammatory effects of the DEX-loaded tNPs and hydrogel on RAW 264.7 macrophages.

1.4. Potential benefits of the study

- The development of a target-specific delivery system with enhanced DEX joint residence time and a sustained DEX release, thereby decreasing frequent injections and chances of infections and increasing patient compliance.

1.5. Novelty of study

- Enhanced drug penetration: The concept of enhancing DEX penetration in the dense and complex joint cartilage by tNPs, especially from the IA administration, is innovative and novel.
- Knee joint simulator: The use of novel and ground-breaking technology such as the knee joint simulator in this study helped to provide more accurate results of DEX release kinetics because unlike conventional drug release methods, it takes into consideration the environment of the joint.

1.6. Synopsis of the dissertation

Chapter 1 will provide a background of the study and outline the conventional treatments of OA. It also highlights the gap within the field which formed the rationale of this research. Furthermore, it will also detail the objectives of the study.

Chapter 2 is a literature review outlining the challenges associated with conventional treatments of OA while highlighting advances in therapies for OA.

Chapter 3 focuses on bridging the gap addressed in Chapter 1. It presents pre-formulation studies and details the materials used for synthesizing the tNPs, providing a rationale for the selection of specific materials. Furthermore, it comprises the designed and developed optimized formulations as well as their various characterizations.

Chapter 4 is a comprehensive conclusion of the study, along with the limitations and future perspective and recommendations

1.7. Concluding Remarks

This chapter provided an introduction, rationale, and insight into the significance of the research undertaken. This study provides insight into designing and developing a drug delivery system that can overcome the current challenges with conventional drug delivery systems. The use of tNPs offers significant advantages, such as enhanced drug stability and targeted delivery, with the tNPs enhancing DEX penetration in the dense and complex joint cartilage, which are crucial for improving the therapeutic outcomes in OA treatment. The use of the hydrogel as a vehicle for the DEX-loaded tNPs provides a platform for the delivery system to therapeutic and structural properties, as the hydrogel can assist with sustained DEX release and offer lubrication between bones at the site of administration in OA. We hoped to demonstrate a novel approach to potentially attenuate OA and improve patient quality of life.

1.8. References

Adebajo, A., 2012. Non-steroidal anti-inflammatory drugs for the treatment of pain and immobility-associated osteoarthritis: consensus guidance for primary care. *BMC family Practice*, *13*(1), pp.1-7.

Bonifacio, B.V., da Silva, P.B., dos Santos Ramos, M.A., Negri, K.M.S., Bauab, T.M. and Chorilli, M., 2014. Nanotechnology-based drug delivery systems and herbal medicines: a review. *International Journal of Nanomedicine*, *9*, p.1.

Brandani, P. and Stroeve, P., 2003. Adsorption and desorption of PEO− PPO− PEO triblock copolymers on a self-assembled hydrophobic surface. *Macromolecules*, *36*(25), pp.9492-9501.

Chinese Orthopaedic Association, 2010. Diagnosis and treatment of osteoarthritis. *Orthopaedic Surgery*, *2*(1), p.1-6.

Deeks, J.J., Smith, L.A. and Bradley, M.D., 2002. Efficacy, tolerability, and upper gastrointestinal safety of celecoxib for treatment of osteoarthritis and rheumatoid arthritis: a systematic review of randomized controlled trials. *Bmj*, *325*(7365), p.619.

Evans, C.J. and Cahill, C.M., 2016. Neurobiology of opioid dependence in creating addiction vulnerability. *F1000Research*, *5*.

Dieppe, P., 2011. Developments in osteoarthritis. *Rheumatology*, *50*(2), pp.245-247.

Gelperina, S., Kisich, K., Iseman, M.D. and Heifets, L., 2005. The potential advantages of nanoparticle drug delivery systems in chemotherapy of tuberculosis. *American Journal of respiratoryJournal of Respiratory and Critical Care Medicine*, *172*(12), pp.1487-1490.

Ghadi, A., Mahjoub, S., Tabandeh, F. and Talebnia, F., 2014. Synthesis and optimization of chitosan nanoparticles: Potential applications in nanomedicine and biomedical engineering. *Caspian Journal of Internal Medicine Journal of Internal Medicine*, *5*(3), p.156.

Glyn-Jones, S. and Palmer, A.J., 2015. Agricola, R.; Price, AJ; Vincent, TL; Weinans, H.; Carr. *AJ Osteoarthritis. Lancet*, *386*(9991), pp.376-387.

Fajardo, M. and Di Cesare, P.E., 2005. Disease-modifying therapies for osteoarthritis. *Drugs & aging*, *22*(2), pp.141-161.

Guermazi, A., Hunter, D.J. and Kloppenburg, M., 2023. Debate: Intra-articular steroid injections for osteoarthritis–harmful or helpful? *Osteoarthritis imaging*, *3*(3), p.100163.

Gupta, R.C., Lall, R., Srivastava, A. and Sinha, A., 2019. Hyaluronic acid: Molecular mechanisms and therapeutic trajectory. *Frontiers in Veterinary Science*, p.192.

He, Y., Li, Z., Alexander, P.G., Ocasio-Nieves, B.D., Yocum, L., Lin, H. and Tuan, R.S., 2020. Pathogenesis of osteoarthritis: risk factors, regulatory pathways in chondrocytes, and experimental models. *Biology*, *9*(8), p.194.

Kleemann, R.U., Krocker, D., Cedraro, A., Tuischer, J. and Duda, G.N., 2005. Altered cartilage mechanics and histology in knee osteoarthritis: relation to clinical assessment (ICRS Grade). *Osteoarthritis and Cartilage*, 13(11), pp.958963.

Kloppenburg, M. and Berenbaum, F., 2020. Osteoarthritis year in review 2019: epidemiology and therapy. *Osteoarthritis and Cartilage*, 28(3), pp.242-248.

Li, X., Dai, B., Guo, J., Zheng, L., Guo, Q., Peng, J., Xu, J. and Qin, L., 2021. Nanoparticle–Cartilage Interaction: Pathology-Based Intra-articular Drug Delivery for Osteoarthritis Therapy. *Nano-Micro Letters*, *13*(1), pp.1-48.

Martel-Pelletier, J., Boileau, C., Pelletier, J.P. and Roughley, P.J., 2008. Cartilage in normal and osteoarthritis conditions. *Best practice & Research Clinical Rheumatology*, 22(2), pp.351-384.

Orchard, J.W., 2020. Is there a place for intra-articular corticosteroid injections in the treatment of knee osteoarthritis? *Bmj*, *368*.

Pizzorno, J.E., Murray, M.T. and Joiner-Bey, H., 2016. *The Clinician's Handbook of Natural Medicine E-Book: The Clinician's Handbook of Natural Medicine E-Book*. Elsevier Health Sciences.

Pujalte, G., 2013. *Orthopedics, An Issue of Primary Care Clinics in Office Practice* (Vol. 40, No. 4). Elsevier Health Sciences.

Rajan, R., Jose, S., Mukund, V.B. and Vasudevan, D.T., 2011. Transferosomes-A vesicular transdermal delivery system for enhanced drug permeation. *Journal of Advanced Pharmaceutical Technology & Research*, *2*(3), p.138.

Singh-Joy, S.D. and McLain, V.C., 2008. Safety assessment of poloxamers 101, 105, 108, 122, 123, 124, 181, 182, 183, 184, 185, 188, 212, 215, 217, 231, 234, 235, 237, 238, 282, 284, 288, 331, 333, 334, 335, 338, 401, 402, 403, and 407, poloxamer 105 benzoate, and poloxamer 182 dibenzoate as used in cosmetics. *International Journal of Toxicology*, *27*, pp.93-128.

Sinusas, K., 2012. Osteoarthritis: diagnosis and treatment. *American Family Physician*, *85*(1), pp.49-56.

Tong, L., Yu, H., Huang, X., Shen, J., Xiao, G., Chen, L., Wang, H., Xing, L. and Chen, D., 2022. Current understanding of osteoarthritis pathogenesis and relevant new approaches. *Bone Research*, *10*(1), p.60.

Yasir, M., Goyal, A., Bansal, P. and Sonthalia, S., 2018. Corticosteroid adverse effects.

Yuan, D., He, H., Wu, Y., Fan, J. and Cao, Y., 2019. Physiologically based pharmacokinetic modeling of nanoparticles. *Journal of Pharmaceutical Sciences*, *108*(1), pp.58-72.

CHAPTER TWO

Recent Advances in Intra-Articular Bioactive Delivery for the Treatment of Osteoarthritis

2.1. Introduction

Osteoarthritis (OA) is the most prevalent form of chronic degenerative joint disease that ultimately leads to an overall decline in the quality of life (He *et al*., 2020). As of 2019, a staggering 528 million individuals worldwide suffered from OA (WHO, 2023). A demographic lens indicates that 73% of OA patients are aged 55 and older, with a striking 60% comprising females. Moreover, knee OA is the most prevalent type, affecting approximately 365 million individuals, followed by hip and hand OA (WHO, 2019). There is currently no definitive cure for OA, and pain generally correlates with disease progression (Hawker and Lohmander, 2021). OA is classified into two major categories: primary and secondary OA. Primary OA arises from age-related mechanical stress and cartilage degeneration. (Loeser, 2010). When cartilage degenerates, it flakes and develops crevasses that lead to pain, inflammation, and friction between bones. In contrast, secondary OA is triggered by external factors such congenital disabilities, joint injuries, or underlying diseases. As a result, secondary OA affects people of all ages (Leung *et al.,* 2014).

Conventional treatment strategies for OA include physiotherapy, aerobic exercise, the use of non-steroidal anti-inflammatory drugs (NSAIDs), glucocorticoids, biologics, and, in severe cases, joint replacement surgery. Among these approaches, the administration of various small-molecule drugs in oral dosage forms is still considered the standard treatment for OA. While their advantages are widely acknowledged, they pose significant drawbacks such as, non-specific drug delivery, poor bioavailability, short half-life, and the necessity for high dosages which can lead to severe adverse reactions such as gastrointestinal bleeding. In contrast to oral delivery, IA injection stands out as a favourable method for treating OA. This approach involves directly administering bioactives into the affected joints, offering several benefits over systemic treatments. These include enhanced safety, decreased joint inflammation, and improved joint function. IA injections also allow for prolonged drug action time with minimal exposure to other parts of the body, cost reductions, and enhanced treatment effectiveness.

While IA delivery has many benefits, it faces challenges, such as the rapid clearance of the injected therapeutic agent solution from the joint cavity, causing short intra-joint retention times, often lasting only a few hours. Given that OA is a chronic condition, frequent injections

are necessary to maintain effective drug concentrations, but this can increase the risk of infections at the injection site or damage to the cartilage, often resulting in poor patient compliance. Consequently, research on sustained-release formulations for IA injections is critically important. Researchers have dedicated significant efforts toward developing innovative strategies that enhance the effectiveness of IA. OA treatment, viz., the quality of life for OA patients.

This review provides comprehensive insights, exploiting various advanced drug delivery systems such as NPs and colloidal hydrogels suitable for IA delivery of anti-OA drugs and biologics in OA therapy. *In vitro* and *in vivo* experiments were investigated to determine the effects of the delivery systems on OA models. Investigations include their anti-inflammatory effects, chondrogenesis, cartilage, and tissue regeneration. Key challenges were identified while offering valuable suggestions and insights to overcome these obstacles contributing towards advancing the attenuation of OA development using NPs and hydrogel-based delivery systems.

2.1.1. Anatomy and Pathogenesis of OA

It was previously believed that OA was only characterized by articular cartilage damage, but recent research suggests that the condition involves histopathological changes in the whole joint (Dieppe, 2011). Apart from the progressive deterioration of articular cartilage, OA is accompanied by subchondral bone remodeling, osteophyte formation, synovial membrane inflammation, and hypertrophic bone changes (Man and Mologhianu, 2014; Chen *et al*., 2020; Gao *et al.*, 2022).

2.1.2. Articular Cartilage Degeneration

Articular cartilage is an aneural connective tissue that serves as a shock absorber and mediates frictionless motion at the joints. It mainly consists of chondrocytes, which are responsible for the secretion of cartilage matrix and maintenance of extracellular matrix (ECM). The ECM primarily consists of approximately 70% water along with collagen (COL) and glycosaminoglycans such as aggrecan (ACAN), chondroitin sulfate, and hyaluronic acid (HA) (Jin, 2020). The large amount of water is essential for the maintenance of resilience in the joint tissues, lubrication, and nutritional purposes (Martell-Pelletier *et al*., 2008). Moreover, the integrity and activity of chondrocytes are influenced by numerous factors that include cytokines, polypeptide growth factors as well as structural and physical stimuli.

Cartilage degradation is exacerbated by biological factors such as reactive oxygen species (ROS), pro-inflammatory enzymes, and proteolytic enzymes (Jin, 2020). While ROS are physiological by-products of mitochondrial respiration in normal metabolism, their excessive

production has been shown to be one of the primary mechanisms of cartilage damage (Henrotin *et al*., 2005). ROS can induce mitochondrial senescence, leading to increased permeability of the mitochondrial membrane, resulting in the increased influx of ROS into the chondrocyte cytosol (Ansari *et al*., 2018; Dan Dunn *et al*., 2015). Once within chondrocytes, ROS disrupts the mitotic phase of the cell cycle, leading to chondrocyte apoptosis (chondroptosis) (Kang *et al*., 2020).

Mechanical stimuli, inflammatory cytokines, as well as oxidative and nitric oxide-mediated stress result in a redox imbalance, which also induces chondroptosis (Charlier *et al*., 2016). Inflammatory cytokines such as interleukin (IL)-1β, IL-6, and tumour necrosis factor (TNF)-α are simultaneously produced with ECM-degrading enzymes like matrix metalloproteinases (MMP) (e.g., MMP-3 and MMP-13) as well as disintegrin and metalloproteinase with thrombospondin motifs (ADAMTS) (Figure 1) (Li *et al*., 2021). IL-1 and TNF-α are potent pro-inflammatory cytokines with the ability to induce the synthesis of MMPs by chondrocytes (Jabłońska-Trypuć *et al*., 2016). The MMPs are secreted as pro-enzymes, which require proteolytic cleavage for activation (Campana and Iredale, 2015).

Under natural conditions, matrix synthetic and degradative enzymes are at equilibrium. However, due to the enhanced synthesis of MMPs in the case of OA, the equilibrium is shifts in favour of the degradative enzymes (Martell-Pelletier *et al*., 2008). This equilibrium shift results in decreased amounts of proteoglycan and collagen in the ECM. Given this, the collagen network weakens, further aiding the degradation process of cartilage. During the initial degenerative stages of articular cartilage, there is cartilage softening, fissuring, and thinning of cartilage (Kleemann *et al*., 2005). Importantly, this collagen loss ultimately leads to chondroptosis. As the disease progresses, inflammatory fluids fill the cavity, therefore causing swelling, stiffness, and heightened pain (Glyn-Jones and Palmer, 2015). Lastly, the destruction of articular cartilage is intricately linked to subchondral bone remodeling in the pathogenesis of OA (Man and Mologhianu, 2014).

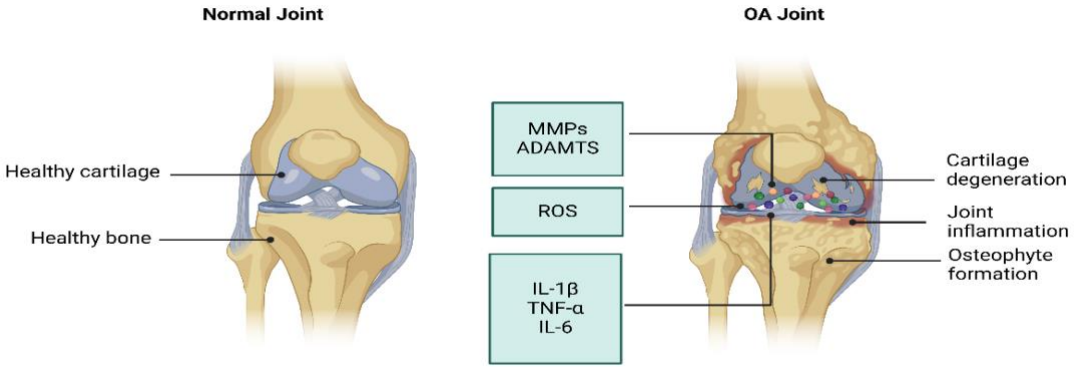


Figure 2.1. Comparison between a normal joint and an OA-affected joint.

2.1.3. Subchondral Bone Remodelling

The subchondral bone is the bony layer situated beneath the cartilage and the tidemark, comprising the bone marrow space, underlying trabecular bone, and the subchondral bone plate (Hu *et al*., 2021). Subchondral bone modeling and thickening are considered as secondary changes in OA pathogenesis (He *et al*., 2020). Over time, as cartilage deteriorates, it becomes thinner and eventually exposes the underlying subchondral bone plate, leading to increased mechanical stress and pain (Man and Mologhianu, 2014). Transforming Growth Factor-β (TGF-β), is a key enzyme secreted by subchondral bone cells that plays a crucial role in maintaining articular cartilage homeostasis and structural integrity. In OA, excessive levels of TGF-β have been observed. In excess, this enzyme can stimulate the production of MMP-13, an enzyme implicated in cartilage degradation (Hu *et al*., 2021). Several theories have been postulated to explain the potential role of subchondral bone remodelling in the pathogenesis of OA. One theory suggests that subchondral bone recovering from a trabecular microfracture or abnormal metabolism of osteoblasts is stiffer and ineffective as a shock absorber, which causes cartilage damage. Another hypothesis posits that by-products produced by osteoclasts, mononuclear cells, and osteoblasts from the subchondral bone can leak through channels and fissures between the cartilage and bones, thereby inducing OA (Ge *et al*., 2006; Zhu *et al*., 2021).

2.2. Current Approaches and Key Limitations of Current OA Therapies

Conventional treatment for OA is palliative, given no curative avenue is available (Chen *et al*., 2021). Treatment aims to improve the overall quality of patients' lives by alleviating symptoms, delaying the progression of the disease, reducing pain, attempting to correct deformities, and improving the functionality of affected joints (Maqbool *et al*., 2021).

Acetaminophen is the standard treatment of care for mild OA because of its efficacy, safety profile, and low cost (Salgado *et al*., 2021). Acetaminophen is indeed a well-tolerated drug with a mild adverse effect profile (Towheed *et al*., 2006). However, where acetaminophen is ineffective, intolerable, or symptoms are severe, NSAIDs are recommended. NSAIDs pose a risk of adverse effects, which may include renal dysfunction, elevated blood pressure, and gastrointestinal bleeding (Pujalte, 2013). Alternatively, COX-2 selective inhibitors, under the NSAIDs class are recommended due to their improved gastrointestinal side effect profile. However, COX-2 selective inhibitors have an increased risk of cardiovascular diseases. Moreover, the COX-2 inhibitors are less cost-effective than the aforementioned options (Deeks *et al*., 2002).

In cases where both acetaminophen and NSAIDs are ineffective, or the side effects are intolerable or contraindicated, opiate drugs can be prescribed with caution (Chen *et al*., 2021). The lowest possible dosage should be used for the shortest period possible to avoid dependence and abuse (Dydyk *et al*., 2023). The challenge is that OA is a chronic disease often requiring long-term management (Charlesworth *et al*., 2019).

Interestingly, the administration of IA class of anti-inflammatory agents, corticosteroids, can also provide short-term (4-6 weeks) pain relief. These are often injected along with local anaesthetics to provide immediate relief (Orchard, 2020). However, administration of injections is only limited to four injections annually (Sinusas, 2012). Repeated injections increase the risk of infection, are not cost-effective, and can potentially lower patient compliance (Martin *et al*., 2000). As a result, it is widely acknowledged that it is crucial to develop a modified-release system for IA OA therapies such as corticosteroids (Bruno *et al*., 2022; Huang *et al*., 2022; Liu *et al.,* 2023). Drugs that are delivered through the IA route have fewer systemic adverse effects and an increased drug concentration at the joint space (Rai and Pham, 2018).

Glucosamine and chondroitin, primary substrates in the biosynthesis of proteoglycan - a constituent of cartilage, can be taken individually or in combination as supplementation, aiding the delay in the natural progression of OA (Meng *et al.,* 2023). Glucosamine and chondroitin assist in the biosynthesis, elasticity, and function of articular cartilage, potentially acting as chondroprotective agents and disease-modifying OA drugs (DMOADs) (James and Uhl, 2001;

Meng *et al.,* 2023). Another important IA OA treatment option is HA, an endogenous glycosaminoglycan found naturally in animal tissue. It has numerous functions, including lubrication to reduce friction between bones, reducing inflammation and stimulation of cartilage, and restoration of rheological properties in the synovial fluid (Gupta *et al*., 2019). Since osteoarthritic joints have a lower concentration of HA compared to healthy joints (Li, *et al*., 2021), exogenous HA can be administered to restore viscoelasticity and cushioning effects in the joints (Bowman *et al*., 2018). Additionally, HA has the ability to induce chondrocyte synthesis, provide chondrocyte protection, promote cartilage regeneration, and reduce pro-inflammatory mediator production (Testa *et al*., 2021). HA can relieve pain and improve OA joints' functionality (Kou *et al*., 2019). Adverse reactions are rare but may arise as severe acute local reactions characterized by acute joint pain, swelling, erythema and restricted mobility of joints following IA HA administration. The onset of these symptoms ranges anywhere from 4 hours to several days post administration (Glinkowski and Tomaszewski, 2025). Monovisc™ and Orthovisc®, high molecular weight (HMW) exogenous HA formulations, are some of the Food and Drug Administration (FDA)-approved IA HA formulations for OA treatment.

Moreover, apart from those previously discussed treatment options, a more recent tool of OA treatment of OA is platelet-rich plasma (PRP) IA injections (Abbas *et al.,* 2023). Specifically, leukocyte-poor PRPs, which possess the capacity to promote cartilage regeneration while decreasing concentrations of pro-inflammatory cytokines (Gupta *et al*., 2023; Su *et al*., 2023). The endogenous nature of PRP makes them desirable as it utilizes patient blood products to stimulate the production of autologous growth factors (Smith, 2016). This is appealing because the risk of rejection is low as the injection is a derivative of the patient's own blood (Foster *et al.,* 2009). Notably, NSAIDs are contraindicated with the use of PRP. This is because they impair normal platelet function in patients on PRP injections leading to a decline in the amount of growth factors released (Schippinger *et al.,* 2015).

Although there have not been any DMOADs currently approved by regulatory bodies such as FDA and European Medicines Agency (EMA) for the treatment of OA, these have shown potential for therapeutic efficacy in ongoing research (Li *et al*., 2023; Rodriguez-Merchan, 2023). In general, these drugs aim to exploit the hallmarks of OA by inhibiting the progression of the disease and providing symptomatic relief by either reducing pain or improving the physical functioning of the joint (Oo *et al*., 2018). DMOADs target, among others, matrix-degrading enzymes, inflammatory cytokines, and inducible nitric oxide synthase (iNOS) (Yazici et al., 2017; Oo *et al*., 2018). However, DMOADs face some hurdles that impede their translation into clinical application (Gao *et al.,* 2022). Insufficient bioavailability of DMOADs in

the joint cavity upon systemic administration has proven to be a prominent challenge, which results in inadequate therapeutic efficacy and unwanted adverse effects (Gao *et al.*, 2022).

2.3. Challenges in IA Delivery

The complex composition of the synovial joint, along with the viscosity of the synovial fluid, presents an unfavourable pharmacokinetic environment for most drugs (Siefen *et al*., 2022). Often, this results in rapid clearance from the synovial cleft into the systemic circulation through lymphatic and blood vessels (Cao *et al*., 2021). This mandates repeated dosing of drugs at high dosages, which in turn results in toxicity and reduced patient compliance. The short residence times of drugs in the OA joint have also been associated with a synovial membrane where macromolecules larger than 100 kDa are well-retained, but smaller molecules, such as NSAIDs, easily leak through the systemic circulation (Rabei *et al*., 2021). The proteoglycan and collagen fibers of cartilage ECM form a dense network with an overall negative charge, which presents a hurdle for the absorption of the drugs and supplements that are negatively charged at physiological pH into the cartilage (Theocharis *et al*., 2016; Li *et al*., 2021). These include dexamethasone (DEX), diclofenac (DIC) and HA (Al-Owaidi *et al*., 2021; Basheeruddin *et al*., 2022; Hintze *et al*., 2022). As a result, the therapeutic efficacy of such agents is maintained by repeated injections, which are indeed unfavourable in terms of cost and increased risk of infections and joint destruction (Martin *et al*., 2000). It is evident that drug delivery systems with the potential to overcome such obstacles to optimize the IA OA treatment are urgently needed. Since small molecules such as corticosteroids and NSAIDs are not effectively retained for sustained periods to exert the required therapeutic effects, using these drugs in their free forms for IA injections faced numerous pharmacokinetic challenges (Mancipe *et al*., 2020).

To this extent, particulate-based technologies for OA therapy have been explored. However, large particles are not considered optimal carriers for IA drug delivery. Although these could be retained for a relatively long period, their larger size impedes their penetration into intricate spaces such as the ECM thus lowering their efficacy (Geiger *et al.*, 2018; Huang *et al.,* 2022). However, the nanoparticle (NPs) carriers have shown better potential for achieving this goal. Due to their smaller size, they are more permeable and, therefore, able to reach their target sites efficiently in OA joints (Wen *et al*., 2023). Taking into consideration, the recent advances in the particulate IA OA therapy space, this study reviews the potential of IA particulate-based therapies to overcome aforementioned problems and attain better therapeutic responses.

2.4. Colloidal Systems for Targeted and Site-Specific OA Therapy

NPs are approximately a thousand times smaller than chondrocytes (Li *et al*., 2021). NPs have the potential to solve issues associated with conventional drug delivery systems, which include

low solubility, retention time, and efficacy of drugs, as well as their susceptibility to acidic or enzymatic degradation (Bonifacio *et al*., 2014). Furthermore, these submicron particles have relatively high stability (long shelf life) and can encapsulate both hydrophobic and hydrophilic drugs (Gelperina *et al.,* 2005). NPs not only effectively shield drugs from enzymatic degradation, extending their lifespan but have also been shown to be biocompatible and biodegradable. They can induce controlled and sustained release of encapsulated cargo and improve site-specificity in turn and improve the side effect profiles of the encapsulated drugs (Mohanraj and Chen 2007, Wilczewska *et al.,* 2012; Gu *et al.,* 2013). NPs are more effectively uptaken by cells such as macrophages, primary inflammatory mediators in OA, than microparticles. This cellular uptake can result in the phenotypic reprogramming of macrophages from the M1 subtype to the M2 subtype, triggering an anti-inflammatory response in OA (Gambaro *et al.,* 2021).

There are various nanocarriers, which are made from different types of biomaterials and therefore offer a variety of properties, including size, morphology, and functionalities (Wang and Wang, 2014). In describing the hierarchical pore structure within cartilage, DiDomenico *et al*. (2018) mentioned that it has a gap ranging from 4 to 6 nm between glycosaminoglycan chains and from 50 to 100 nm gap between collagen fibers. Therefore, particles with a size equal to or less than 100 nm would be ideal for penetration (Rothenfluh *et al*., 2008; Sophia *et al.,* 2009; DiDomenico *et al*., 2018). On the other hand, the entry of macromolecules and larger-sized NPs can be challenging (Sophia *et al.,* 2009). However, larger molecules (MW up to 500 kDa) have been shown to diffuse through the dense cartilage matrix, although the transport mechanism is still unclear due to the unsolved complex structure of articular cartilage (DiDomenico *et al*., 2018). Either way, unlike with microparticles, the relatively small size of NPs allows their easy penetration through the dense matrix of the ECM to reach target sites, which can potentially improve their retention time and chondro-regeneration for those that possess such properties. Apart from size, the surface charge is also an important factor as the ECM is negatively charged; cationic NPs have the potential to improve the cellular uptake of negatively charged drugs (Honary and ZAhir, 2013). Importantly, the electrostatic interactions between cationic NPs and ECM increase the retention of the drug (Lei *et al*., 2022).

Forming electrostatic forces with endogenous HA, a negatively charged molecule, Bajpayee and co-workers (2014) showed that NeutrAvidin, the neutral counterpart of Avidin, exhibited a 400-fold lower absorption than Avidin (a highly cationic protein). Furthermore, cartilage explants retained >90% of the absorbed Avidin for at least 15 d (Bajpayee *et al*., 2014). As a result, cationic molecules have shown higher uptake and faster penetration as well as prolonged release profiles and retention times compared to their neutral and anionic

counterparts (Vedadghavami *et al*., 2020). However, this can lead to excess accumulation of the cationic NPs leading to cytotoxicity through cell membrane disruption and ultimate cellular death (Guo *et al*., 2024).

In general, NPs as carriers can be used to improve the pharmacokinetic profiles of drugs for IA administration into the joint space. Interestingly, their size is well suited to evade the dense network of the ECM, allowing drugs to reach the site of action at required therapeutic concentrations and possibly extend their retention times. Different types of nanosystems, including micelles, liposomes, polymeric and lipidic NPs, exosomes, and inorganic NPs (Figure 2.7), have been previously studied for application in the treatment of OA and further discussed below and summarized in Table 2.1.

Table 2.1. Summary of recent (2019-2024) advances in OA drug delivery systems with potential IA application.

Type of NPs	Components	Bioactive	Observed biological activities	Reference
Micelles	ACP micelles	Curcumin	• Reduction in the concentrations of ROS in the RAW264.7 cells and in levels of TNF-α and IL-1β in OA mice models. This leads to reduced inflammation both *in vivo* and *in intro.*	Kang *et al.*,2020
	sPLA2 inhibitor-loaded micellar NPs	Thioetheramide-PC	• Prolonged retention of thioetheramide-PC in the joint space of OA mice. • Decreased concentration of ECM degrading MMP-13, and ADAMTS-5 *in-vitro* in OA mouse cartilage explants lead to inhibition of cartilage degradation. • Increased expression of COL2A1 and ACAN in OA mouse cartilage explants promoting cartilage regeneration.	Wei *et al*., 2021
Liposomes	HA-Lipo-DIC/DEX	Dexamethasone and Diclofenac	• The *in vitro* cytotoxicity profile of HA-Lipo-DIC/DEX was superior to that of free DIC/DEX in SW 1353 chondrocytes. • HA-Lipo-DIC/DEX showed visibly reduced inflammation on the front paws of mice more effectively than free DIC and DEX	Chang *et al*., 2021
	DEX-loaded liposomes	DEX	• Improved from 24 to 72 h showing sustained release. • *In vivo* macrophage repolarization reduced pro-inflammatory cytokines	Teng *et al*., 2023

			TNF-α, IL-1β, and IL-6 levels in OA mice models. • Enhanced *in vivo* expression of anti-inflammatory cytokine IL-10 in OA mice models.	
	Lipo-RvD1	Resolvin D1	• Improved retention of Resolvin D1 in the joint cavity of mice for 11 d. • M1-to-M2 polarization of macrophages resulting in: ➢ Reduced synovitis as a result of M2 macrophage infiltration in chondrocytes. ➢ Suppression of ADAMTS-5 and MMP-13 suggesting blockage of cartilage degradation in chondrocytes of OA mice models. ➢ Suppression of the formation of the osteophytes, thus slowing OA progression *in vivo*.	Dravid *et al.,* 2023
	Triamcinolone acetonide-liposomes	Triamcinolone acetonide	• Retention for 28 d in joint cavity • Macrophage polarization from M1 to M2 • Decrease in pro-inflammatory cytokines, chemokines, and matrix-degrading proteins: ➢ TNF-α, IL-1β, and IL-6,	Deng *et al*., 2023

			➢ Chemokine (C-X-C motif) ligand 2 and chemokine (C-C motif) ligand 2 ➢ MMP-1, MMP-3, MMP-13, ADAMTS-3, and ADAMTS-14	
Polymeric NPs	Self-assembled polymeric NPs	Triamcinolone acetonide	• *In vivo* inhibition of MMP-3 and MMP-13 expression: ➢ inhibition of pro-inflammatory cytokines IL-6, TNF-α ➢ promotion of anti-inflammatory cytokines IL-4, IL-10, and IL-13	Seo *et al.,* 2021
	Berberine Opsonized NPs	Berberine	• Improved berberine release profile • Effective reduction of the mRNA expression of iNOS, TNF-α, IL-1β, and IL-6 • Effective promotion of anti-inflammatory mediators IL-10 and Arg-1 compared to the untreated control and LPS stimulation group • The M1 to M2 polarization signaled by A significant increase in the Arg-1 of the macrophages occurred	Kou *et al.*, 2022
	PLGA-PEG-PLGA	ETX	• Higher expression of COL2A and ACAN in the ETXNPs group of isolated human OA chondrocytes. • A decline in the expression of MMP-13 and ADAMTS-5 in the ETXNPs group of isolated human OA chondrocytes.	Liu *et al.,*2019

Rh-PLGA-NPs@NH_4	Rhein	• Sustained release of Rhein for over 20 d. • Significant reduction of pro-inflammatory markers ROS and IL-1 in human chronic myeloid leukaemia cell lines like THP-1 leading to reduced inflammation in OA. • Slight decrease in levels of pro-inflammatory cytokine TNF-α in the THP-1 cell line.	Hu *et al*., 2020
PDA NPs	Polydopamine	• Reduced *in vitro* chondrocyte apoptosis • Reduced levels of ROS, a mediator for cartilage degradation. • Elevation of the levels of proteoglycan suggesting ECM regeneration. • Inhibition of subchondral bone remodeling in OA rat models.	Wang *et al*., 2021
Carboxymethyl chitosan-assisted MnOx	Carboxymethyl	• Increased expression of ACAN and COL2A1 promoting chondrogenesis in chondro-induced BMSCs. • Decreased expression of MMP-13 suggesting decreased cartilage degeneration in OA rats.	Lin *et al*., 2022
Rebamipide-loaded NPs	Rebamipide	• In vitro and in vivo dose-dependent reduction in the mRNA levels of MMP-3 and MMP-13 and pro-inflammatory cytokines IL-1β, IL-6 and TNF-α	Kim *et al.,* 2022

			• Reduction of pro-inflammatory mediator cyclo-oxygenase-2. • Attenuated cartilage degeneration better than the pure rebamipide solution	
	HA-NPs	HA	• Resistance to digestion by hyaluronidase • Reduced PGE_2 production • HA-NPs outperformed free high molecular weight HA	Kang *et al*., 2021
	Superoxide dismutase polymersomes	Superoxide dismutase	• Prolonged retention of superoxide dismutase in mouse joint ➢ Accumulation occurred in the synovium rather than the articular cartilage	Gui *et al.,* 2022
Inorganic NPs	Gold NPS	Gold	• Reduced concentrations of pro-inflammatory cytokines • Enhanced levels of: ➢ liver and kidney indices ➢ oxidative stress markers	Abdel-Aziz *et al.,* 2021
	Triamcinolone-gold NPs	Triamcinolone	• Superior expression of anti-inflammatory cytokines IL-10, IL-4, and Arg-1 in fibroblast-like synoviocytes. • Reduced expression of pro-inflammatory cytokines TNF-α, IL-1-β, IL-6, MMP-1, and matrix degrading protein MMP-3 in fibroblast-like synoviocytes.	Park *et a*l. 2020
	PEG-MnO_2 NPs	MnO_2	• Decreased levels of matrix-degrading entities NOS, MMP-1, MMP-13, and ADAMTS-5 in chondrocytes	Kumar *et al*., 2019

			• Retention for 7 d in the joint cavity of OA rat models.	
	TP-Au@PCN	Tea polyphenol	• Effective repair of cartilage-damaged mitochondria and promoted cartilage regeneration in chondrocytes: ➢ TP-Au@PCN showed a significant reduction in levels of ROS compared to pristine tea polyphenol. ➢ MMP-13 was reduced significantly in chondrocytes treated with TP-Au@PCN compared to other treatment groups. ➢ . TP-Au@PCN significantly increased the expression of COL2 and SOX9 in chondrocytes.	Xu *et al.,* 2023
Microspheres	(sPL)-loaded PLGA/chitosan/gelatin microspheres	Growth factors: IGF, TGF, and VEGF	• Elevation of COL2A1, ACAN, and SOX9 promoting cartilage proliferation. • Reduced number of osteophytes and subsequent reduction of OA progression of in rat models. • Cartilage regeneration presented by smoothened cartilage surfaces and increased integrity of cartilage.	Li *et al.,* 2021
Microplates	DEX-loaded microplates	DEX	• Inhibition of pro-inflammatory cytokines IL-1β, IL-6, and TNF-α in ATCD5 chondrocytes. • Inhibition of pro-inflammatory cytokines IL-1β, IL-6, and TNF-α in conjunction with matrix degrading protein MMP-13 in over-load induced mice.	Di Francesco *et al,* 2021

2.4.1. Micelles

Micelles are amphiphilic nanostructures composed of a hydrophobic core and a hydrophilic shell, typically ranging between 10 and 200 nm in size (Owen *et al*., 2012). Accordingly, this structural composition allows for the encapsulation of hydrophobic drugs in the lipophilic core, while hydrophilic drugs are bound to the hydrophilic shell (Ghezzi *et al.,* 2021). This means that, unlike most types of NPs, micelles can carry a variety of types of cargo, making them advantageous for OA therapy. Given their low critical micelle concentration, polymeric micelles are more stable and enforce controlled and sustained drug release (Jones and Leroux, 1999). Nevertheless, the application of micelles is limited because of their toxicity, dependence on critical micelle concentration, poor uptake by cells, loading efficiency, and stability (Kim *et al*., 2010).

In an effort to harness the benefits of micelles, Wei *et al.* (2021) employed cationic secretory phospholipase A2 inhibitor (thioether amide-PC)-loaded micellar NPs ($sPLA_2i$-NPs) for an IA injection in OA mouse models. Their findings showed a significant decrease in overall OA progression, whereby articular cartilage degeneration was attenuated. Comparatively, groups treated with $sPLA_2i$ showed increased subchondral bone plate sclerosis and osteophyte formation, effects that were not observed in the $sPLA_2i$-NPs group. This indicates the attenuation of late-stage OA by $sPLA_2i$-NPs compared to free $sPLA_2i$. In comparison to free secretory phospholipase A2 inhibitor, the phenotype and integrity of the articular cartilage improved whereby the cartilage surface was almost completely intact with no proteoglycan loss for up to 4 months following the NP-based drug injection in surgically induced OA mice (Wei *et al*., 2021). Given the current challenges in achieving complete cartilage regeneration, these results highlight the potential of micellar systems for long-term OA management (Wei *et al*., 2021).

Curcumin, the main active component of turmeric, has been reported to have favourable therapeutic properties, such as potent antioxidant and anti-inflammation activities, for the treatment of OA (Tanvir *et al*., 2017; Peng *et al.,* 2021). Despite its potential, the effectiveness of curcumin is hampered by its low retention, rapid metabolism, poor absorption, and low water solubility (Tabanelli *et al.,* 2021). As a result, the potential of polymeric micelles to overcome these drawbacks was explored by developing an acid-activatable curcumin polymer, an anti-inflammatory polymeric prodrug of curcumin (ACP) (Kang *et al*., 2020). Interestingly, polymeric prodrugs have been shown to retain approximately 60% of the drug as the polymers degrade, which helps with the sustained release of the drug (Luliński, 2017).

In this study, ACP could self-assemble into micelles under aqueous conditions and disassemble under acidic conditions which would allow for a targeted release triggered by changes in pH found in synovial joints of osteoarthritic joints. Previous work has stated that the pH of synovial joints of osteoarthritic joints can be weakly acidic because of the resulting inflammation (Xiong *et al*., 2020), though conflicting reports indicate no significant pH differences between normal and osteoarthritic joints (Gerwin *et al*., 2006; Milošev *et al.*, 2017). The ACP micelles displayed an increase in size in the acidic conditions, further illustrating their dependence on pH as a result of protonated tertiary amine groups in the ACP's backbone. The release profiles at different pHs showed that in acidic conditions (pH 6.0), the ACP micelles released four times more drug in 7 d than at physiological pH (7.4) conditions.

Biological studies showed that ACP micelles demonstrated better viability against RAW 264.7 cells compared to free curcumin at equivalent concentrations making them more biocompatible. Although curcumin could suppress the ROS production independently, it was more effective than the ACP micelle. The study further showed that ACP micelles reduced the pro-inflammatory markers TNF-α and IL-1β levels better than the free curcumin suggesting an improvement in biological activity. More interestingly, the NPs did not show any toxicity to chondrocytes (Kang *et al*., 2020).

2.4.2. Liposomes

Liposomes, typically formed with phospholipids, are spherical lipid vesicles with at least one lipid bilayer that surrounds an aqueous center (Pande, 2023). Since they have both hydrophobic and hydrophilic moieties, liposomes can encapsulate both hydrophobic and hydrophilic drugs (Sercombe *et al*., 2015). For example, hydrophilic DIC sodium and hydrophobic DEX can be co-encapsulated in the same liposomal system with high entrapments (Chang *et al*. 2021). Liposomes fuse with the cell membrane at the site of inflammation to release the payload (Liu *et al*., 2021). This unique ability is useful for targeted drug delivery as it would enhance the efficiency of drug delivery in OA joints. Although liposomes are good carriers, they have drawbacks, such as leakage of cargo and short shelf life. This means that they cannot be used for chronic diseases as they degrade quickly, and the leakage of drugs would not be sustainable. Liposomes and other lipid-based NPs can also be exploited as potential lubricants as a result of phospholipids present within thus reducing bone-to-bone friction in OA.

In a study, Chang *et al*. (2021) developed hyaluronan-loaded liposomal dexamethasone–diclofenac NPs (HA-Lipo-DIC/DEX) with HA of MW from 130,000–150,000 to target OA intra-articularly. DIC is an NSAID that is generally viewed as an alternative to DEX, a glucocorticoid, for the anti-inflammatory effects in OA (Alsaif *et al*., 2021;). The liposomes, of ~103nm,

displayed an impressive DIC and DEX entrapment efficiency (EE) of 90.5 ± 5.6% and 94.7 ± 2.4%, respectively. *In vitro* studies exhibited sustained release of DIC and DEX over 160 h. Importantly, HA-Lipo-DIC/DEX demonstrated superior chondrocyte cell survival rates (93.65 ± 3.77%) compared to free DIC/DEX-treated groups (65.48 ± 4.01%) at 24 h with equivalent concentrations. This nanosystem displayed continued cell viability for 72 h, exhibiting improved biocompatibility compared to that of the combination of the free drugs. The *in vivo* studies on mice further validated the HA-Lipo-DIC/DEX nanosystem's anti-inflammatory effects by significantly reducing OA-induced inflammation better than free DIC and DEX on the paws of mice (Figure 2.2) (Chang *et al*., 2021).

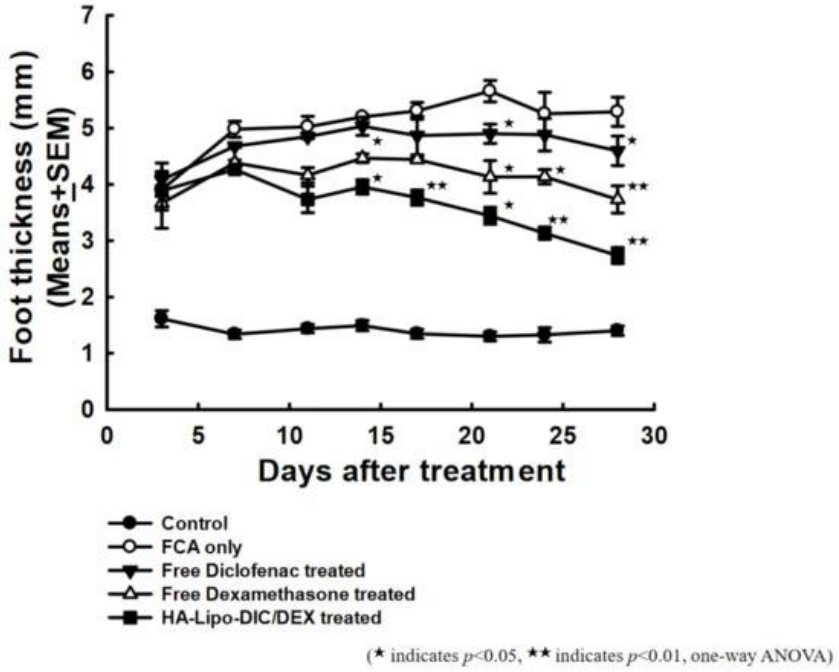


Figure 2.2. Effects of HA-Lipo-DIC/DEX in suppressing OA in the paws of mice (adapted from an open access article; Chang et al., Copyright @ 2021 Adapted under a Creative Commons Attribution (CC BY)).

In another study, Teng *et al*. (2023) conducted a study on DEX-loaded liposomes on OA (Figure 2.3A). The *in vitro* drug release profile of the DEX-loaded liposomes showed sustained release whereby 80% of free DEX was released within 24 h; it improved to 72 h in the DEX-loaded liposomes. Immunofluorescent staining of DEX-loaded liposomes showed a prominent decrease in expression of CD86, an M1 macrophage marker, compared to that of cells treated with free DEX. Notably, there was an increase in the expression of M2 macrophages (Figure 2.3B). This supports a phenotypic change from M1 to M2 macrophages, which promoted anti-inflammatory activity in mice. This was corroborated by the quantification of pro- and anti-inflammatory cytokines, where the DEX-loaded liposomes reduced TNF-α and IL-1β levels better than free DEX while IL-6 levels were similar in both treatment groups, and the expression of anti-inflammatory cytokine IL-10 was improved after treatment of the mice with

DEX-loaded liposomes compared to free DEX. This indicated that the DEX-liposome could suppress OA inflammation better than free DEX and, therefore, ameliorate OA more efficiently (Teng *et al.,* 2023).

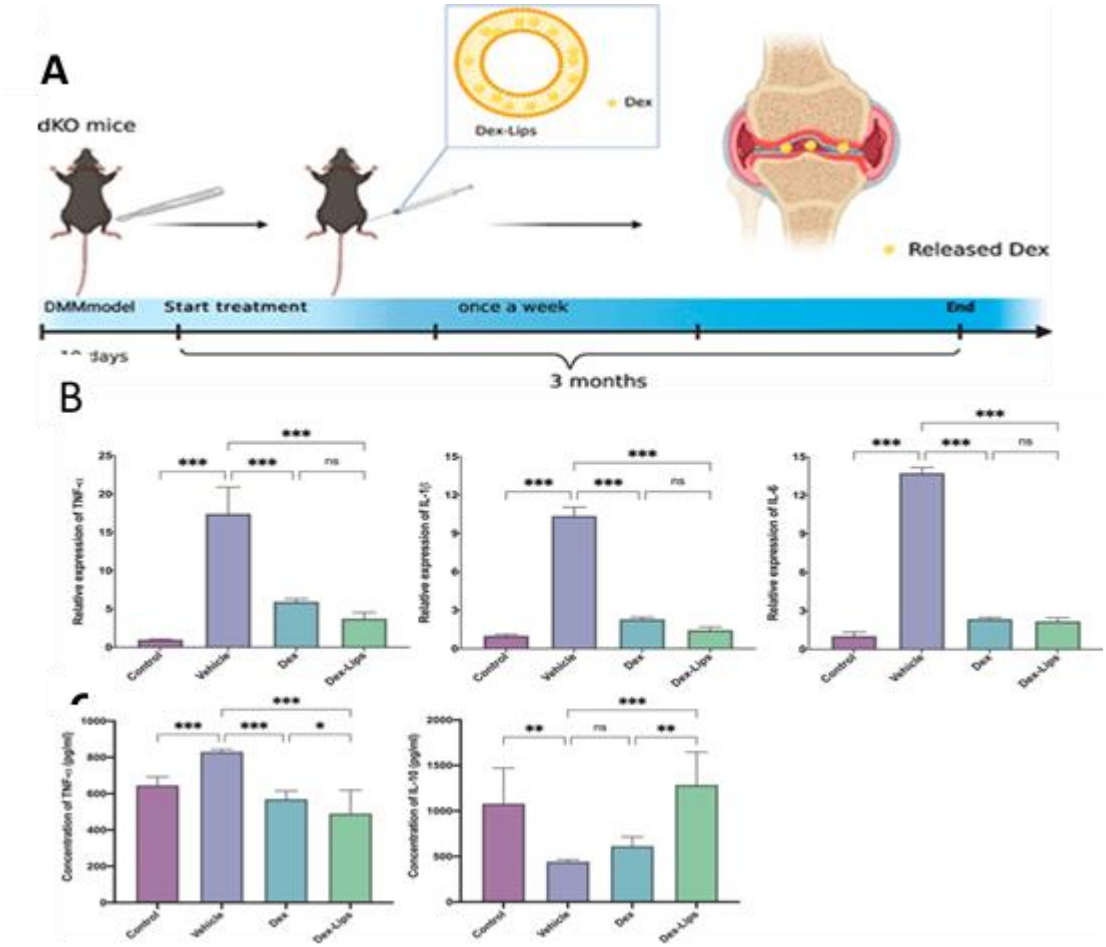


Figure 2.3. Effects of DEX-Liposomes on expression levels of (A) TNF-α, IL-1β, and IL-6 in the femoral head and the (B) Concentrations of TNF-α and IL-10 in the serum, reprinted from Teng *et al*., Copyright © 2023. Reproduced with permission from The Journal of the American Chemical Society.

Since small molecules are rapidly cleared by the lymphatic system thus mandating repeated IA administrations/injections (Rabei *et al*., 2021). Dravid *et al* (2023) encapsulated Resolvin D1 (RvD1) into liposomes, forming a Lipo-RvD1 formulation to achieve sustained release of RvD1. This formulation attained prolonged release of RvD1 for ~11 d with close to 10% of the drug still available at that endpoint. Lipo-RvD1 promoted the M2-type polarization of macrophages in the synovium which exerts anti-inflammatory effects. Lipo-RvD1 also reduced the levels of pro-inflammatory M1 cells more effectively as compared to free RvD1 joints. Since M1 macrophages are a major source of pro-inflammatory cytokines which contribute to cartilage damage, their reduction suggests that inflammation and cartilage damage were mitigated in the treated mice. Additionally, Lipo-RvD1 reduced synovitis, a hallmark of OA, by

preventing the infiltration of leukocytes into the inflammatory milieu in obese mice (Dravid *et al.,* 2023).

Similarly, Deng *et al*. (2023) targeted synovial macrophages and fibroblasts to attenuate OA (Deng *et al*. 2023). In this effort, triamcinolone acetonide was encapsulated into apoptotic neutrophil membrane-camouflaged liposomes and administered intra-articularly to rodents. Findings reveal that the liposomes were successfully retained in the joint cavity for 28 d while facilitating the effective repolarization of M1-type macrophages to the M2 phenotype. Free triamcinolone acetonide demonstrated moderate downregulation of M1-related pro-inflammatory cytokines (TNF-α, IL-1β, IL-6, and iNOS) in RAW 264.7 cells. The macrophage repolarization was proven by upregulation of the genes of M2 macrophage markers such as CCAAT/enhancer-binding protein beta and suppressor of cytokine signaling 2.

Upon induction, pro-inflammatory M1-type macrophages secrete pro-inflammatory cytokines including IL-12, IL-6, IL-1β and TNF-α. Conversely, M2-type macrophages secrete IL-4 and IL-10 which exert anti-inflammatory effects (Mushenkova *et al*., 2022). There was a marked decrease in TNF-α, IL-1β, and IL-6 levels, alongside reduced expression of chemokines CXCL2 and CCL2. Moreover, the genes encoding ECM-degrading proteins such as MMP-1, MMP-3, MMP-13, ADAMTS-3, and ADAMTS-14 were also significantly downregulated in OA joints compared to the control group. Dissimilarly, genes associated with M2-type macrophages were upregulated, supporting the presence of decreased inflammation in triamcinolone acetonide liposome-treated rodents compared to the free triamcinolone acetonide. This suggested that the triamcinolone acetonide liposomes had a better inflammation inhibitory effect compared to free triamcinolone acetonide (Deng *et al*., 2023).

2.4.3. Polymeric NPs

Polymeric NPs (PNPs) are solid NPs with a size of 10-1000 nm synthesized from biocompatible and biodegradable synthetic and natural polymers (Zielińska *et al*., 2020). PNPs with smaller sizes can be efficiently delivered through the tightly wound ECM making them particularly suitable for IA delivery in OA joints. Synthetic polymers include poly (lactide) (PLA), poly (lactide-co-glycolide) copolymers (PLGA), poly (ε-caprolactone) (PCL) and natural polymers including albumin, chitosan, alginate, and gelatin. As a result of their biocompatibility and biodegradability, PNPs reduce the risk of accumulation in OA joints, mitigating possible adverse reactions such as toxicity. There are two types of PNPs, namely nanocapsules and nanospheres (Gagliardi *et al*., 2018, Palma *et al.,* 2018). Encapsulated drugs are uniformly dispersed within the polymer matrix of nanospheres, within a reservoir core, or bound to the inner surface of nanocapsules (Jin, 2020). This enables the efficient delivery of a variety of therapeutics, including hydrophilic and hydrophobic drugs and compounds of varying

molecular weights, such as proteins and small molecules directly to the affected joint cavity, improving efficacy and reducing systemic side effects (Wang and Wang, 2014).

Targeted therapy can be advanced further through functionalization of the surface of PNPs by adding specific ligands which are compatible with inflamed tissue or cartilage, enhancing specificity thus minimizing off-target adverse effects (Wen *et al*., 2023). An example is how Seo *et al,* 2021 encapsulated triamcinolone acetonide into self-assembled polymeric NPs through the interaction between the hydrophobic core of the polymer-poly(organophosphazene) with hydrophobic parts of the TCA to induce chronic anti-inflammatory modulation in OA (Seo *et al.,* 2022). A one-time injection of the NPs exhibited improved inflammation profiles with *in vivo* promotion of the expression of IL-4, IL-10, and IL-13 and the suppression of IL-6, TNF-α MMP-3 & 13 expression (Seo *et al*., 2022). This repolarization mechanism effectively mitigates inflammation in macrophages and synoviocytes by suppressing pro-inflammatory responses while amplifying anti-inflammatory signaling pathways (Yuan *et al.,* 2024).

Kou *et al* investigated a similar approach by encapsulating berberine, an anti-inflammatory agent, within opsonized NPs made from a bilirubin grafted polylysine biomaterial (oxidant-responsive) and a layer of immunoglobulin IgG (IgG/Bb@BRPL) (Kou *et al*., 2022). The system prolonged the release of berberine, whereby free berberine was completely released after approximately 50 h; at the same period, only a maximum of approximately 57% of berberine was released from the system. Although free berberine and the blank NPs both exerted had an anti-inflammatory effect on macrophages, the nanotherapeutic system loaded with berberine reduced the mRNA expression of iNOS, TNF-α, IL-1β, and IL-6 and promoted IL-10 and Arg-1 more effectively compared to the control groups but similar to that of free berberine (Figure 2.4 A-F). It is possible that polylysine and berberine exerted a synergistic anti-inflammatory effect. A significant increase in the Arg-1 signals and the diminished fluorescence of CD86 staining confirmed that macrophage polarization had occurred which signified an anti-inflammatory response thus attenuating OA (Figure 2.4 L).

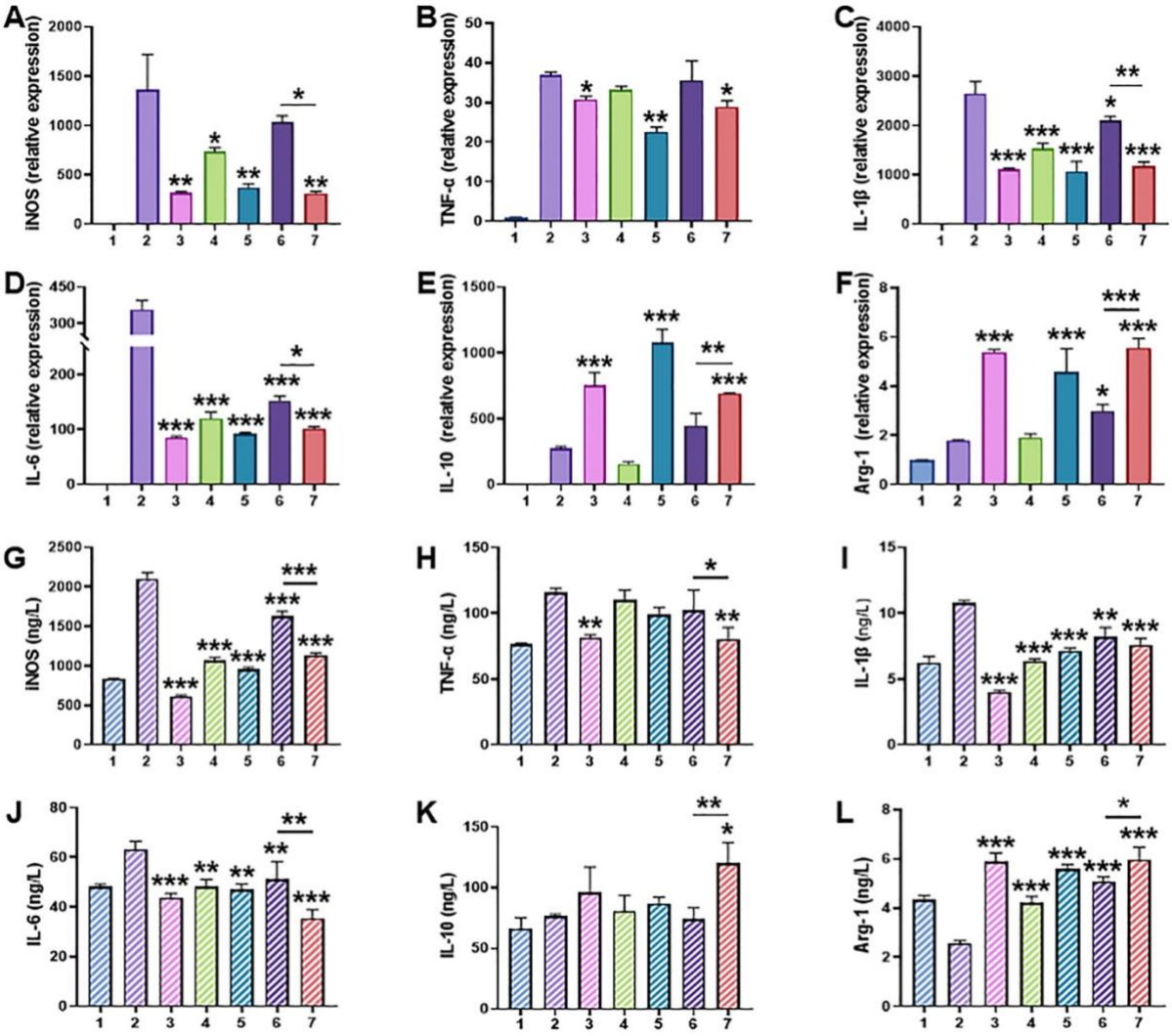


Figure 2.4. *In vitro* In vitro assessment of the anti-inflammatory effects of IgG/Bb@BRPL. The experimental groups include untreated RAW 264.7 macrophage cells (column 1), LPS-stimulated cells (column 2), free Bb treatment (column 3), BRPL treatment (column 4), Bb@BRPL treatment (column 5), BSA/Bb@BRPL treatment (column 6), and IgG/Bb@BRPL treatment (column 7) (Kou et al., 2022). Adapted with permission from Elsevier.

Liu and colleagues (2019), encapsulated etoricoxib (ETX), a COX-2 selective NSAID, in PLGA and polyethylene glycol (PEG) (PLGA-PEG-PLGA) triblock copolymeric NPs for application in the treatment of OA. The ETX release kinetics indicated that there was a burst release of ETX within the first 3 d but showed sustained release over approximately 30 d (Liu *et al.,* 2019). The cell viability study demonstrated high biocompatibility of ETX-loaded NPs towards chondrocytes (Liu *et al.,* 2019). The study revealed a higher expression of COL2 and ACAN in the ETX-loaded NPs group in comparison to the free ETX groups. This suggested that the integrity of the matrix in the chondrocytes improved, and therefore, the ETX-loaded NPs attenuated OA. Additionally, the expression of ECM-degrading enzymes MMP-13 and ADAMTS-5 in the ETX-loaded NPs group was more suppressed in comparison to the free ETX group. This indicated that the ETX-loaded NPs could inhibit the activity of ECM degrading

enzymes, hence maintaining the cartilage integrity. The mice treated with ETX-loaded NPs also showed superior osteochondral interface compared to the free ETX-treated subjects, supporting cartilage regeneration as a result of ETX-loaded NPs (Liu *et al.,* 2019).

Hu *et al.* (2020) used Rhein (Rh), an anti-inflammatory drug, to develop pH-sensitive Rh and ammonium bicarbonate (NH_4HCO_3) laden PLGA NPs (Rh-PLGA-NPs@NH_4). An improved Rh release profile was observed in a synovial fluid environment with lower pHs. Rh-PLGA-NPs@NH_4 showed more sustained release in a simulated synovial fluid environment than in a buffer with pH 7.4 and pH 5. and a more rapid release in a Notably, the Rh-PLGA-NPs@NH_4 improved the release profile kinetics of Rh from 1 d to 30 d (Figure 2.5). There was a significant reduction of OA markers ROS and IL-1 and a slight decline in the concentrations of TNF-α. Interestingly, the toxicity study revealed an increase in cytotoxicity that was directly proportional to the concentration of Rh. However, Rh-PLGA-NPs@NH_4 exerted a higher toxicity than Rh-PLGA-NPs, as a result of the addition of NH_4 (Hu *et al*., 2020).

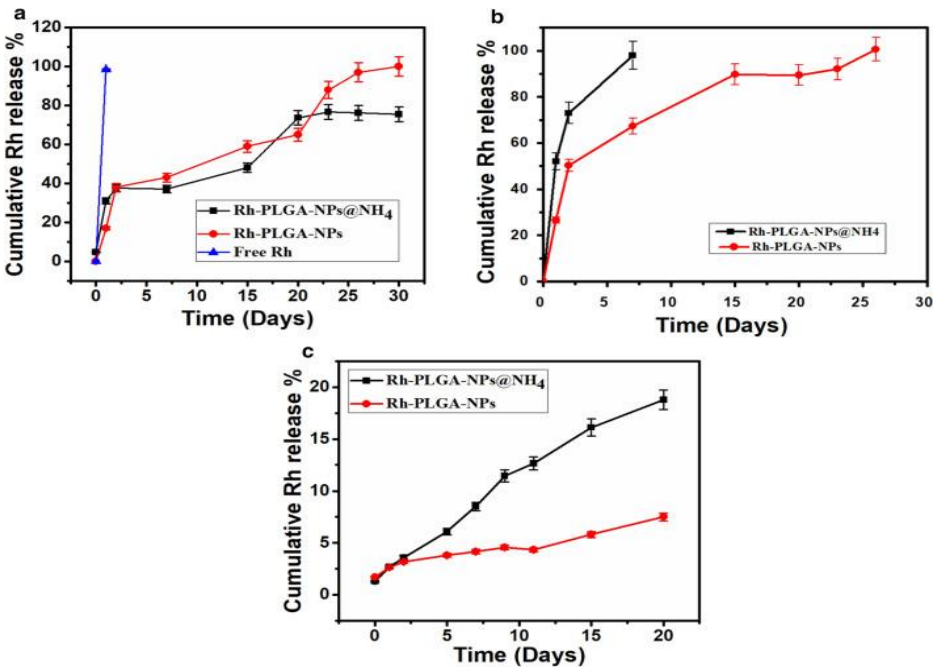


Figure 2.5. *In vitro* release profile of Rh from Rh-PLGA-NPs@NH4 under different conditions: (A) phosphate buffer at pH 7.4, (B) phosphate buffer at pH 5.4, and (C) simulated fluid environment (SFE). Figure adapted from Hu et al. (2020) and distributed under the terms of the Creative Commons CC BY license).

In a different study, Wang and colleagues (2021) introduced a polydopamine NPs (PDA NPs) antioxidative/anti-inflammatory dual task nanoplatform to treat OA. The PDA NPs acted as a dual task platform by serving as reducing agents directly scavenging ROS and by regulating ROS generation in mitochondria resulting in antioxidant and anti-inflammatory effects. The treatment exhibited excellent biocompatibility of PDA NPs at low doses and lower incubation periods and reduced chondroptosis (53.72%) and intracellular ROS levels compared to the

lipopolysaccharide group. This suggested that the PDA NPs had a potent *in vitro* chondroprotection effect against lipopolysaccharide-induced chondrocyte apoptosis. *In vivo*, studies showed increased levels of proteoglycans and effects against subchondral bone remodeling, and which are typically decreased during OA and result in matrix degradation, and this supported the alleviation of OA (Wang *et al*., 2021).

Lin and co-workers (2022) assessed the potential of carboxymethyl chitosan-assisted manganese oxide NPs (WY-CMC-MnOx NPs) in early OA management. Having shown good viability of the tested MC3T3-E1 and L929 cells, the WY-CMC-MnOx NPs elevated the expressions of ACAN better than the carboxymethyl chitosan group by upregulating SRY-box transcription factor 9 (SOX9), a pivotal transcription factor in the synthesis of the ECM of cartilage (Lefebvre *et al*., 2019). Therefore, these NPs could further promote the *in vitro* synthesis of cartilage ECM. Furthermore, the WY-CMC-MnOx NPs also induced a superior mRNA expression of ACAN and COL2 in comparison to the pristine carboxymethyl chitosan, suggesting that the NPs had a better impact on attenuation of OA. (Lin *et al*., 2022).

PLGA NPs have emerged as promising vehicles in the targeted delivery of small molecules for treating OA. Kim and colleagues (2022) entrapped rebamipide in NPs that were synthesized by using a blend of polymers - PLGA and methoxy poly(ethylene glycol)-b-poly(D,l-lactide) (mPEG-PDLLA) to attenuate joint cartilage destruction and progression of OA in rat models (Kim *et al., 2022)*. Rebamipide, an amino acid analogue of 2 (1H)-quinolinone, possesses antioxidant effects that can help combat oxidative stress and inflammation, key factors recognized in the development and progression of OA (Kudur *et al.,* 2013). *In vitro* and *in vivo* results showed a dose-dependent reduction in the mRNA levels of MMP-3 & 13 and pro-inflammatory mediators IL-1β, IL-6, and TNF-α and COX-2. Moreover, macroscopic, radiographic, and histological evaluations confirmed that IA injections of rebamipide-NPs effectively prevented cartilage degradation more than the pure rebamipide solution. This indicates that the rebamipide-NPs improved the inflammatory response while simultaneously decreasing joint degradation and OA progression (Kim *et al., 2022)*.

It has been well established that endogenous concentrations and distribution of HA in OA decrease as OA progresses (Altman *et al*., 2015). In response, Kang and colleagues (2021) used self-assembling HA-based NPs (HA-NPs) with HA with MW of 10 000 Da to combat cartilage degradation in OA. HA-NPs demonstrated resistance to hyaluronidase-mediated degradation and exhibited prolonged retention within the knee joint. Additionally, they inhibited IL-1β and CD44-induced NF-κB activation, leading to reduced collagenase activity and prostaglandin E2 (PGE2) production. Since PGE2 is highly secreted in the subchondral bone of OA patients and promotes OA progression through osteoclast-induced angiogenesis (Sun

et al., 2022). Intriguingly, HA-NPs showed better protection against OA than free high MW HA, a current treatment option of OA. Given the data, HA-NPs provided *in vitro* and *in vivo* protection against CD44-mediated cartilage destruction (Kang *et al*., 2021).

Although not extensively researched in OA therapy, polymeric systems such as polymersomes have shown great promise in OA therapy showing prolonged retention time compared to phospholipid liposomes. This property is essential because OA treatment is usually not retained in the joint for a sustained period, creating a need for repeated injections resulting in poor patient compliance. In an investigation by Gui *et al* (2022), polymersomes were used to deliver exogenous superoxide dismutase, the major catalytic antioxidant in joint tissues whose delivery is hindered by factors such as low retention and rapid degradation. Superoxide dismutase scavenges ROS by catalyzing the conversion of superoxide radicals to hydrogen peroxide. The Superoxide dismutase-NPs exhibited prolonged retention in mouse joints, with the majority of the system accumulating in the synovium rather than the articular cartilage, thus effectively targeting the disease. The porous nature allowed for improved intrinsic membrane permeability, allowing the superoxide dismutase to penetrate the joint tissues and have full access to ROS once delivered. The study demonstrated that the porous superoxide dismutase polymersomes were more efficient than free superoxide dismutase in the treatment of OA (Gui *et al.,* 2022).

PNPs have emerged as a promising therapeutic strategy for the treatment of OA. Their ability to deliver drugs in a targeted and controlled manner directly to the affected joint enhances therapeutic efficacy while minimizing off-target side effects.

2.4.4. Inorganic Nanoparticles (INPs)

INPs are composed of inorganic materials such as metals and carbon compounds. INPs exhibit high biocompatibility and good stability; however, concerns regarding their potential toxicity and poor solubility persist (Wen *et al*., 2023). Common types of INPs include superparamagnetic iron oxide NPs (SPIONs), metal NPs, carbon fibers, and mesoporous silica NPs (Slowing *et al.,* 2007).

Some INPs have shown anti-osteoarthritic activitiy (Sarkar *et al*., 2019; Abdel-Aziz *et al*., 2021), potentially enhancing delivery of OA treatment through synergistic mechanisms. For example, gold NPs (GNPs) possess antioxidant activities and have been shown to suppress IL-1β, PGE_2, and COX-2, which have been proven to contribute to the etiology of OA (Sarkar *et al.,* 2019). Abdel-Aziz *et al* (2021) showed that the combined treatment of Diacerein® (anthraquinone IL-1 inhibitor-Rhein) and GNPs improved levels of cytokines, kidney and liver function markers as well as oxidative stress markers associated with OA better than either

treatment alone. Diacerein® is an anti-OA drug possessing anti-inflammatory, and anabolic properties on cartilage and subchondral bone (Pavelka *et al.,* 2016).

In their study, untreated OA rats showed a notable rise in renal and hepatic indices (Alanine Aminotransferase, Aspartate Aminotransferase, Alkaline Phosphatase, creatinine, and urea). While the administration of Diacerein® and GNPs individually led to a reduction in all these markers in healthy rats, GNPs alone significantly increased hepatic and renal markers in OA rats. However, the combined treatment of Diacerein® and GNPs (Diacerein®-GNPs) proved more effective than individual treatments, significantly improving hepatic and renal oxidative stress markers (superoxide dismutase, malondialdehyde, and glutathione peroxidase). A significant decrease in inflammatory cytokines (IL-1β, IL-6, and TNF-α) was observed in rats that received Diacerein®-GNPs compared with the untreated group. The combination therapy (Diacerein®-GNPs) proved more effective than either treatment alone, demonstrating superior anti-inflammatory and subchondral bone-protective effects s (Abdel-Aziz *et al.,* 2021).

Taking this further into OA drug delivery application, Park *et al*. (2020) synthesized triamcinolone-loaded GNPs for IA delivery of OA. The triamcinolone-loaded GNPs elicited greater levels of anti-inflammatory cytokines (IL-10 and IL-4) and arginase 1 in synoviocytes accompanied by a reduction of pro-inflammatory cytokines (TNF-α, IL-1-β, and IL-6) and ECM degenerating enzymes (MMP-1, and MMP-3). Unlike free triamcinolone, which failed to elicit an anti-inflammatory response or induce macrophage repolarization, the triamcinolone-loaded GNPs formulation effectively mitigated OA progression by reducing inflammation and inhibiting cartilage degradation (Park *et al*. 2020).

Despite their potential, GNPs present safety concerns. Zhang *et al.* (2014) reported that exposure to GNPs in osteoblasts led to elevated Alkaline Phosphatase levels, which are already heightened in OA. Although not directly linked to the disease, elevated Alkaline Phosphatase contributes to bone remodeling, potentially exacerbating OA progression (Zhang *et al.,* 2014).

Following articular damage, the occurrence and accumulation of oxidative stress within the OA joint eventually leads to the progression of OA. Excessive ROS causes mitochondrial damage to chondrocytes, leading to the impaired function of chondrocytes, resulting in apoptosis (Hou *et al.,* 2021). Therefore, the effective scavenging of ROS can be instrumental in treating the treatment of OA. Xu and co-workers (2023) developed a near-infrared light-sensitive tea polyphenol-modified zirconium-based porphyrin metal-organic framework (TP-Au@PCN) to repair impaired chondrocytes in OA (Xu *et al*., 2023). Tea polyphenol is a free radical scavenger that prevents oxidative damage mediated inflammation (Musial *et al.*, 2020). Although both pristine tea polyphenol and TP-Au@PCN showed significant reduction in levels

of ROS, the TP-Au@PCN was more effective in reducing the levels of ROS than pristine tea polyphenol. Both pristine tea polyphenol and TP-Au@PCN significantly reduced ROS levels, however TP-Au@PCN exhibited superior efficacy, reducing MMP-13 expression while increasing COL2 and SOX9 levels, thereby effectively promoting cartilage repair. (Hou *et al.,* 2021).

Other metals possess properties that can be beneficial for the attenuation of OA, these metals can be used in conjunction with OA therapies to combat OA. Kumar and colleagues (2019) utilized manganese dioxide (MnO_2) NPs to evaluate their ability to penetrate and be retained in the joint. Findings revealed that MnO2 NPs exhibited no cytotoxic effects on murine chondrocytes, synovial cells, mesenchymal stem cells (MSCs), or bone marrow-derived macrophages. Furthermore, treatment with these NPs significantly reduced the expression of key cartilage degradation markers, including nitric oxide synthase (NOS), MMP-1, MMP-13, and ADAMTS-5 (Figure 2.6). The PEG-MnO_2 NPs demonstrated prolonged *in vivo* retention in the joint cavity for at least 7 d after IA administration (Kumar *et al*., 2019). The incorporation of an OA drug would help exploit the properties of a nanosystem of this kind and possibly improve the properties of the drug.

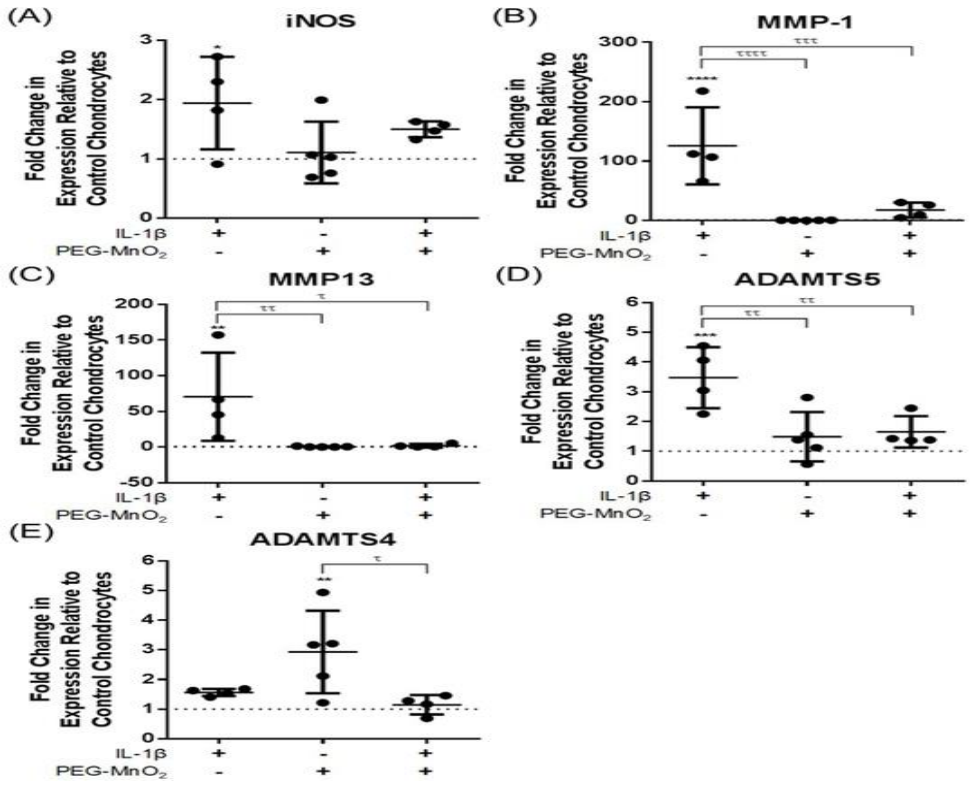


Figure 2.6. Effects of PEG-MnO2 NPs on expression of catabolic mediators (A) iNOS, (B) MMP-1, (C) MMP-13, (D) ADAMTS-5and (E) ADAMTS-4 in chondrocytes (Kumar et al., 2019). Reproduced with permission from Elsevier.

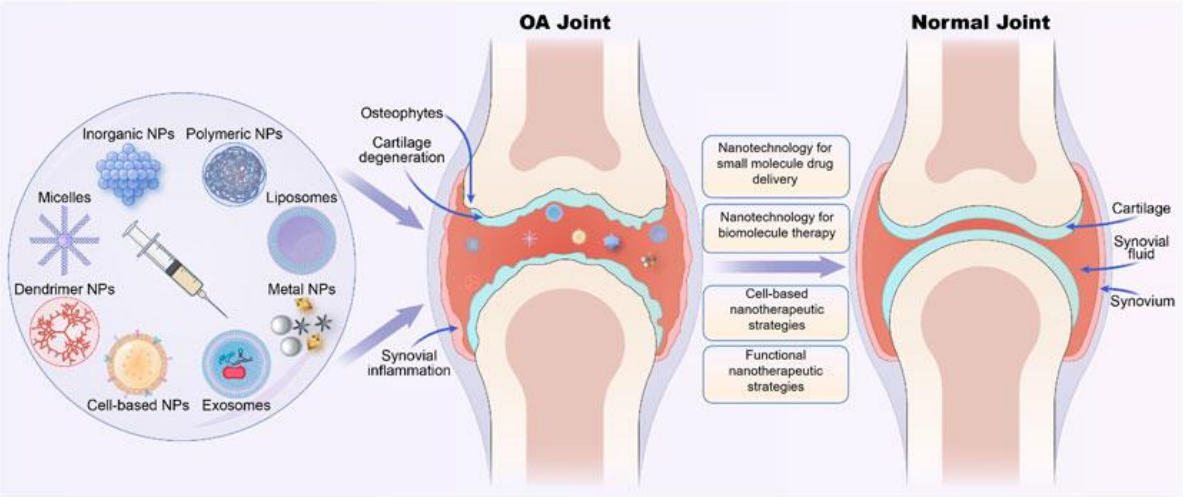


Figure 2.7. Structures of nanoparticles used as drug delivery systems in the treatment of OA (image adapted from the open-access article; Guo *et al*., 2022). Adapted under the terms of the Creative Commons Attribution License (CC BY).

Microparticles are defined as spherical particles between 1 and 1000 μm in diameter mainly classified as either microcapsules or microspheres (Cao *et al*., 2021). The particle size presents an advantage over NPs because of the larger surface-to-volume ratio (Stack *et al.*, 2019). This large size allows the entrapment of larger molecules such as proteins and peptides in greater quantities compared to NPs, which is essential for chronic diseases such as OA. Furthermore, once administered, microparticles are less likely to be rapidly eliminated via small capillary networks provided that they can penetrate the ECM in the joint, therefore improving retention of biologics delivered, a property necessary for chronic diseases such as OA (Colella *et al*., 2020).

Li and collaborators (2021) used super-activated platelet lysate (sPL)-loaded PLGA/chitosan/gelatin microspheres for IA delivery to inhibit and promote cartilage repair in OA rats. Growth factors IGF, TGF, and VEGF were released from the sPL-loaded microspheres within the first 3 d followed by stabilization and sustained release of all three growth factors thereafter for the remaining 17 d of the study. Treatment with the sPL-loaded microspheres resulted in increased expression of COL2A, ACAN, and SOX9 in OA chondrocytes which promote cartilage synthesis better than in the control group. The Micro-CT scan results (Figure 2.8) showed new cartilage filling within deeper cartilage layers as well as smoothened joint surfaces, and minimal osteophytes (Li *et al.,* 2021).

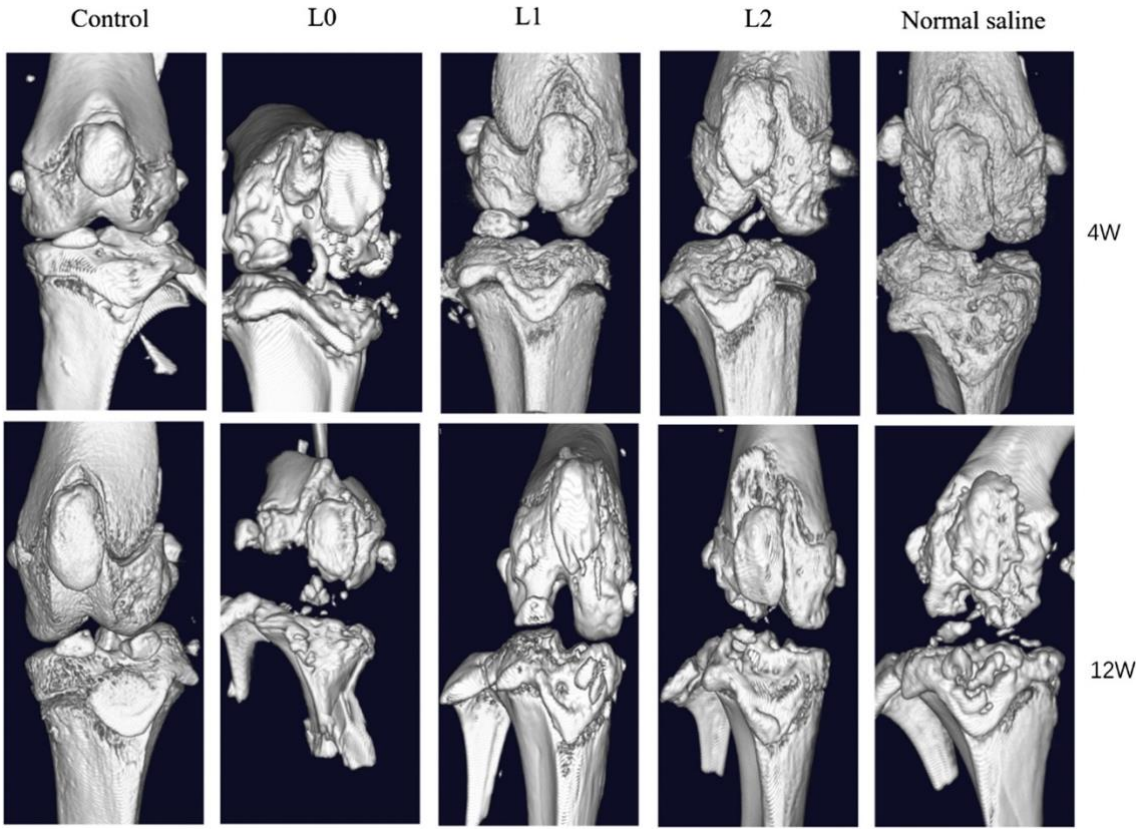


Figure 2.8. Micro-CT scans showing the effect of the microspheres on bone and articular cartilage injury. (Adapted from an open-access article; Li *et al.,* 2021, licensed under a Creative Commons Attribution 4.0 International License).

Another avenue of microparticles is microplates; Di Francesco and colleagues (2021) deployed DEX-loaded microplates for the IA delivery in OA mice (Di Francesco *et al.,* 2021). Although both free DEX and DEX-loaded microplates suppressed the amount of pro-inflammatory cytokines (IL-1β, IL-6, and TNF-α), the DEX-loaded microplates were more effective in inhibiting IL-6, and TNF-α than free DEX in ATCD5 chondrocytes. *In vivo* studies on over-load induced mice also showed that the DEX-loaded microplates had more effective inhibitory properties of IL-1β, IL-6, and TNF-α, as well as key matrix degradation protein MMP-13 than the free DEX. This suggested that DEX-loaded microplates were more effective as anti-inflammatory and anti-matrix degradation agents than free DEX in OA mice (Di Francesco *et al,* 2021).

In general, NPs and microparticles bear potential for their application in OA IA-delivered therapies due to their unique properties, such as targeted delivery and controlled and sustained drug delivery, all while minimizing systemic side effects.

2.5. Specialised Bioactives' Carriers in OA Therapy

Although much progress has been made, traditional drug delivery systems (e.g., liposomes) still have limitations such as short half-life, low encapsulation efficiency of hydrophobic drugs,

membrane instability making them leaky, and lack of flexibility (Opatha *et al*., 2020). To overcome these drawbacks, novel vesicular drug carriers such as exosomes, tNPs, and niosomes have emerged as promising platforms due to their unique structural properties and mechanisms of action.

2.5.1. Exosomes

Exosomes are extracellular nanovesicles with an average size of ~ 100 nm. These vesicles can be secreted by almost all cell types and are found in all body fluids and tissues including blood, urine, and adipose tissue (Kalluri and LeBleu, 2020). Exosomes have various endogenous functions, which include transporting nucleic acids (DNA, mRNA, siRNA, microRNA, and lncRNA), proteins, metabolites, and bioactive lipids (Tran *et al*., 2020). Additionally, exosomes have low immunogenicity, good tissue penetration, low toxicity, and are stable under physiological conditions (Chen *et al*., 2021; Hu *et al*., 2020). Exosomes are usually harvested from chondrocytes and MSCs for OA treatment (Liang *et al.,* 2024). Liang *et al.* (2022) developed chondrocyte-targeting exosomes (Figure 2.9 A) to encapsulate and intra-articularly deliver CRISPR/Cas9 plasmid (Cas9 sgMMP-13). Upon delivery to chondrocytes, the plasmid Cas9 sgMMP-13 knocked down MMP-13. This resulted in the prevention of COL2 degradation and the increase of ACAN (Figure 2.9 B), preventing cartilage degradation in *vitro* and *in vivo* (rat) OA models (Liang *et al.,* 2022).

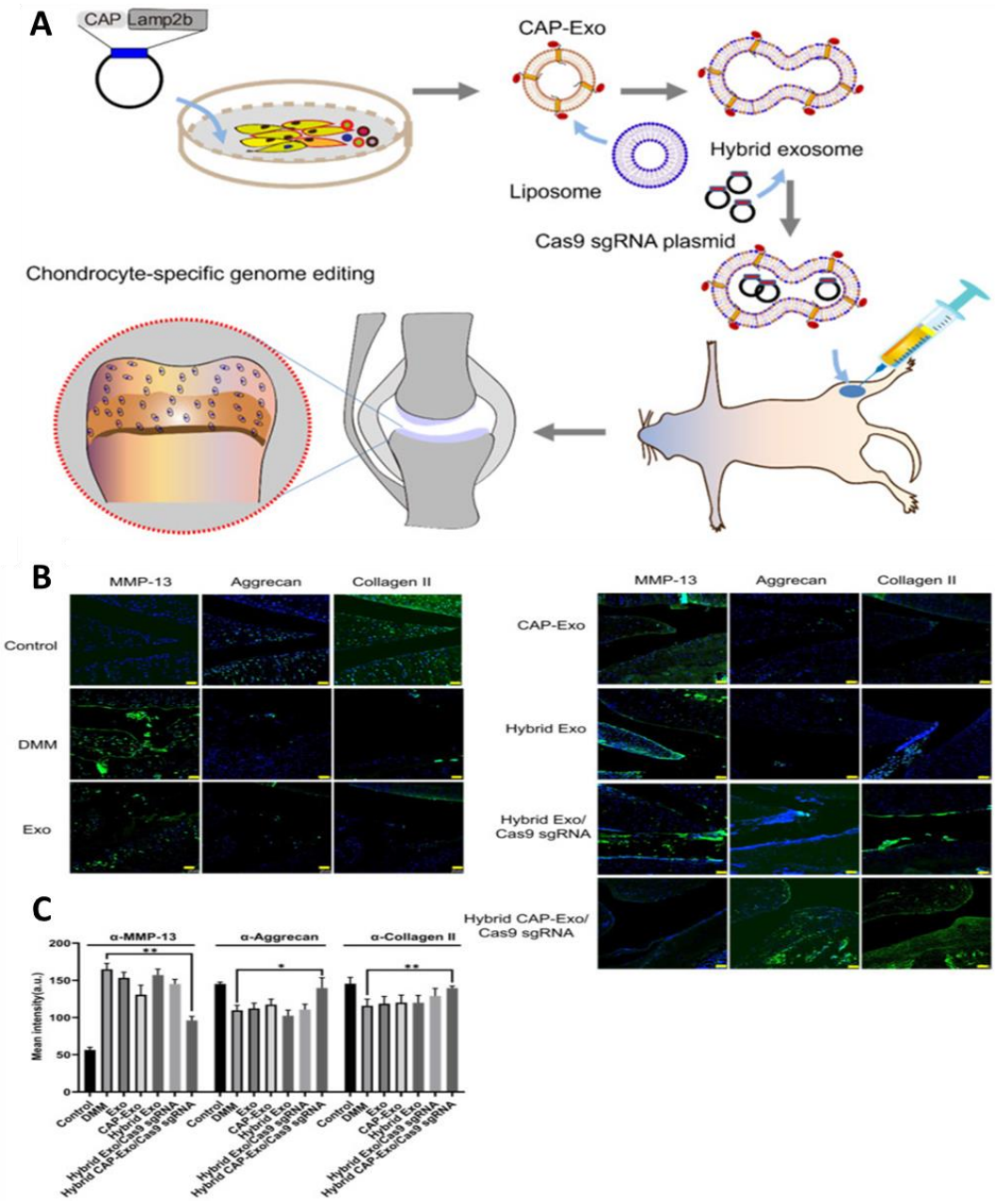


Figure 2.9. Schematic illustration of the concept and function of chondrocyte-specific genome editing by the synthesized hybrid exosomes (B) The effect of Cas9 sgMMP-13 on MMP-13, ACAN, and COL2 levels in chondrocytes of the knee joints in rats (adapted from an open-access article; Liang *et al.,* 2022.) Reproduced under the terms of Creative Commons CC BY.

Kartogenin (KGN) is a small molecule that possesses the capacity to stimulate chondrogenesis by inducing chondrocyte differentiation of MSCs (Johnson *et al*.,2012). Despite this, the clinical application of KGN has been hampered due to its poor solubility, this makes dose control and administration very complex. Xu *et al.,* (2021) encapsulated KGN into E7 peptide-exosomes and delivered into synovial fluid-MSCs to induce chondrogenesis. The superior expression of COL2A and ACAN in MSCs treated with E7-Exo/KGN compared to those of free KGN led to elevated MSC chondrogenic differentiation. This not only suggests

that E7-Exo/KGN has higher chondrogenesis capacity but also shows that the use of exosomes as carriers improved the solubility and in turn the bioavailability of KGN. The E7-Exo/KGN treated group also showed improved cartilage regeneration in OA rat models compared to those treated with free KGN. This was evident by the presence of clear layers of the perichondrium and smooth cartilage surfaces from E7-Exo/KGN-treated OA rats compared to coarse, eroded cartilage surfaces in OA rats treated with free KGN (Xu *et al.*, 2021).

Similar to inorganic NPs, non-medicated exosomes have the capacity to induce therapeutic effects on OA. For example, He and collaborators (2020) demonstrated the possibility of using bone marrow MSC-derived exosomes (BMSC-derived exosomes) as a delivery system to target chondrocytes. This is because MSCs have the capacity to enhance and promote endogenous cell regeneration and cell viability. In OA, MSCs function to maintain chondrocyte homeostasis, promote cartilage regeneration, and expedite tissue repair. (Lei *et al.,* 2022). The BMSC-derived exosomes led to significant *in vitro* upregulation of COL2A1 and downregulation of MM-P13, an enzyme associated with cartilage degradation in chondrocytes. Moreover, the BMSC-derived exosomes treated OA rats showed upregulated COL2A1 and downregulated MMP-13 compared to untreated rats. In general, BMSC-derived exosomes decreased cartilage destruction both *in vitro* and *in vivo* followed by inducing a cartilage repair *in vivo* (He *et al*., 2020).

Zhang *et al* (2020) assessed the possibility of repairing cartilage using BMSC-derived exosomes that possess bio-actives (proteins, lipids, and nucleic acids). Western blots showed enhanced concentrations of COL2 and SOX9 were increased, which promotes cartilage synthesis. Further, the results exhibited macrophage polarization to the M2 phenotype, subsequently leading to decreased levels of IL-1β, IL-6, and TNF-α (pro-inflammatory cytokines) as well as increased levels of IL-10 (anti-inflammatory cytokine), compared to the phosphate buffered saline group. The macrophage phenotypic change to M2-subtype favours an anti-inflammatory response (Strizova *et al*., 2023). Therefore, BMSC-derived exosomes displayed the potential to act as inflammation mediators and induce cartilage regeneration in OA rats (Zhang *et al*., 2020).

2.3.5. tNPs

tNPs are lipid-based nano-vesicular systems that consists of “at least one inner aqueous compartment”, a lipid bilayer (phospholipids) as well as an edge activator (EA) (Rai *et al*., 2017). In a literature review, Opatha *et al*. (2019) discussed that tNPs are both biodegradable and biocompatible as they are comprised of natural phospholipids and EAs (Opatha *et al*., 2020). Because they are biocompatible, tNPs are well suitable for prolonged retention periods,

critical for OA therapy as it will mitigate the need for multiple injections, making patients liable to possible infections and reducing patient compliance. The presence of the aqueous layer contributes to these vesicles' elasticity. This property is important as it makes it easy for tNPs to distort and wedge through constrictions that are smaller than their own diameter to reach the target site intact. This flexibility allows these NPs to be able to evade the dense network of the ECM. This results in controlled and sustained drug delivery, thus displaying high penetration resulting in targeted drug delivery in the joints (Rajan *et al*., 2011). Using tNPs that have an appropriate size to fit in the ECM, charge for solubility (cationic), and flexibility is critical for the treatment of OA as they can manoeuvre around the negative densely packed ECM (Li *et al*., 2021). Phospholipids in the tNPs may also serve as lubricants for the joints to assist in combating joint inflammation by reducing bone-to-bone friction in the OA joint microenvironment (Petelska *et al*., 2019). The deformability degree depends on the ratio of the EA to the lipid mixture. Because EAs are amphiphilic surfactants with lipophilic and hydrophilic moieties, they help with increasing solubility and entrapping of a wide range of drugs. EAs bring about membrane ultra-flexibility by acting as membrane destabilizing factors (Opatha *et al*., 2020).

They also help keep the membranes intact and offer protection against fragmentation of the membrane after penetration into pores smaller (up to a tenth smaller) than their diameter whilst protecting their cargo from metabolic degradation. EAs also affect vesicle size and drug encapsulation efficiency; the higher the concentration of the EA in the formulation, the smaller the vesicles formed. Conversely, the encapsulation efficiency decreases with the increased concentration of the surfactant (Akram *et al* 2022). As a result, tNPs can be used to carry a diverse selection of molecules almost independent of their size, MW, or structure (Opatha *et al*., 2020). The hydrophilic compartment of tNPs stores hydrophilic cargo such as chondroitin sulfate, while the hydrophobic compartment carries hydrophobic cargo such as DIC and curcumin within the lipid bilayers (Çağdaş *et al*., 2014; Chauhan *et al*., 2018).

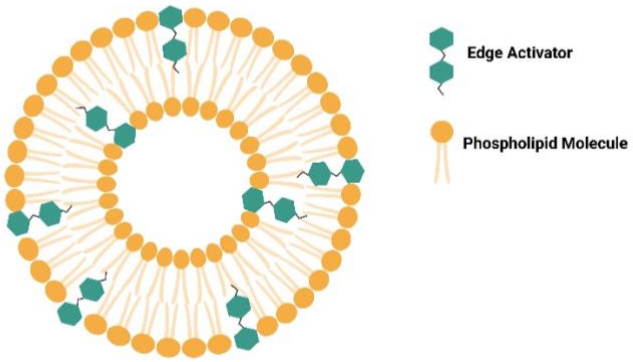


Figure 2.10. The general structure of a tNPs.

In the treatment of OA, tNPs have been mainly delivered transdermally (Rother *et al.,* 2009; Abada *et al.*, 2021; Rasheed *et al.,* 2022). (Marwah *et al*., 2022). EAs enable tNPs to create a trans-epidermal gradient, facilitating the ultra-deformable nanovesicles to squeeze through the stratum corneum and carry large molecules across the skin barrier. An osmotic gradient is created by the difference in water concentrations between the epidermis and stratum, facilitating the passage of tNPs from a higher to a lower gradient, thus delivering the cargo to its target across the skin barriers (Walve *et al*., 2011).

Rasheed *et al*. (2022) delivered glucosamine sulfate transdermally using tNPs to investigate improved drug delivery for glucosamine for OA treatment in rabbits (Rasheed *et al*., 2022). Similar to IA delivery, transdermal delivery has fewer side effects and potentially higher bioavailability compared to oral delivery, given that the drugs bypass hepatic first-pass metabolism. Glucosamine sulfate, a precursor of glycosaminoglycans, is well suited as a supplement to cartilage ECM, and a study by Towheed *et al.* (2005) suggested that glucosamine sulfate is as symptomatically effective as NSAIDs in the short-term management of OA (Towheed *et al.*, 2005). In the study by Rasheed and colleagues (2022), a tNPs -loaded glucosamine sulphate formulation was used to treat OA in papain-induced OA rabbits. One month post treatment, results showed an improvement in cartilage regeneration in rabbits treated with the transfersomal formulation; while on the other hand, there was no improvement in the rabbits treated with the liposomal formulation (Figure 2.11). This could possibly be attributed to the lack of permeability across the skin, as liposomes are more rigid than tNPs (Rasheed *et al.,* 2022). Additionally, since IA delivery is more site-specific, the transfersomal formulations being delivered directly to the joint along with their high permeability across the ECM, would increase the concentration of the drug in the joint space.

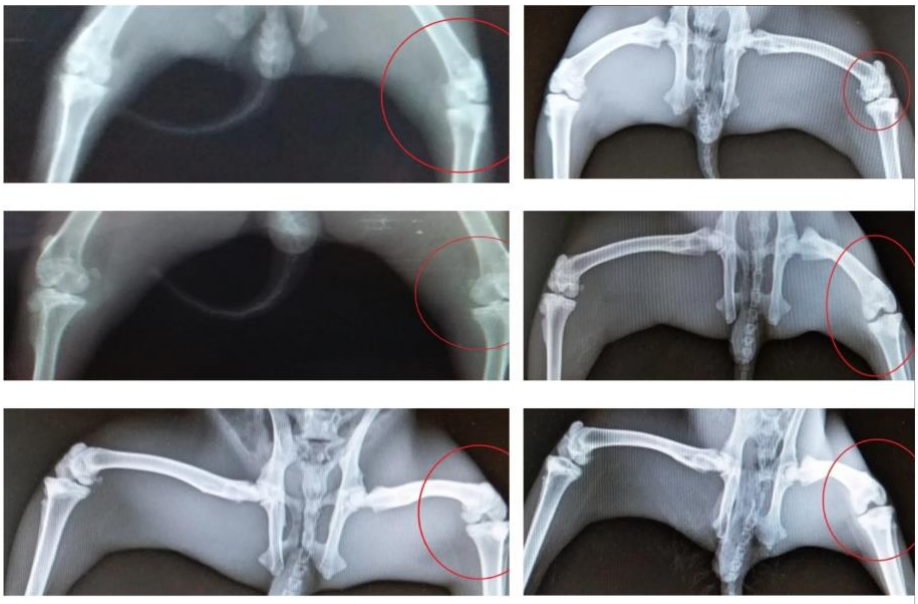


Figure 2.11. Radiological study results and observation before (A) and after treatment of OA rabbits. Adapted with no changes from Rasheed *et al*., 2022 under licensed under a Creative Commons Attribution CC BY license.

2.3.6. Niosomes

Usman *et al*. (2017) defined niosomes as "amphiphilic nanovesicles" capable of improving the pharmacokinetic properties of therapeutic compounds (Usman *et al.,* 2017). The lipid bilayer in the structure of niosomes is primarily based on the presence of non-ionic surfactants and lipid compounds (Akbarzadeh *et al*., 2021). As a result of their special geometry, niosomes can entrap both hydrophilic and hydrophobic drugs (Figure 2.12). Similar to tNPs, niosomes also possess the potential to safeguard encapsulated cargo from degradation upon administration, provide sustained release of therapeutic agents, are convenient, and achieve targeted drug delivery in OA joints. This, in turn, has the potential to mitigate the toxicity of administered agents, making them ideal for the treatment of chronic diseases such as OA (Masjedi and Montahaei 2021). Niosomes and liposomes have similar structures; however, the key difference is that niosomes comprise of non-ionic single-chain surfactants and cholesterol, while liposomes are made up of double-chain phospholipids (Gharbavi *et al*., 2018). Furthermore, niosomes are considered to be better nanocarriers compared to traditional liposomes as have a superior drug entrapment capacity, higher chemical stability, and greater bioavailability (Opatha *et al,* 2020). Therefore, niosomes can carry higher quantities of therapeutics, which is helpful for sustained release in OA, reducing the need for repeated administration. Although niosomes exhibit great promise as carriers, not enough studies have been conducted on their toxicity as they have endless permutations for combinations of surfactants and lipids (Gharbavi *et al*., 2018). However, like tNPs, niosomes have been primarily researched for topical delivery in OA, and no research was available

during the compilation of this review on their IA delivery in OA, also highlighting an area for future exploration by researchers.

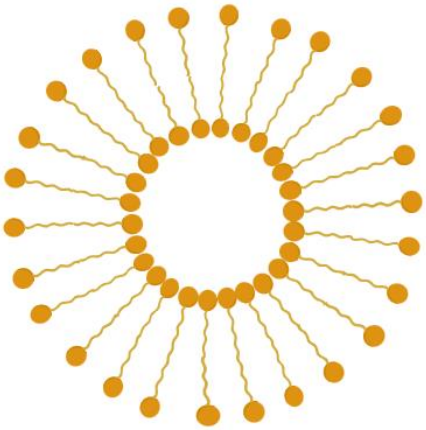


Figure 2.12. The general structure of a noisome.

Niosomes are innovative drug delivery systems designed to hurdle hinderances associated with traditional lipid-based delivery systems (Opatha *et al*., 2020). In general, tNPs and niosomes comprise the EAs and aqueous compartments that contribute to their flexibility and permeability through the dense ECM, making them suitable for application in IA OA treatment (Li *et al*., 2021; Kazi *et al*., 2010). The ultra-elasticity of tNPs allows them to traverse through constricted areas thus enabling efficient drug delivery (Rai *et al*., 2017). Conversely, niosomes are slightly more rigid but are more chemically stable than other vesicles (Mashal *et al*., 2023). Based on their biocompatibility, biodegradability, and site-specificity, both tNPs and niosomes hold great potential as drug carriers for OA treatment (Ag Seleci *et al*., 2016; Akram *et al.,* 2022).

Similar to tNPs and niosomes, hydrogels, a large class of polymers that have a high aqueous capacity to aid their structural flexibility hence potential application in OA therapy (Parhi, 2017). For this reason, the loading of vesicular OA formulations into the hydrogel systems bears great promise, given their compatibility in terms of structural deformability.

2.4. Hydrogels in OA Therapy

Hydrogels are three-dimensional cross-linked polymer networks containing hydrophilic functional groups, enabling them to absorb water up to several times their weight (Parhi, 2017). The extent of water absorption is directly influenced by the number of hydrophilic groups within the polymer structure. Due to this property, hydrogels serve as efficient drug carriers in smart delivery systems, promoting sustained drug release (Nunes *et al*., 2022). Their key attributes include biodegradability, biocompatibility, non-toxicity, and non-

immunogenicity, making them suitable for biomedical applications (He *et al*., 2017). Hydrogels can be synthesized from natural or synthetic polymers, with common synthetic polymers including polyethylene glycol (PEG), poly(lactic acid) (PLA), poly(lactic-co-glycolic acid) (PLGA), and polyvinyl alcohol (PVA) (Bashir *et al*., 2020). Conversely, natural hydrogel polymers, such as chitosan, HA, collagen, alginic acid, and carrageenan, are often derived from ECM proteins, enhancing their compatibility with the osteoarthritic joint matrix.

The high-water content exhibited by hydrogels allows them to undergo swelling and shrinkage in response to external stimuli, such as temperature and pH. Temperature-responsive hydrogels rely on polymers with a lower critical solution temperature (LCST) (Zhuo *et al*., 2022). Above the LCST, hydrophobic interactions cause polymer contraction, leading to phase separation and gel collapse. Below the LCST, hydrophilicity increases, causing water absorption and hydrogel expansion (Peppas and Hoffman, 2020). This unique property enables phase transitions between sol and gel states, facilitating controlled drug release (Abou-Shamat *et al*., 2020). pH-sensitive hydrogels, on the other hand, consist of ionic polymers containing acidic (e.g., carboxylic acid) or basic (e.g., amine) functional groups (Tan *et al*., 2022). Under specific pH and ionic conditions, these groups ionize, generating electrostatic repulsions that induce gelation and enhance drug release efficiency (Bustamante-Torres *et al.,* 2021).

NP-loaded hydrogel systems integrate the benefits of both NPs and hydrogels to optimize drug delivery. A compelling example is the study by Yang *et al*. (2020), where KGN-loaded GelMA@Lipo microgels extended KGN release for over three weeks, significantly longer than the 25-day release observed with KGN-loaded liposomes alone. Furthermore, GelMA@Lipo@KGN demonstrated the highest proteoglycan accumulation in bone marrow-derived stem cells (BMSCs), surpassing both Lipo@KGN and control groups, indicating enhanced chondrogenesis due to the sustained release of KGN via the GelMA system. The formulation also elevated the expression of COL2A1, ACAN, and SOX9, supporting its potential to promote chondrogenic differentiation in BMSCs (Yang *et al.,* 2020). Similarly, Han *et al* (2021) developed methacrylate gelatin (GelMA) microspheres embedded with dopamine-modified poly(N, N-dimethylacrylamide) (DMA) and 2-methacryloyloxyethyl phosphorylcholine (MPC) (GelMA@DMA-MPC). This system significantly improved lubrication and provided sustained diclofenac (DIC) release in OA rat models (Figure 2.13). Additionally, the delivery system upregulated ACAN and COL2A1 expression while downregulating MMP-13 and ADAMTS-5, thereby promoting cartilage regeneration and preventing further degradation (Han *et al*., 2021).

Another notable example is the study by Lei and co-workers (2022) in which rapamycin's water solubility was enhanced through encapsulation in cationic liposomes, forming rapamycin-liposome-incorporating HA-based hydrogel microspheres (RAPA@Lipo@HMs). The results demonstrated that liposomes improved the pharmacokinetic profile of rapamycin, while RAPA@Lipo@HMs extended drug release from 21 to 28 d. Interestingly, the RAPA@Lipo@HMs also functioned as a bio-lubricant, reducing joint wear in vivo and further supporting their potential in OA therapy

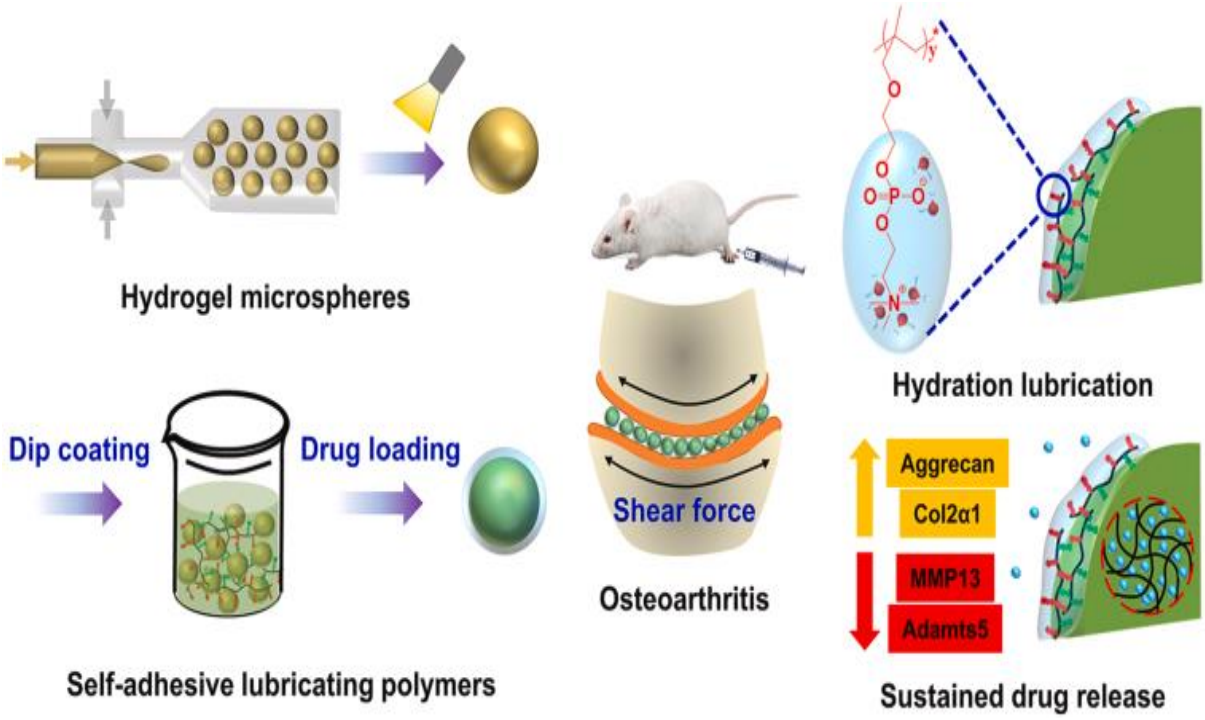


Figure 2.13. Formulation process and principle of the GelMA@DMA-MPC microspheres in OA (Reprinted from an open-access article Han *et al.,* 2021 rats. Reproduced under the terms of Creative Commons under the CC BY-NC-ND license.

Li and colleagues (2021) addressed articular cartilage degeneration by utilizing a nano-micron system composed of G5-AHP (a multifunctional gene vector modified with arginine, histidine, and phenylalanine) and microRNA-140 (miR-140) to form G5-AHP/miR-140 NPs encapsulated within hydrogel microspheres. This system demonstrated high gene transfection efficiency, increasing COL2 expression by over threefold compared to the control. Additionally, ADAMTS-5 and MMP-13 expression levels were reduced by approximately 0.7-fold and 0.5-fold, respectively, in chondrocyte cells, thereby preserving cartilage matrix homeostasis in a murine OA model (Li *et al*., 2021).

In another study, Seo *et al.* (2022) encapsulated triamcinolone acetonide into PNPs within an intra-articularly injectable hydrogel to manage OA-related inflammation in mice. This system significantly reduced the expression of pro-inflammatory cytokines IL-6 and TNF-α over four weeks, whereas free triamcinolone acetonide failed to achieve long-term suppression,

indicating inferior efficacy. The hydrogel also enhanced the secretion of anti-inflammatory cytokines IL-4, IL-10, and IL-13, further supporting its superior long-term anti-inflammatory effects. Additionally, it effectively inhibited matrix-degrading proteins MMP-3 and MMP-13, preventing cartilage degeneration. Free triamcinolone acetonide, in contrast, was unable to sustain these effects over the same period (Seo *et al*., 2022).

Tsubosaka *et al*. (2020) explored the application of eicosapentaenoic acid (EPA) encapsulated within micelles and further incorporated into a gelatin hydrogel for IA OA treatment. EPA, known for its anti-inflammatory and immunomodulatory properties, reduced inflammatory cytokine synthesis (Curtis et al., 2002). The EPA-hydrogel formulation demonstrated superior suppression of IL-1β, MMP-3, and MMP-13 compared to free EPA, suggesting its potential in mitigating inflammation and protecting cartilage integrity in OA models. (Tsubosaka *et al*., 2020).

Cai *et al.* (2019) synthesized a vinyl sulfone-modified HA crosslinked with dithiol-terminated poly (ethylene glycol). While the unmodified HA solution degraded entirely within 2 d, the modified HA hydrogel resisted enzymatic degradation for up to 7 d. Additionally, the modified HA exhibited enhanced viscoelastic properties, making it a promising candidate for OA treatment (Cai *et al.* 2019).

Biomimetic viscosupplementation strategies have also been explored to restore joint lubrication. Mou and colleagues (2021) formulated an HA-chitosan-based supramolecular hydrogel for OA therapy, demonstrating effective pain relief and inflammatory suppression by inhibiting TNF-α, IL-1β, IL-6, and IL-17 more efficiently than plain HA. Rat models treated with this hydrogel displayed smooth, intact cartilage surfaces with thicker layers, signifying enhanced cartilage regeneration compared to HA alone. The formulated HA-chitosan-based hydrogel was significantly better than the plain HA-formulation in attenuating OA in rodents by decreasing inflammation and inducing cartilage regeneration (Mou *et al*., 2021).

Leone and colleagues crosslinked gellan gum (Leone *et al*., 2020), a water-soluble anionic polysaccharide with PVA, yielding improved mechanical properties. The formulation exhibited enhanced elastic and viscous moduli compared to the polysaccharide core, indicating superior thixotropic properties and resistance to degradation. Approximately 70% of HA was released initially, followed by sustained release over the next 23.5 h. (Leone *et al*., 2020).

Jahanbekam *et al.* (2023) developed an ultrasound-triggered mixed-micelle HA hydrogel containing hydrocortisone for IA OA therapy (Jahanbekam *et al*., 2023). Ultrasound waves elevated the local temperature, triggering drug release by disrupting micelles through shear stress. Free hydrocortisone was fully released within 2 h, while hydrocortisone from the HA hydrogel and mixed-micelle hydrogels (containing Capryol® and Brij®) exhibited extended

release over approximately 4–8 h. The formulation incorporating Tween® 60 exhibited the most controlled and prolonged release. This is critical because it shows that the different surfactants had an influence on the drug release and that the formulation containing Tween® 60 will prolong the release of hydrocortisone in the joint, highlighting its potential for reducing the frequency of IA injections in OA management.

Diaz-Rodriguez and colleagues (2021) engineered a HA-based thermos-responsive hydrogel that would release beta-lapachone (βLap), a natural naphthoquinone with anti-inflammatory activity. This hydrogel transitioned from sol-to-gel at 30 °C. The gel displayed rheological properties favourable for the treatment of OA as well as a decrease in the secretion of IL-6 in both free βLap and βLap loaded in the HA hydrogel from an *ex vivo* OA model. This suggested that βLap in both states could decrease pro-inflammatory cytokine IL-6; however, hydrogel-loaded βLap reduced IL-6 secretion better than free βLap. In addition, the secretion of pro-inflammatory chemokine CXCL8 was more effectively reduced by the hydrogel-loaded βLap compared to free βLap. Conversely, free βLap reduced the secretion of matrix-degrading protein MMP-13 better than βLap embedded in the hydrogel formulation. Therefore, the hydrogel formulation had superior anti-inflammatory effects and slightly inferior cartilage regeneration effects compared to free βLap (Diaz-Rodriguez *et al*., 2021).

The incorporation of metal NPs into hydrogels has also been explored for OA treatment; Li and colleagues (2024) combined the antioxidant properties of cerium oxide-NPs with cartilage-repairing properties of platelet lysate together with an HA hydrogel for IA delivery in OA (Li *et al.,* 2024). This hybrid system increased the expression of COL2 and ACAN while inhibiting COL10, MMP-13, ADAMTS-5, and ADAMTS-9 in chondrocytes (Figure 2.14) indicating the hydrogel's potential to effectively promote cartilage regeneration while suppressing matrix degradation. (Li *et al.,* 2024).

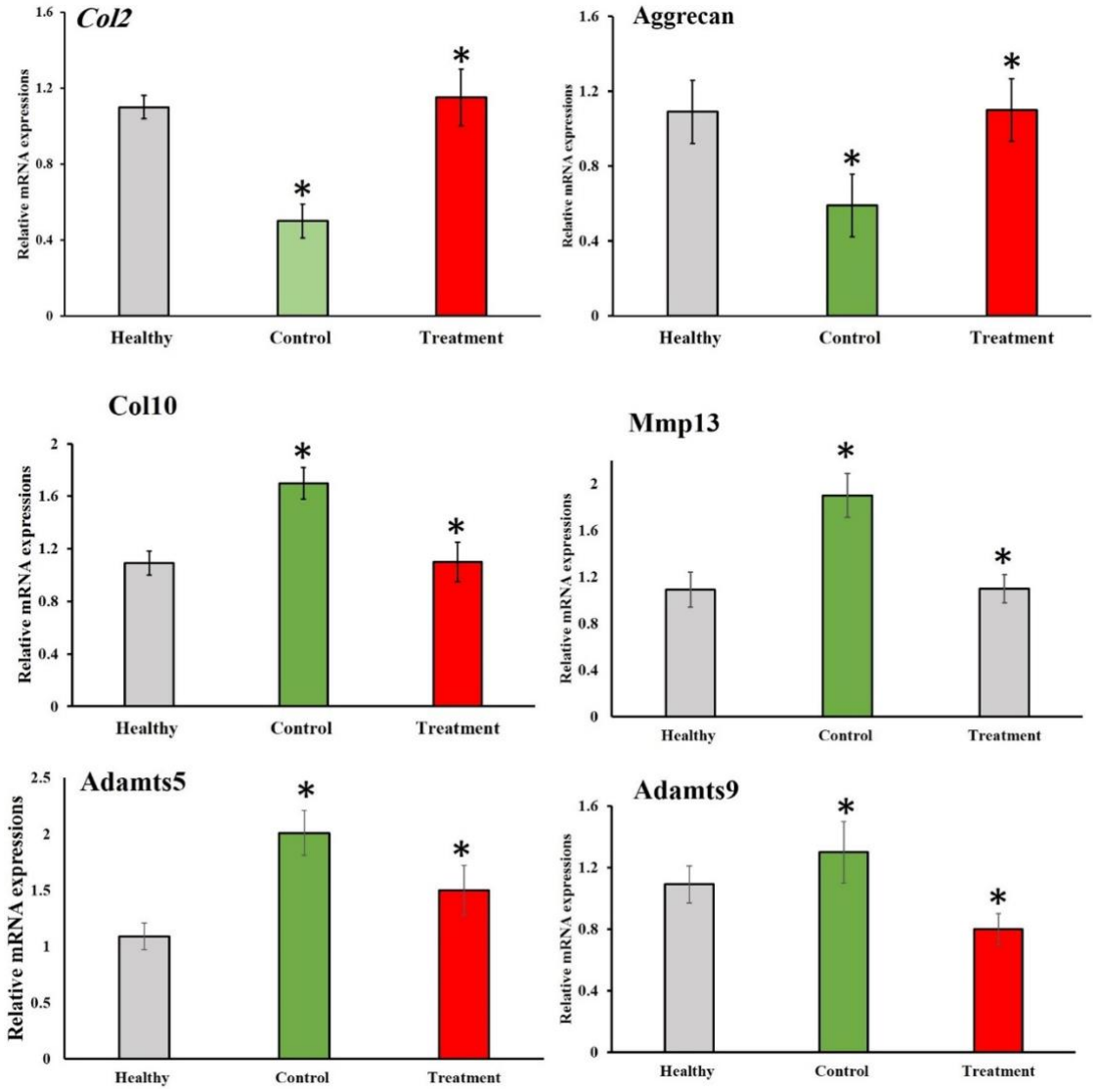


Figure 2.14. The effect of cerium oxide-NPs on mRNA expressions of Col2, ACAN, Col10, MMP-13, ADAMTS-5, ADAMTS-9 genes in chondrocytes (Li et al., 2024). Figure adapted an open access article and reproduced with permission from Elsevier.

2.5. Molecularly Imprinted Materials with Potential to Treat OA

Amongst many approaches investigated to address drawbacks connected to conventional delivery systems in OA, molecularly imprinted materials provide a promising platform for potentially target-specific smart drug delivery systems.

Molecular imprinting technology provides a versatile tool for fabrication of highly selective polymeric materials, viz. molecularly imprinted polymers (MIPs) (BelBruno, 2018). The high selectivity of MIPs towards target compounds is derived from the chemically modified surfaces of resulting material. The surface modification is a result of the synthetic process that is executed in the presence of a template molecule (Janczura *et al.,* 2021). MIPs are obtained in three key steps: the synthetic formation of a prepolymerization adduct, polymerization and template removal, resulting in modified polymer surface regions that are complementary to

the distribution of electrostatic potentials to the template. A prepolymerization adduct can be created via two distinct approaches: (i) a covalent strategy, where stable chemical bonds are formed between the template and the functional monomers providing a functionalized molecule, most commonly, possessing vinyl groups capable of polymerization or a (ii) non-covalent strategy where different non-covalent interactions, such as van der Waals forces hydrogen bonds or electrostatic forces stabilize the prepolymerization complex between the template and the monomers.

The covalent strategy offers high durability of the functionalized compound, making it advantageous under harsh polymerization conditions, but requires confirmation of the compound's structural integrity and purity prior to the polymerization process. Moreover, the template needs to possess functional groups that are able to react with functional monomers forming ester or imine bonds. Unfortunately, this method necessitates hydrolysis of the template at the removal step, which can potentially alter the polymer's structure. Conversely, the non-covalent strategy simplifies the synthesis process and reduces synthesis time, but its lower stability often results in greater heterogeneity in the binding sites of the final polymer. The selection of a pertinent strategy is largely contingent on the template structural properties, availability and the intended application of MIPs (Liu *et al*., 2024).

In most cases the template molecule and the target compound used in the synthesis of MIPs are the same chemical entities. However, limited availability or high costs of certain templates are limiting factors in the synthesis of MIPs. In such a case, MIPs can be obtained using structural analogues of target compounds as alternative templates (Chen *et al.*, 201). Careful selection of the template also mitigates the risk of template leaching—an undesirable phenomenon where residual template molecules affect the performance of the synthesized MIP. Literature has shown the effectiveness of providing selective MIPs. The efficiency of molecular imprinting is typically assessed using the imprinting factor, which is calculated as the ratio of the template’s adsorption capacity on the MIP to that on a non-imprinted reference polymer. To ensure accuracy, the non-imprinted polymer must be synthesized under identical conditions, omitting the template molecule (Lamaoui *et al.,* 2024).

It has to be mentioned that both highly cross-linked rigid polymers and low cross-linked hydrogels can be effectively obtained through molecular imprinting. In highly cross-linked hydrogels, the rigidity of the polymers maintains the geometry of their modified surface regions, preserving electrostatic potential distributions even after template removal, thus ensuring selective adsorption of the target molecule. Conversely, low cross-linked hydrogels exhibit flexible polymer chains, allowing imprinting to function as a macromolecular memory process. Multiple interactions between the template and functional monomers during

synthesis drive the hydrogel's polymer chains into an energetically favorable conformation. Upon template removal, complementary binding interactions between the target molecule and the hydrogel network facilitate adsorption through conformational adjustments, ensuring high-affinity binding (Kakkar and Narula, 2022).

The desorption of target molecules from MIPs or hydrogels is governed by the diffusion and the relaxation of the material network. For highly cross-linked polymers, the degree of cross-linking affects diffusion, making the desorption process less diffusion-dependent. In contrast, low cross-linked hydrogels, the macromolecular relaxation upon medium absorption induces swelling of the material. Despite this swelling, numerous spatially oriented functional groups within the hydrogel network interact with the target molecule (e.g., a drug), thereby modulating its release. The modified kinetics of the drug release process depend on the strength of those interactions. The migration of the drug through the polymer matrix, from one macromolecular memory region to another with various binding interactions creates a "tumbling effect", creating efficient complexes by minimizing entropically unfavourable translational and rotational free energies (Venkatesh *et al*.,2008).

Among the various forms of MIPs, 'surface imprinting' has emerged as a notable advanced molecular imprinting strategy. This technique allows us to provide a thin molecularly imprinted layer on the surface of core forming composite materials (Kumar *et al.,* 2024). Moreover, surface-imprinted MIPs provide a versatile platform for 'epitope imprinting', a protocol very effective for the synthesis of protein-targeted MIPs. Epitope imprinting involves using peptide fragments specific to a target protein, thus enhancing the selectivity of the resulting material (Dietl *et al.*, 2021). Facile functionalization of MIP layers with different cores is an important advantage as this enables further modifications allowing additional properties to the material such as integrating magnetic susceptibility properties. Additionally, surface imprinting improves the diffusion kinetics, expediting the effectiveness of the adsorption process. This technique is commonly applied in cancer diagnostics and therapy, where MIPs are employed for targeted drug delivery through the recognition of specific cell surface domains (Balcer *et al.,* 2023).

MIPs exhibit selectivity comparable to that of antibodies while offering greater chemical and thermal stability. Unlike biologics, MIPs do not require specialized storage conditions, making them a more practical alternative to antibodies and biological receptors. Their robust nature compensates for the challenges associated with antibody manufacturing, particularly stability and shelf-life limitations (Liu *et al.,* 2024). MIPs have been extensively utilized in analytical chemistry, primarily as selective sorbents in the solid-phase extraction, selectors in chromatography and recognition elements of sensors (Sobiech and Luliński, 2024; Su *et*

al.,2024). Despite numerous commercial applications, their potential in drug delivery remains an active area of research (Luliński, 2017; Haupt *et al*., 2020). Recent studies have validated multiple MIPs as effective operative diagnostic tools or drug delivery devices. Notably, MIPs have not yet been utilized for IA delivery of therapeutics for OA therapy. In OA, MIPs may be designed to trigger the degradation of hydrogel matrices to release drugs/drug-loaded NPs into target areas upon the recognition of hallmarks of OA, such as pro-inflammatory cytokines and matrix-degrading proteins (Gagliardi, 2023). This would potentially allow specific and targeted release and enhance retention times of therapeutics by providing a specific binding site to trigger their release. Thus, in our opinion, a few approaches discussed below could be beneficial to progress IA bioactive delivery for the treatment of OA.

As mentioned, MIPs reveal potential for facile integration with other materials resulting in composites which increases their value by presenting additional advantages. The resulting hybrid materials could serve dual functions, such as serving as carriers for delivery of anti-inflammatory agents and simultaneously as selective adsorbents of the inflammatory cytokines. To the best of our knowledge, literature survey shows no reports of MIP-based systems that combines these functions for IA treatment of OA thus providing an opportunity for further investigations. However, it has to underlined that the investigations of specific MIP systems for anti-inflammatory drug deliveries and towards inflammatory cytokines have been carried out. Most recent and pronounced achievements are briefly discussed below.

In a very interesting paper, Parisi and co-workers (2018) developed a ‘smart bandage’ incorporating MIPs for DIC, an anti-inflammatory drug, for topical administration, to combat localized pain and inflammation. The ‘smart bandage’ prepared using MIP loaded with DIC exhibited drug release of 24% within the 6 h and 92% of DIC released after 72 h. In contrast, the non-imprinted smart bandage’ loaded with DIC released 51% of the drug within the first 6 h and was completely released (100%) after 72 h. The MIP-integrated version of the smart bandage demonstrated prolonged drug release and improved diffusion kinetics compared to the non-imprinted version, ensuring sustained therapeutic effects. (Parisi *et al.,* 2018).

As an example, for the delivery for steroid anti-inflammatory drug, Wei et al. (2019) reported a pH-responsive molecularly imprinted hydrogel for DEX delivery. Dopamine, acrylamide and acrylic acid were utilized as functional monomers to synthesize the hydrogel and DEX as the template molecule. After immersion in DEX solutions, the molecularly imprinted hydrogel had a significantly higher drug loading rate compared to that of non-imprinted hydrogel. While the release rate of non-molecularly imprinted exhibited an excess of 80% DEX release after 24 hrs, approximately 60% of DEX was released from molecularly imprinted hydrogel in the same period. The molecularly imprinted hydrogel sustained DEX release for up to 7 days. (Wei *et*

al., 2019). In another study, Zahedi and co-workers integrated MIP NPs within electrospun poly(ε-caprolactone) nanofibers for the release of DEX. The MIP NPs were made using methacrylic acid and ethylene glycol dimethacrylate as functional monomers and DEX served as the template molecule. Biodegradability could be considered as an advantageous property of MIPs for drug delivery. Here, poly(ε-caprolactone) combined with MIP prolonged DEX release following the Fickian diffusion mechanism, confirming their potential for sustained drug release. (Zahedi *et al.,* 2017).

MIPs have also been explored for cytokine detection. Choi and co-workers (2022) developed a double layer MIP-based sensor for IL-1β detection using poly(1,2-phenylenediamine) and poly(2-(phenylazo)chromotropic acid) as functional monomers and IL-1β as the template. The MIP layer showed high IL-1β adsorption compared to IL-1α, IL-6, and TNF-α (Choi *et al.,* 2022). In another paper, Chen and co-workers proposed defect‑engineered graphene nanoribbons as substrate material to fabricate MIP via electropolymerization, utilizing IL-6 as the template and producing a material selective towards IL-6 (Chen *et al*., 2024). Yang *et al* (2023) fabricated MIP-based chemosensors using gold-dendritic electrodes for TNF-α detection, achieving precise cytokine recognition and quantification. The selectivity of these sensors was validated against IL-1β and IL-6. (Yang *et al*., 2023). Simultaneously, Yellin et al. (2023) further validated the effectiveness of protein-imprinted polymers in selectively adsorbing TNF-α, with in vitro studies demonstrating biocompatibility and reduced TNF-α-induced cell death (Yellin et al., 2023).

Other studies have extended MIP applications to matrix metalloproteinase (MMP) detection, as seen in work by Lee et al. (2023) and Zito et al. (2024), who developed MIP-based photonic nanostructures for MMP-1 and TGF-β, respectively.

The potential of MIPs in OA treatment remains largely unexplored. However, emerging studies underscore their utility in drug delivery applications with prolonged release profiles. The adaptability of MIPs for integration with various biomaterials highlights opportunities for designing innovative therapeutic strategies, particularly for inflammatory disease management. Future advancements in MIP technology could facilitate the development of multi-functional MIP composites tailored for OA treatment, combining targeted drug delivery with cytokine modulation for enhanced therapeutic efficacy

2.6. Current Clinical Trials on Intra-Articular OA Therapy

In overall, the number of clinical trials on intra-articularly administered drug delivery systems for OA is inadequate (Li *et al*., 2021). Clinical trials focused on OA play a pivotal role in

advancing researchers' progress in understanding the effect of medical interventions on this debilitating joint disorder in humans. These trials are critical for developing and evaluating novel OA therapies, assisting researchers in gaining insights into essential parameters such as their safety, efficacy, and tolerability (Holford *et al*., 2000). Though a plethora of research has been conducted on IA drug delivery in OA treatment, their translation into clinical applicability is underwhelming. This failure might be because of the use of small animals for testing and absentia of best-practice standards for animal testing (Mak *et al.,* 2014). Small animals like mice and rabbits are commonly used in the *in vivo* studies and can be useful for preliminary studies; however, large animals must be used for validity before conducting clinical trials in humans. Another possible reason can be the failure to simulate the environment of the joint when conducting *in vitro* tests such as *in vitro* drug release. The wide translation gap remains an enormous hurdle, with concerns such as safety and efficacy at the forefront. As a result, the development of strategies that aim to eradicate this gap is of paramount importance. Table 2.2 summarizes clinical trials focused on IA drug delivery in OA (ClinicalTrials.gov).

TLC599, a liposome formulation of dexamethasone sodium phosphate (DSP), showed a significant Western Ontario and McMaster Universities Osteoarthritis Index-pain (WOMAC) reduction and improved function for up to 24 weeks in a phase 3 clinical study of knee OA (NCT02803307) (Table 2.2). Similarly, Cingal® is a hydrogel that was a formulated as a crosslinked HA viscosupplement loaded with a corticosteroid triamcinolone hexacetonide, for IA injection (Hangody *et al*., 2018). Cingal® is Anika Therapeutics next-generation formulation constructed from the base of Monovisc™, their FDA-approved non-drug-loaded HA viscosupplementation product. Clinical trial studies showed that Cingal® possessed superior WOMAC pain scores than the saline group and exhibited better pain relief for the first 3 weeks, followed by similar pain relief through the remaining 23 weeks (ClinicalTrials.gov). Seikagaku co-developed SI-613, a conjugate of HA and DIC (Gao *et al*., 2022). Safety and efficacy studies revealed that SI-613 outperformed the placebo, showing a significantly improved WOMAC pain subscale score over 12 weeks. However, further safety evaluations are needed, as anaphylactic reactions were observed (Gao *et al*., 2022).

In another study, the safety and efficacy of high-purity synthetic trans-capsaicin (CNTX-4975) were evaluated in moderate to severe knee OA (Ghouri and Conaghan, 2019). CNTX-4975 exhibited dose-dependent improvement in knee OA–associated pain through 24 weeks. FX006, a formulation of triamcinolone acetonide (TCA) encapsulated PLGA microspheres DeJulius *et al.*, 2021). Efficacy studies revealed that FX006 provided sustained clinical improvement in knee OA compared to saline-placebo regardless of the baseline inflammation. Studies on FX006 also showed that treatment-emergent adverse events were similar to saline elucidating the tolerability of the drug delivery system. Generally, the results from the majority

of the aforementioned studies showed longer duration than that reported for existing IA treatments in OA (Hangody *et al*., 2018; Gao *et al*., 2022). Table 2.2. summarizes clinical trials focused on IA drug delivery in OA.

Table 2.2. List of clinical trials for IA drug delivery in OA from clinicaltrials.gov.

Product	Aim	Drug(s)	Delivery system	Type of Study	Phase	OA type	Identifier
TLC 599	Evaluate the efficacy and safety	Dexamethasone sodium phosphate (DSP)	Liposomes	Randomised, double-blinded placebo- and active-controlled	III	Knee OA	NCT02803307
CiNGAL	Relieve symptoms and treatment	Triamcinolone Hexacetonide (TH)	Hydrogel	Randomized, double-blind, placebo-controlled	III	Knee OA	NCT04231318
CNTX- Capsaincin 4975	Relieve OA knee pain	Capsaincin	N/A	Randomized, double-blind, placebo-controlled	III	Knee OA	NCT03429049
FX006	Efficacy and safety assessment	TCA IR 40	Polymeric NPs	Double-blind, randomized	II	Knee OA	NCT02357459
FX-201	Safety and tolerability assessment	Recombinant human interleukin-1 receptor antagonist protein	HDAd vector	Non-randomized	I	Knee OA	NCT04119687
SI-613	Efficacy and safety assessment	Diclofenac etalhyaluronate & HA	Hydrogel	Randomized, double-blind	III	Knee OA	NCT03209362

2.7. Review Summary: Colloidal Systems in OA Treatment

In OA, nano-, micro-formulations, and hydrogels have been shown, both individually and in combination, to be superior to conventional formulations. Therapeutic agents are encapsulated into these delivery systems to potentially increase the therapeutic agents' potency, allow for a higher concentration of drugs within the joint, leading to faster and more effective treatment. Given that, this, in turn, can potentially improve the side effect profiles of these agents and the frequency of administration through targeted and localized delivery of bioactives (Huang *et al*., 2022).

Both *in vitro* and *in vivo* studies have shown promising results, with bioactive-loaded delivery systems effectively suppressing key pro-inflammatory cytokines, including TNF-α, IL-1β, IL-6, and iNOS, in OA joints. These findings suggest that targeted drug delivery can alleviate the inflammation associated with the pathogenesis of OA and potentially attenuate the progression of the disease. Furthermore, certain hydrogel-based delivery systems promoted macrophage repolarization from the pro-inflammatory M1-subtype to the anti-inflammatory M2-subtype, which is characterized by the secretion of cytokines such as IL-4 and IL-10 (Pérez and Rius-Pérez, 2022; Strizova *et al.*, 2023).

Additionally, the reviewed delivery platforms consistently demonstrated the ability to inhibit matrix-degrading enzymes such as ADAMTS-5, MMP-1, MMP-3 and MMP-13, which are key contributors to cartilage degeneration (Kumar *et al*., 2019; Liu *et al.,*2019; Park *et a*l. 2020; Wei *et al*., 2021; Lei *et al*., 2022; Dravid *et al.,* 2023; Deng *et al*., 2023). The suppression of these enzymes in chondrocytes has resulted in cartilage regeneration evident by the restoration of previously degraded cartilage in animal OA (Li *et al.,* 2021; Mou *et al*., 2021; Xu *et al*., 2021). Therefore, delivery platforms such as microspheres and MSC-derived exosomes have the capacity to aid the preservation of cartilage integrity and prevention of further cartilage degeneration. It was also observed that nano- and hydrogel-based delivery systems improved drug retention and provided sustained drug release compared to free drugs within the joint space, leading to prolonged therapeutic effects (Kumar *et al*., 2019; Hu *et al*., 2020; Wei *et al*., 2021; Teng *et al*., 2023; Dravid *et al.,* 2023; Deng *et al*., 2023).

Considering the aforementioned information, designing a system that enhances controlled and sustained drug release is crucial, positioning hydrogels as an ideal candidate (Nunes *et al*., 2022). In OA, hydrogels act as lubricants and shock absorbers, reducing bone-to-bone friction, thus alleviating pain and possibly inflammation (Lin and Klein, 2022). However, incorporating NPs and microparticles into hydrogels can offer dual structural and therapeutic benefits, as the gel

regulates drug release while simultaneously reducing mechanical stress within the joint (Lin and Klein, 2022). Moreover, exogenous hydrogel components derived from ECM can help mimic and confer desirable properties that can potentially benefit the joint's health.

Interestingly, hydrogels can be engineered to possess properties that can increase the specificity of nano-systems. Modifications include the incorporation of the stimuli-responsiveness characteristics to the hydrogel (Kung *et al*., 2023; Neumann *et al*., 2023). When acted upon by certain stimuli such as pH and temperature, hydrogels can respond by transitioning from solution-to-gel therefore preventing the likelihood of them clotting in the vessels on the occasion that they are administered into the wrong areas (El-Husseiny *et al.,* 2023). Stimuli-responsive hydrogels present a compelling strategy for addressing the constraints associated with the traditional conventional administration of drugs in OA. They enable site-specific, controlled, and sustained release of therapeutic agents, therefore, improving therapeutic efficacy, minimizing premature drug release, and reducing systemic toxicity.

2.8. Conclusion and Future Research Perspectives

This literature review explored a selection of developments and advancements in IA therapies for OA within the past 5 years. The investigation also sheds light on the innovative strategies and therapeutic modalities developed to overcome the complexities of this prevalent and incapacitating joint disorder. It is evident that studies mostly focus on articular cartilage, but there are other hallmarks that not only affect the primary progression of the disease but also secondary developments, such as subchondral bone remodeling. A comprehensive understanding of the disease would benefit the advancement of therapies.

There have been remarkable developments in IA therapies, including viscosupplementation and sustained release injections, which involve modern methods of nanomedicine. While NPs and microparticles provide a promising platform for IA drug delivery in the treatment of OA, it is, however, noted that incorporating the drug-loaded particles into hydrogel achieves superior biological results. The examined literature offers compelling evidence supporting the effectiveness of advanced drug delivery systems, particularly NP-loaded hydrogels in OA treatment. Future studies may invest more in assessing the safety and efficacy of these in clinical trials.

2.9. References

Abbas, S., Asad, M., Bukhari, A., Adil, S., Rutherford, J. and Bilal, B., 2023. Do Platelet-Rich Plasma Injections for Knee Osteoarthritis Work?. *Cureus*, *15*(2).

Abdel-Aziz, M.A., Ahmed, H.M., El-Nekeety, A.A., Sharaf, H.A., Abdel-Aziem, S.H. and Abdel-Wahhab, M.A., 2021. Biosynthesis of gold nanoparticles for the treatment of osteoarthritis alone or in combination with Diacerein® in a rat model. *Inflammopharmacology*, *29*(3), pp.705-719.

Abou-Shamat, M.A., Stair, J.L., Kirton, S.B., Calvo-Castro, J. and Cook, M.T., 2020. A Design-of-Experiments approach to developing thermoresponsive gelators from complex polymer mixtures. *Molecular Systems Design & Engineering*, 5(9), pp.1538-1546.

Ag Seleci, D., Seleci, M., Walter, J.G., Stahl, F. and Scheper, T., 2016. Niosomes as nanoparticular drug carriers: fundamentals and recent applications. *Journal of Nanomaterials*, *2016*.

Akbarzadeh, I., Sedaghatnia, K., Bourbour, M., Moghaddam, Z., Moghtaderi, M., Samimi-Sohrforozani, E., Quazi, S. and Far, B., 2021. Niosomes: A novel targeted drug delivery system.

Akram, M.W., Jamshaid, H., Rehman, F.U., Zaeem, M., Khan, J.Z. and Zeb, A., 2022. Transfersomes: a Revolutionary nanosystem for efficient transdermal drug delivery. *AAPS PharmSciTech*, *23*, pp.1-18.

Al-Owaidi, M.F., Alkhafaji, S.L. and Mahood, A.M., 2021. Quantitative determination of dexamethasone sodium phosphate in bulk and pharmaceuticals at suitable pH values using the spectrophotometric method. *Journal of Advanced Pharmaceutical Technology & Research*, *12*(4), p.378.

Alsaif, A., Karam, M., Al-Naseem, A., Almuhanna, A., Aldubaikhi, A., Aljebreen, M. and Alfreihi, S., 2021. Diclofenac versus dexamethasone following strabismus surgery: a systematic review and meta-analysis. *Journal of Ocular Pharmacology and Therapeutics,* 37(6), pp.343-353.

Altman, R.D., Manjoo, A., Fierlinger, A., Niazi, F. and Nicholls, M., 2015. The mechanism of action for hyaluronic acid treatment in the osteoarthritic knee: a systematic review. *BMC Musculoskeletal disorders*, *16*(1), pp.1-10.

Ansari, M.Y., Khan, N.M., Ahmad, I. and Haqqi, T.M., 2018. Parkin clearance of dysfunctional mitochondria regulates ROS levels and increases survival of human chondrocytes. *Osteoarthritis and Cartilage*, *26*(8), pp.1087-1097.

Balcer, E., Sobiech, M. and Luliński, P., 2023. Molecularly imprinted carriers for diagnostics and therapy—A critical appraisal. *Pharmaceutics*, *15*(6), p.1647.

Bajpayee, A.G., Wong, C.R., Bawendi, M.G., Frank, E.H. and Grodzinsky, A.J., 2014. Avidin as a model for charge driven transport into cartilage and drug delivery for treating early stage post-traumatic osteoarthritis. *Biomaterials*, *35*(1), pp.538-549.

Bartold, K., Iskierko, Z., Borowicz, P., Noworyta, K., Lin, C.Y., Kalecki, J., Sharma, P.S., Lin, H.Y. and Kutner, W., 2022. Molecularly imprinted polymer-based extended-gate field-effect transistor (EG-FET) chemosensor for selective determination of matrix metalloproteinase-1 (MMP-1) protein. *Biosensors and Bioelectronics*, *208*, p.114203.

Basheeruddin, M., Khan, S., Ahmed, N. and Jamal, S., 2022. Effect of pH on Diclofenac–Lysozyme Interaction: Structural and Functional Aspect. *Frontiers in Molecular Biosciences*, *9*, p.872905.

Bashir, S., Hina, M., Iqbal, J., Rajpar, A.H., Mujtaba, M.A., Alghamdi, N.A., Wageh, S., Ramesh, K. and Ramesh, S., 2020. Fundamental concepts of hydrogels: Synthesis, properties, and their applications. *Polymers*, *12*(11), p.2702.

BelBruno, J.J., 2018. Molecularly imprinted polymers. *Chemical Reviews*, *119*(1), pp.94-119.

Bowman, S., Awad, M.E., Hamrick, M.W., Hunter, M. and Fulzele, S., 2018. Recent advances in hyaluronic acid based therapy for osteoarthritis. *Clinical and Translational Medicine*, *7*(1), pp.1-11.

Bruno, M.C., Cristiano, M.C., Celia, C., d'Avanzo, N., Mancuso, A., Paolino, D., Wolfram, J. and Fresta, M., 2022. Injectable drug delivery systems for osteoarthritis and rheumatoid arthritis. *ACS nano*, *16*(12), pp.19665-19690.

Bustamante-Torres, M., Romero-Fierro, D., Arcentales-Vera, B., Palomino, K., Magaña, H. and Bucio, E., 2021. Hydrogels classification according to the physical or chemical interactions and as stimuli-sensitive materials. *Gels*, *7*(4), p.182.

Çağdaş, M., Sezer, A.D. and Bucak, S., 2014. Liposomes as potential drug carrier systems for drug delivery. *Application of Nanotechnology in Drug Delivery*, *1*, pp.1-50.

Cai, Z., Zhang, H., Wei, Y., Wu, M. and Fu, A., 2019. Shear-thinning hyaluronan-based fluid hydrogels to modulate viscoelastic properties of osteoarthritis synovial fluids. *Biomaterials Science*, *7*(8), pp.3143-3157.

Campana, L. and Iredale, J., 2015. Matrix metalloproteinases and their inhibitors. *In Stellate Cells in Health and Disease* (pp. 107-124). Academic Press.

Cao, Y., Ma, Y., Tao, Y., Lin, W. and Wang, P., 2021. Intra-Articular Drug Delivery for Osteoarthritis Treatment. *Pharmaceutics*, *13*(12), pp.2166-2166.

Chang, Ming-Cheng, Ping-Fang Chiang, Yu-Jen Kuo, Cheng-Liang Peng, Kuan-Yin Chen, and Ying-Cheng Chiang. "Hyaluronan-loaded liposomal dexamethasone–diclofenac nanoparticles for local osteoarthritis treatment." *International Journal of Molecular Sciences* 22, no. 2 (2021): 665.

Charlier, E., Relic, B., Deroyer, C., Malaise, O., Neuville, S., Collée, J., Malaise, M.G. and De Seny, D., 2016. Insights on molecular mechanisms of chondrocytes death in osteoarthritis. *International Journal of Molecular Sciences*, *17*(12), p.2146.

Charlesworth, J., Fitzpatrick, J., Perera, N.K.P. and Orchard, J., 2019. Osteoarthritis-a systematic review of long-term safety implications for osteoarthritis of the knee. *BMC Musculoskeletal Disorders*, *20*, pp.1-12.

Chauhan, P. and Tyagi, B.K., 2018. Herbal novel drug delivery systems and transfersomes. *Journal of Drug Delivery and Therapeutics*, 8(3), pp.162-168.

Chen, W., Chen, F., Wu, Y., Xie, M., Lin, S., Zhao, Y., Li, Y. and Lai, Y., 2024. Defect-engineered graphene nanoribbons based molecularly imprinting voltammetric sensor for sensitive determination of interleukin-6. *International Journal of Electrochemical Science*, *19*(9), p.100706.

Chen, T., Ehnert, S., Tendulkar, G., Zhu, S., Arnscheidt, C., Aspera-Werz, R.H. and Nussler, A.K., 2020. Primary Human Chondrocytes Affected by Cigarette Smoke—Therapeutic Challenges. *International Journal of Molecular Sciences*, *21*(5), p.1901.

Chen, R.N., Kang, S.H., Li, J., Lu, L.N., Luo, X.P. and Wu, L., 2021. Comparison and recent progress of molecular imprinting technology and dummy template molecular imprinting technology. *Analytical Methods*, *13*(39), pp.4538-4556.

Chen, H., Wang, L., Zeng, X., Schwarz, H., Nanda, H.S., Peng, X. and Zhou, Y., 2021. Exosomes, a new star for targeted delivery. *Frontiers in Cell and Developmental Biology*, p.2827.

Chen, T., Weng, W., Liu, Y., Aspera-Werz, R.H., Nüssler, A.K. and Xu, J., 2021. Update on novel non-operative treatment for osteoarthritis: current status and future trends. *Frontiers in Pharmacology*, *12*, p.755230.

Choi, D.Y., Yang, J.C., Hong, S.W. and Park, J., 2022. Molecularly imprinted polymer-based electrochemical impedimetric sensors on screen-printed carbon electrodes for the detection of trace cytokine IL-1β. *Biosensors and Bioelectronics*, *204*, p.114073.

Colella, F., Garcia, J.P., Sorbona, M., Lolli, A., Antunes, B., D'Atri, D., Barré, F.P., Oieni, J., Vainieri, M.L., Zerrillo, L. and Capar, S., 2020. Drug delivery in intervertebral disc degeneration and osteoarthritis: Selecting the optimal platform for the delivery of disease-modifying agents. *Journal of Controlled Release*, *328*, pp.985-999.

Dan Dunn, J., Alvarez, L.A., Zhang, X. and Soldati, T., Reactive oxygen species and mitochondria: A nexus of cellular homeostasis. *Redox Biology*. 2015; 6: 472–85.

Deeks, J.J., Smith, L.A. and Bradley, M.D., 2002. Efficacy, tolerability, and upper gastrointestinal safety of celecoxib for treatment of osteoarthritis and rheumatoid arthritis: systematic review of randomised controlled trials. *Bmj*, *325*(7365), p.619.

DeJulius, C.R., Gulati, S., Hasty, K.A., Crofford, L.J. and Duvall, C.L., 2021. Recent Advances in Clinical Translation of Intra-Articular Osteoarthritis Drug Delivery Systems. *Advanced Therapeutics*, *4*(1), p.2000088.

Deng, C., Chen, Y., Zhao, X., Yu, L., Xiao, Y., Li, H., Zhang, Y., Ai, K., Zhou, D., Bai, X. and Gong, T., 2023. Apoptotic neutrophil membrane-camouflaged liposomes for dually targeting

synovial macrophages and fibroblasts to attenuate osteoarthritis. *ACS Applied Materials & Interfaces*, *15*(33), pp.39064-39080.

Diaz-Rodriguez, P., Marino, C., Vázquez, J.A., Caeiro-Rey, J.R. and Landin, M., 2021. Targeting joint inflammation for osteoarthritis management through stimulus-sensitive hyaluronic acid based intra-articular hydrogels. *Materials Science and Engineering: C*, *128*, p.112254.

DiDomenico, C.D., Lintz, M. and Bonassar, L.J., 2018. Molecular transport in articular cartilage—what have we learned from the past 50 years?. *Nature Reviews Rheumatology*, 14(7), pp.393-403.

Dieppe, P., 2011. Developments in osteoarthritis*. Rheumatology*, 50(2), pp.245-247

Dietl, S., Sobek, H. and Mizaikoff, B., 2021. Epitope-imprinted polymers for biomacromolecules: Recent strategies, future challenges and selected applications. *TrAC Trends in Analytical Chemistry*, *143*, p.116414.

Di Francesco, M., Bedingfield, S.K., Di Francesco, V., Colazo, J.M., Yu, F., Ceseracciu, L., Bellotti, E., Di Mascolo, D., Ferreira, M., Himmel, L.E. and Duvall, C., 2021. Shape-defined microplates for the sustained intra-articular release of dexamethasone in the management of overload-induced osteoarthritis. *ACS Applied Materials & Interfaces*, *13*(27), pp.31379-31392.

Dravid, A.A., Dhanabalan, K.M., Naskar, S., Vashistha, A., Agarwal, S., Padhan, B., Dewani, M. and Agarwal, R., 2023. Sustained release resolvin D1 liposomes are effective in the treatment of osteoarthritis in obese mice. *Journal of Biomedical Materials Research Part A*, *111*(6), pp.765-777.

Dydyk, A.M., Jain, N.K. and Gupta, M., 2023. Opioid use disorder. In *StatPearls [Internet]*. StatPearls Publishing.

El-Husseiny, H.M., Mady, E.A., El-Dakroury, W.A., Doghish, A.S. and Tanaka, R., 2023. Stimuli-responsive hydrogels: Smart state of-the-art platforms for cardiac tissue engineering. *Frontiers in Bioengineering and Biotechnology*, 11.

Foster, T.E., Puskas, B.L., Mandelbaum, B.R., Gerhardt, M.B. and Rodeo, S.A., 2009. Platelet-rich plasma: from basic science to clinical applications. *The American Journal of Sports Medicine*, *37*(11), pp.2259-2272.

Gagliardi, M., 2023. Design and development of molecularly imprinted biodegradable polymers for nanomedicine. *Advanced Industrial and Engineering Polymer Research*, *6*(4), pp.396-406.

Gagliardi, A., Paolino, D., Iannone, M., Palma, E., Fresta, M., and Cosco, D. (2018). Sodium deoxycholate-decorated zein nanoparticles for a stable colloidal drug delivery system. *Int. J. Nanomed.* 13, 601–614. doi:10.2147/IJN.S156930

Gambaro, F.M., Ummarino, A., Torres Andon, F., Ronzoni, F., Di Matteo, B. and Kon, E., 2021. Drug delivery systems for the treatment of knee osteoarthritis: a systematic review of in vivo studies. *International Journal of Molecular Sciences*, *22*(17), p.9137.

Gao, J., Xia, Z., Mary, H.B., Joseph, J., Luo, J.N. and Joshi, N., 2022. Overcoming barriers for intra-articular delivery of disease-modifying osteoarthritis drugs. *Trends in Pharmacological Sciences*.

Ge, Z., Hu, Y., Heng, B.C., Yang, Z., Ouyang, H., Lee, E.H. and Cao, T., 2006. Osteoarthritis and therapy. *Arthritis Care & Research*, *55*(3), pp.493-500.

Gerwin, N., Hops, C. and Lucke, A., 2006. Intraarticular drug delivery in osteoarthritis. *Advanced Drug Delivery Reviews*, *58*(2), pp.226-242.

Gharbavi, M., Amani, J., Kheiri-Manjili, H., Danafar, H. and Sharafi, A., 2018. Niosome: a promising nanocarrier for natural drug delivery through blood-brain barrier. *Advances in Pharmacological and Pharmaceutical Sciences*, *2018*.

Ghouri, A. and Conaghan, P.G., 2019. Update on novel pharmacological therapies for osteoarthritis. *Therapeutic Advances in Musculoskeletal Disease*, *11*, p.1759720X19864492.

Glinkowski, W.M and Tomaszewski, W., 2025. Intra-Articular Hyaluronic Acid for Knee Osteoarthritis: A Systematic Umbrella Review*. Journal of Clinical Medicine, 14(4), p.1272.*

Guo, X., Lou, J., Wang, F., Fan, D. and Qin, Z., 2022. Recent advances in nano-therapeutic strategies for osteoarthritis. *Frontiers in Pharmacology*, *13*, p.924387.

Gupta, R.C., Lall, R., Srivastava, A. and Sinha, A., 2019. Hyaluronic acid: Molecular mechanisms and therapeutic trajectory. *Frontiers in veterinary science*, p.192.

Glyn-Jones, S. and Palmer, A.J., 2015. Agricola, R.; Price, AJ; Vincent, TL; Weinans, H.; Carr. *AJ Osteoarthritis. Lancet*, *386*(9991), pp.376-387.

Gui, T., Luo, L., Chhay, B., Zhong, L., Wei, Y., Yao, L., Yu, W., Li, J., Nelson, C.L., Tsourkas, A. and Qin, L., 2022. Superoxide dismutase-loaded porous polymersomes as highly efficient antioxidant nanoparticles targeting synovium for osteoarthritis therapy. *Biomaterials*, *283*, p.121437.

Hangody, L., Szody, R., Lukasik, P., Zgadzaj, W., Lénárt, E., Dokoupilova, E., Bichovsk, D., Berta, A., Vasarhelyi, G., Ficzere, A. and Hangody, G., Intraarticular injection of a cross-linked sodium hyaluronate combined with triamcinolone hexacetonide (Cingal) to provide symptomatic relief of osteoarthritis of the knee: a randomized, double-blind, placebo-controlled multicenter clinical trial. *Cartilage*. 2018; 9 (3): 276-83.

Haupt, K., Medina Rangel, P.X. and Bui, B.T.S., 2020. Molecularly imprinted polymers: Antibody mimics for bioimaging and therapy. *Chemical Reviews*, *120*(17), pp.9554-9582.

Hawker, G.A. and Lohmander, L.S., 2021. What an earlier recognition of osteoarthritis can do for OA prevention. *Osteoarthritis and Cartilage*, *29*(12), pp.1632-1634.

He, Z., Wang, B., Hu, C. and Zhao, J., 2017. An overview of hydrogel-based intra-articular drug delivery for the treatment of osteoarthritis. *Colloids and Surfaces B: Biointerfaces*, *154*, pp.33-39.

He, L., He, T., Xing, J., Zhou, Q., Fan, L., Liu, C., Chen, Y., Wu, D., Tian, Z., Liu, B. and Rong, L., 2020. Bone marrow mesenchymal stem cell-derived exosomes protect cartilage damage and relieve knee osteoarthritis pain in a rat model of osteoarthritis. *Stem Cell Research & Therapy*, *11*, pp.1-15.

Henrotin, Y., Kurz, B. and Aigner, T., 2005. Oxygen and reactive oxygen species in cartilage degradation: friends or foes?. *Osteoarthritis and Cartilage*, *13*(8), pp.643-654.

Hintze, V., Schnabelrauch, M. and Rother, S., 2022. Chemical modification of hyaluronan and their biomedical applications. *Frontiers in Chemistry*, *10*, p.830671.

Holford, N.H., Kimko, H.C., Monteleone, J.P. and Peck, C.C., 2000. Simulation of clinical trials. *Annual review of pharmacology and toxicology*, *40*(1), pp.209-234.

Honary, S. and Zahir, F., 2013. Effect of zeta potential on the properties of nano-drug delivery systems-a review (Part 1). *Tropical Journal of Pharmaceutical Research*, *12*(2), pp.255-264.

Honary, S. and Zahir, F., 2013. Effect of zeta potential on the properties of nano-drug delivery systems-a review (Part 2). *Tropical Journal of Pharmaceutical Research*, *12*(2), pp.265-273.

Hou, W., Ye, C., Chen, M., Gao, W., Xie, X., Wu, J., Zhang, K., Zhang, W., Zheng, Y. and Cai, X., 2021. Excavating bioactivities of nanozyme to remodel microenvironment for protecting chondrocytes and delaying osteoarthritis. *Bioactive Materials*, *6*(8), pp.2439-2451.

Hu, Q., Su, H., Li, J., Lyon, C., Tang, W., Wan, M. and Hu, T.Y., 2020. Clinical applications of exosome membrane proteins. *Precision Clinical Medicine*, *3*(1), pp.54-66.

Hu, Y., Chen, X., Wang, S., Jing, Y. and Su, J., 2021. Subchondral bone microenvironment in osteoarthritis and pain. *Bone Research*, *9*(1), p.20.

Hu, B., Gao, F., Li, C., Zhang, B., An, M., Lu, M., Liu, Y. and Liu, Y., 2020. Rhein laden pH-responsive polymeric nanoparticles for treatment of osteoarthritis. *AMB Express*, *10*, pp.1-10.

Hua, S., De Matos, M.B. and Metselaar, J.M., 2018. Current trends and challenges in the clinical translation of nanoparticulate nanomedicines: pathways for translational development and commercialization. *Frontiers in Pharmacology*, *9*, p.403086.

Huang, H., Lou, Z., Zheng, S., Wu, J., Yao, Q., Chen, R., Kou, L. and Chen, D., 2022. Intra-articular drug delivery systems for osteoarthritis therapy: Shifting from sustained release to enhancing penetration into cartilage. *Drug Delivery*, *29*(1), pp.767-791.

Jabłońska-Trypuć, A., Matejczyk, M. and Rosochacki, S., 2016. Matrix metalloproteinases (MMPs), the main extracellular matrix (ECM) enzymes in collagen degradation, as a target for anticancer drugs. *Journal of Enzyme Inhibition and Medicinal Chemistry*, *31*(sup1), pp.177-183.

James, C.B. and Uhl, T.L., 2001. A review of articular cartilage pathology and the use of glucosamine sulfate. *Journal of Athletic Training*, *36*(4), p.413.

Janczura, M., Luliński, P. and Sobiech, M., 2021. Imprinting technology for effective sorbent fabrication: Current state-of-art and future prospects. *Materials*, *14*(8), p.1850.

Jin, G.Z., 2020. Current nanoparticle-based technologies for osteoarthritis therapy. *Nanomaterials,* 10(12), p.2368.

Kalluri, R. and LeBleu, V.S., 2020. The biology, function, and biomedical applications of exosomes. *Science*, *367*(6478), p.eaau6977.

Ghezzi, M., Pescina, S., Padula, C., Santi, P., Del Favero, E., Cantù, L. and Nicoli, S., 2021. Polymeric micelles in drug delivery: An insight of the techniques for their characterization and assessment in biorelevant conditions. *Journal of Controlled Release*, *332*, pp.312-336.

Gu, W., Wu, C., Chen, J. and Xiao, Y., 2013. Nanotechnology in the targeted drug delivery for bone diseases and bone regeneration. *International Journal of Nanomedicine*, pp.2305-2317.

Jahanbekam, S., Mozafari, N., Bagheri-Alamooti, A., Mohammadi-Samani, S., Daneshamouz, S., Heidari, R., Azarpira, N., Ashrafi, H. and Azadi, A., 2023. Ultrasound-responsive hyaluronic acid hydrogel of hydrocortisone to treat osteoarthritis. *International Journal of Biological Macromolecules*, *240*, p.124449.

Kakkar, V. and Narula, P., 2022. Role of molecularly imprinted hydrogels in drug delivery-A current perspective. *International Journal of Pharmaceutics*, *625*, p.121883.

Kang, C., Jung, E., Hyeon, H., Seon, S. and Lee, D., 2020. Acid-activatable polymeric curcumin nanoparticles as therapeutic agents for osteoarthritis. *Nanomedicine: Nanotechnology, Biology and Medicine*, 23, p.102104.

Kang, L.J., Yoon, J., Rho, J.G., Han, H.S., Lee, S., Oh, Y.S., Kim, H., Kim, E., Kim, S.J., Lim, Y.T. and Park, J.H., 2021. Self-assembled hyaluronic acid nanoparticles for osteoarthritis treatment. *Biomaterials*, 275, p.120967.

Kazi, K.M., Mandal, A.S., Biswas, N., Guha, A., Chatterjee, S., Behera, M. and Kuotsu, K., 2010. Niosome: a future of targeted drug delivery systems. *Journal of Advanced Pharmaceutical Technology & research*, *1*(4), p.374.

Kim, S.E., Choi, S.J., Park, K., Kim, H.J., Song, G.G. and Jung, J.H., 2022. Intra-articular injection of rebamipide-loaded nanoparticles attenuate disease progression and joint destruction in osteoarthritis rat model: a pilot study. *Cartilage*, *13*(1), p.19476035211069250.

Kleemann, R.U., Krocker, D., Cedraro, A., Tuischer, J. and Duda, G.N., 2005. Altered cartilage mechanics and histology in knee osteoarthritis: relation to clinical assessment (ICRS Grade). *Osteoarthritis and Cartilage*, *13*(11), pp.958-963.

Kou, L., Xiao, S., Sun, R., Bao, S., Yao, Q. and Chen, R., 2019. Biomaterial-engineered intra-articular drug delivery systems for osteoarthritis therapy. *Drug Delivery*, *26*(1), pp.870-885.

Kou, L., Huang, H., Tang, Y., Sun, M., Li, Y., Wu, J., Zheng, S., Zhao, X., Chen, D., Luo, Z. and Zhang, X., 2022. Opsonized nanoparticles target and regulate macrophage polarization

for osteoarthritis therapy: A trapping strategy. *Journal of Controlled Release*, *347*, pp.237-255.

Kudur, M.H. and Hulmani, M., 2013. Rebamipide: A novel agent in the treatment of recurrent aphthous ulcer and Behcet's syndrome. *Indian Journal of Dermatology*, *58*(5), pp.352-354.

Kumar, Shreedevi, Isaac M. Adjei, Shannon B. Brown, Olivia Liseth, and Blanka Sharma. "Manganese dioxide nanoparticles protect cartilage from inflammation-induced oxidative stress." *Biomaterials* 224 (2019): 119467.

Kumar, A., Kashap, S., Mazahir, F., Sharma, R. and Yadav, A.K., 2024. Unveiling the potential of molecular imprinting polymer-based composites in the discovery of advanced drug delivery carriers. *Drug Discovery Today*, p.104164.

Kung, Y., Chien, W.C., Shen, H.H., Chen, S.L., Yu, W.L., Wang, Y.C., Chen, W.S. and Wu, C.H., 2023. Potential of thermoresponsive hydrogel as an alternative therapy for rat knee osteoarthritis. *Journal of Biomaterials Applications*, *38*(5), pp.707-718.

Lee, M.H., Lin, C.C., Kutner, W., Thomas, J.L., Lin, C.Y., Iskierko, Z., Ku, Y.S., Lin, C.Y., Borowicz, P., Sharma, P.S. and Lan, Y.W., 2023. Peptide-imprinted conductive polymer on continuous monolayer molybdenum disulfide transferred electrodes for electrochemical sensing of Matrix Metalloproteinase-1 in lung cancer culture medium. *Biosensors and Bioelectronics: X*, *13*, p.100258.

Lei, Y., Wang, Y., Shen, J., Cai, Z., Zhao, C., Chen, H., Luo, X., Hu, N., Cui, W. and Huang, W., 2022. Injectable hydrogel microspheres with self-renewable hydration layers alleviate osteoarthritis. *Science Advances*, *8*(5), p.eabl6449.

Lei, Y., Zhang, Q., Kuang, G., Wang, X., Fan, Q. and Ye, F., 2022. Functional biomaterials for osteoarthritis treatment: from research to application. *Smart Medicine*, *1*(1), p.e20220014.

Leone, G., Consumi, M., Pepi, S., Pardini, A., Bonechi, C., Tamasi, G., Donati, A., Lamponi, S., Rossi, C. and Magnani, A., 2020. Enriched Gellan Gum hydrogel as visco-supplement. *Carbohydrate Polymers*, *227*, p.115347.

Leung, G.J., Rainsford, K.D. and Kean, W.F., 2014. Osteoarthritis of the hand I: aetiology and pathogenesis, risk factors, investigation and diagnosis. *Journal of Pharmacy and Pharmacology*, 66(3), pp.339-346.

Loeser, R.F., 2010. Age-related changes in the musculoskeletal system and the development of osteoarthritis. *Clinics in Geriatric Medicine*, *26*(3), pp.371-386.

Li, S., Cao, P., Chen, T. and Ding, C., 2023. Latest insights in disease-modifying osteoarthritis drugs development. *Therapeutic Advances in Musculoskeletal Disease*, *15*, p.1759720X231169839.

Li, J., Liu, N., Huang, Z., Wang, W., Hou, D. and Wang, W., 2021. Intra-articular injection of loaded sPL sustained-release microspheres inhibits osteoarthritis and promotes cartilaginous repairs. *Journal of Orthopaedic Surgery and Research*, 16, pp.1-9.

Li, X., Dai, B., Guo, J., Zheng, L., Guo, Q., Peng, J., Xu, J. and Qin, L., 2021. Nanoparticle–cartilage interaction: pathology-based intra-articular drug delivery for osteoarthritis therapy. *Nano-micro Letters*, *13*(1), p.149.

Li, X., Duan, H., Wang, G., Li, M., Zhou, L., Jiang, X., Hu, M., Fan, X., Shi, T. and Gao, F., 2024. Anti-osteoarthritis effects of injectable hyaluronic acid hydrogel loaded with platelet lysate and cerium oxide nanoparticle by regulating TNF-α: An in vitro model. *Arabian Journal of Chemistry*, *17*(2), p.105488.

Liang, Y., Xu, X., Xu, L., Iqbal, Z., Ouyang, K., Zhang, H., Wen, C., Duan, L. and Xia, J., 2022. Chondrocyte-specific genomic editing enabled by hybrid exosomes for osteoarthritis treatment. *Theranostics*, *12*(11), p.4866.

Liang, Q., Cheng, Z. and Qin, L., 2024. Advanced nanoparticles in osteoarthritis treatment. *Biomaterials Translational*, *5*(2), p.95.

Lin, T., Zhao, Y., Chen, J., Wu, C., Li, Z., Cao, Y., Lu, R., Zhang, J., Zhao, C. and Lu, Y., 2022. Carboxymethyl chitosan-assisted MnOx nanoparticles: Synthesis, characterization, detection and cartilage repair in early osteoarthritis. *Carbohydrate Polymers*, *294*, p.119821.

Liu, P., Gu, L., Ren, L., Chen, J., Li, T., Wang, X., Yang, J., Chen, C. and Sun, L., 2019. Intra-articular injection of etoricoxib-loaded PLGA-PEG-PLGA triblock copolymeric nanoparticles attenuates osteoarthritis progression. *American Journal of Translational Research*, 11(11), p.6775.

Liu, K., Zhang, D. and Wang, W., 2021. Nanoparticle-Based Drug Delivery System—A Target Strategy for Osteoarthritis Treatment. *Journal of Nanomaterials*, *2021*, pp.1-15.

Liu, L., Tang, H. and Wang, Y., 2023. Nanotechnology-Boosted Biomaterials for Osteoarthritis Treatment: Current Status and Future Perspectives. *International Journal of Nanomedicine*, pp.4969-4983.

Liu, Y., Wang, L., Li, H., Zhao, L., Ma, Y., Zhang, Y., Liu, J. and Wei, Y., 2024. Rigorous recognition mode analysis of molecularly imprinted polymers—Rational design, challenges, and opportunities. *Progress in Polymer Science*, p.101790.

Luliński, P., 2017. Molecularly imprinted polymers based drug delivery devices: A way to application in modern pharmacotherapy. A review. *Materials Science and Engineering: C*, *76*, pp.1344-1353.

Lusina, A. and Cegłowski, M., 2022. Molecularly Imprinted Polymers as State-of-the-Art Drug Carriers in Hydrogel Transdermal Drug Delivery Applications. *Polymers*, *14*(3), p.640.

Johnson, K., Zhu, S., Tremblay, M.S., Payette, J.N., Wang, J., Bouchez, L.C., Meeusen, S., Althage, A., Cho, C.Y., Wu, X. and Schultz, P.G., 2012. A stem cell–based approach to cartilage repair. Science, 336(6082), pp.717-721.

Jones, M.C. and Leroux, J.C., 1999. Polymeric micelles–a new generation of colloidal drug carriers. *European Journal of Pharmaceutics and Biopharmaceutics*, *48*(2), pp.101-111.

Ma, D., 2019. Hybrid nanoparticles: an introduction. In *Noble metal-metal oxide hybrid nanoparticles* (pp. 3-6). Woodhead Publishing.

Mak, I.W., Evaniew, N. and Ghert, M., 2014. Lost in translation: animal models and clinical trials in cancer treatment. *American Journal of Translational Research*, *6*(2), p.114.

Man, G.S. and Mologhianu, G., 2014. Osteoarthritis pathogenesis–a complex process that involves the entire joint. *Journal of Medicine and Life*, *7*(1), p.37.

Mancipe Castro, L.M., Sequeira, A., García, A.J. and Guldberg, R.E., 2020. Articular cartilage- and synoviocyte-binding poly (ethylene glycol) nanocomposite microgels as intra-articular drug delivery vehicles for the treatment of osteoarthritis. *ACS Biomaterials Science & Engineering*, *6*(9), pp.5084-5095.

Martel-Pelletier, J., Boileau, C., Pelletier, J.P. and Roughley, P.J., 2008. Cartilage in normal and osteoarthritis conditions. *Best Practice & research Clinical Rheumatology*, *22*(2), pp.351-384.

Marwah, M.K., Shokr, H., Sanchez-Aranguren, L., Badhan, R.K.S., Wang, K. and Ahmad, S., 2022. Transdermal delivery of a hydrogen sulphide donor, ADT-OH using aqueous gel formulations for the treatment of impaired vascular function: an ex vivo study. *Pharmaceutical Research*, *39*(2), pp.341-352.

Masjedi, M. and Montahaei, T., 2021. An illustrated review on nonionic surfactant vesicles (niosomes) as an approach in modern drug delivery: Fabrication, characterization, pharmaceutical, and cosmetic applications. *Journal of Drug Delivery Science and Technology*, *61*, p.102234.

Mashal, M., Attia, N., Grijalvo, S., Eritja, R., Puras, G. and Pedraz, J.L., 2023. Stability of polymeric cationic niosomes and their plasmid DNA-based complexes as gene delivery carriers. *Drug delivery*, *30*(1), p.2219420.

Maqbool, M., Fekadu, G., Jiang, X., Bekele, F., Tolossa, T., Turi, E., Fetensa, G. and Fanta, K., 2021. An up to date on clinical prospects and management of osteoarthritis. *Annals of Medicine and Surgery*, *72*, p.103077.

Meng, Z., Liu, J. and Zhou, N., 2023. Efficacy and safety of the combination of glucosamine and chondroitin for knee osteoarthritis: a systematic review and meta-analysis. *Archives of Orthopaedic and Trauma Surgery*, 143(1), pp.409-421.

Metselaar, J.M. and Lammers, T., 2020. Challenges in nanomedicine clinical translation. *Drug Delivery and Translational Research*, *10*, pp.721-725.

Milošev, I., Levašič, V., Vidmar, J., Kovač, S. and Trebše, R., 2017. pH and metal concentration of synovial fluid of osteoarthritic joints and joints with metal replacements. *Journal of Biomedical Materials Research Part B: Applied Biomaterials*, 105(8), pp.2507-2515.

Mohanraj, V.J. and Chen, Y.J.T.J.O.P.R., 2006. Nanoparticles-a review. *Tropical Journal of Pharmaceutical Research*, *5*(1), pp.561-573.

Mou, D., Yu, Q., Zhang, J., Zhou, J., Li, X., Zhuang, W. and Yang, X., 2021. Intra-articular injection of chitosan-based supramolecular hydrogel for osteoarthritis treatment. *Tissue Engineering and Regenerative Medicine*, *18*, pp.113-125.

Mota, A.H., Direito, R., Carrasco, M.P., Rijo, P., Ascensão, L., Viana, A.S., Rocha, J., Eduardo-Figueira, M., Rodrigues, M.J., Custódio, L. and Kuplennik, N., 2019. Combination of

hyaluronic acid and PLGA particles as hybrid systems for viscosupplementation in osteoarthritis. *International Journal of Pharmaceutics*, *559*, pp.13-22.

Mushenkova, N.V., Nikiforov, N.G., Shakhpazyan, N.K., Orekhova, V.A., Sadykhov, N.K. and Orekhov, A.N., 2022. Phenotype diversity of macrophages in osteoarthritis: implications for development of macrophage modulating therapies. *International Journal of Molecular Sciences*, 23(15), p.8381.

Musial, C., Kuban-Jankowska, A. and Gorska-Ponikowska, M., 2020. Beneficial properties of green tea catechins. *International Journal of Molecular Sciences*, *21*(5), p.1744.

Orchard, J.W., 2020. Is there a place for intra-articular corticosteroid injections in the treatment of knee osteoarthritis?. *Bmj*, *368*.

Nelson, K.M., Dahlin, J.L., Bisson, J., Graham, J., Pauli, G.F. and Walters, M.A., 2017. The essential medicinal chemistry of curcumin: miniperspective. *Journal of Medicinal Chemistry*, *60*(5), pp.1620-1637.

Neumann, M., di Marco, G., Iudin, D., Viola, M., van Nostrum, C.F., van Ravensteijn, B.G. and Vermonden, T., 2023. Stimuli-Responsive Hydrogels: The Dynamic Smart Biomaterials of Tomorrow. *Macromolecules*, *56*(21), pp.8377-8392.

Nunes, D., Andrade, S., Ramalho, M.J., Loureiro, J.A. and Pereira, M.C., 2022. Polymeric nanoparticles-loaded hydrogels for biomedical applications: A systematic review on in vivo findings. *Polymers*, *14*(5), p.1010.

Opatha, S.A.T., Titapiwatanakun, V. and Chutoprapat, R., 2020. Transfersomes: A promising nanoencapsulation technique for transdermal drug delivery. *Pharmaceutics*, *12*(9), p.855.

Palma, E., Pasqua, A., Gagliardi, A., Britti, D., Fresta, M., and Cosco, D. (2018). Antileishmanial activity of amphotericin B-loaded-PLGA nanoparticles: an overview. *Materials* 11, E1167. doi:10.3390/ma11071167

Pande, S., 2023. Liposomes for drug delivery: review of vesicular composition, factors affecting drug release and drug loading in liposomes. *Artificial Cells, Nanomedicine, and Biotechnology*, *51*(1), pp.428-440.

Parisi, O.I., Ruffo, M., Scrivano, L., Malivindi, R., Vassallo, A. and Puoci, F., 2018. Smart bandage based on molecularly imprinted polymers (MIPs) for diclofenac controlled release. *Pharmaceuticals*, *11*(4), p.92.

Parhi, R., 2017. Cross-linked hydrogel for pharmaceutical applications: a review. *Advanced Pharmaceutical Bulletin*, *7*(4), pp.515-530.

Park, J.Y., Kwon, S., Kim, S.H., Kang, Y.J. and Khang, D., 2020. Triamcinolone–Gold Nanoparticles Repolarize Synoviocytes and Macrophages in an Inflamed Synovium. *ACS Applied Materials & Interfaces*, 12(35), pp.38936-38949.

Pavelka, K., Bruyere, O., Cooper, C., Kanis, J.A., Leeb, B.F., Maheu, E., Martel-Pelletier, J., Monfort, J., Pelletier, J.P., Rizzoli, R. and Reginster, J.Y., 2016. Diacerein: benefits, risks and place in the management of osteoarthritis. An opinion-based report from the ESCEO. *Drugs & Aging*, *33*, pp.75-85.

Peng, Y., Ao, M., Dong, B., Jiang, Y., Yu, L., Chen, Z., Hu, C. and Xu, R., 2021. Anti-inflammatory effects of curcumin in the inflammatory diseases: Status, limitations and countermeasures. *Drug design, Development and Therapy*, pp.4503-4525.

Peppas, N.A. and Hoffman, A.S., 2020. Hydrogels. In *Biomaterials Science* (pp. 153-166). Academic Press.

Pérez, S. and Rius-Pérez, S., 2022. Macrophage polarization and reprogramming in acute inflammation: a redox perspective. *Antioxidants*, *11*(7), p.1394.

Rai, S., Pandey, V., Rai, G., Pharmaceutics, R. and Khasla, R., Transfersomes as versatile and flexible nano-vesicular carriers in skin cancer therapy: the state of the art. *Nano Rev Exp*. 2017; 8 (1): 1325708.

Rai, M.F. and Pham, C.T., 2018. Intra-articular drug delivery systems for joint diseases. *Current opinion in pharmacology*, *40*, pp.67-73.

Rajan, R., Jose, S., Mukund, V.B. and Vasudevan, D.T., 2011. Transferosomes-A vesicular transdermal delivery system for enhanced drug permeation. *Journal of Advanced Pharmaceutical Technology & Research*, *2*(3), p.138.

Ramesh, M. and Sakthishobana, K., 2021. Significance of biosurfactants in oil recovery and bioremediation of crude oil. In *Green Sustainable Process for Chemical and Environmental Engineering and Science* (pp. 211-226). Elsevier.

Rasheed, M.S., Ansari, S.F. and Shahzadi, I., 2022. Formulation, characterization of glucosamine loaded transfersomes and in vivo evaluation using papain induced arthritis model. *Scientific Reports*, *12*(1), p.19813.

Rodriguez-Merchan, E.C., 2023. The current role of disease-modifying osteoarthritis drugs. *Archives of Bone and Joint Surgery*, *11*(1), p.11.

Rother, M., Seidel, E.J., Clarkson, P.M., Mazgareanu, S., Vierl, U. and Rother, I., 2009. Efficacy of epicutaneous Diractin®(ketoprofen in Transfersome® gel) for the treatment of pain related to eccentric muscle contractions. *Drug Design, Development and therapy*, pp.143-149.

Rothenfluh, D.A., Bermudez, H., O'Neil, C.P. and Hubbell, J.A., 2008. Biofunctional polymer nanoparticles for intra-articular targeting and retention in cartilage. *Nature materials*, *7*(3), pp.248-254.Salgado, C., Jordan, O. and Allémann, E., 2021. Osteoarthritis in vitro models: applications and implications in development of intra-articular drug delivery systems. *Pharmaceutics*, *13*(1), p.60.

Sarkar, A., Carvalho, E., D'souza, A.A. and Banerjee, R., 2019. Liposome-encapsulated fish oil protein-tagged gold nanoparticles for intra-articular therapy in osteoarthritis. *Nanomedicine*, *14*(7), pp.871-887.

Schippinger, G., Prüller, F., Divjak, M., Mahla, E., Fankhauser, F., Rackemann, S. and Raggam, R.B., 2015. Autologous platelet-rich plasma preparations: influence of nonsteroidal anti-inflammatory drugs on platelet function. *Orthopaedic Journal of Sports Medicine*, *3*(6), p.2325967115588896.

Seo, B.B., Kwon, Y., Kim, J., Hong, K.H., Kim, S.E., Song, H.R., Kim, Y.M. and Song, S.C., 2022. Injectable polymeric nanoparticle hydrogel system for long-term anti-inflammatory effect to treat osteoarthritis. *Bioactive Materials*, *7*, pp.14-25.

Sercombe, L., Veerati, T., Moheimani, F., Wu, S.Y., Sood, A.K. and Hua, S., 2015. Advances and challenges of liposome assisted drug delivery. *Frontiers in Pharmacology*, *6*, p.286.

Shewaiter, M.A., Selim, A.A., Rashed, H.M., Moustafa, Y.M. and Gad, S., 2023. Niosomal formulation of mefenamic acid for enhanced cancer targeting; preparation, characterization and biodistribution study using radiolabeling technique. *Journal of Cancer Research and Clinical Oncology*, *149*(20), pp.18065-18080.

Sinusas, K., 2012. Osteoarthritis: diagnosis and treatment. *American Family Physician*, *85*(1), pp.49-56.

Slowing, I.I., Trewyn, B.G., Giri, S. and Lin, V.Y., 2007. Mesoporous silica nanoparticles for drug delivery and biosensing applications. *Advanced functional materials*, *17*(8), pp.1225-1236.Sophia Fox, A.J., Bedi, A. and Rodeo, S.A., 2009. The basic science of articular cartilage: structure, composition, and function. *Sports Health*, *1*(6), pp.461-468.

Smith, P.A., 2016. Intra-articular autologous conditioned plasma injections provide safe and efficacious treatment for knee osteoarthritis: an FDA-sanctioned, randomized, double-blind, placebo-controlled clinical trial. *The American Journal of Sports Medicine*, *44*(4), pp.884-891.

Sobiech, M. and Luliński, P., 2024. Molecularly imprinted solid phase extraction–recent strategies, future prospects and forthcoming challenges in complex sample pretreatment process. *TrAC Trends in Analytical Chemistry*, p.117695.

Stack, M., Parikh, D., Wang, H., Wang, L., Xu, M., Zou, J., Cheng, J. and Wang, H., 2019. Electrospun nanofibers for drug delivery. *In Electrospinning: Nanofabrication and Applications* (pp. 735-764). William Andrew Publishing.

Strizova, Z., Benesova, I., Bartolini, R., Novysedlak, R., Cecrdlova, E., Foley, L.K. and Striz, I., 2023. M1/M2 macrophages and their overlaps–myth or reality?. *Clinical Science*, *137*(15), pp.1067-1093.

Su, H., Ren, H., Maimaitikelimu, X., Xu, J., Bian, F. and Wang, H., 2024. Molecularly and ionically imprinted polymers-based chemical sensors in chemical assays. *Chemical Engineering Journal*, p.156315.

Su, F., Tong, M.W., Lansdown, D.A., Luke, A., Ma, C.B., Feeley, B.T., Majumdar, S. and Zhang, A.L., 2023. Leukocyte-poor platelet-rich plasma injections improve cartilage T1ρ and T2 and patient-reported outcomes in mild-to-moderate knee osteoarthritis. *Arthroscopy, Sports Medicine, and Rehabilitation*, *5*(3), pp.e817-e825.

Tabanelli R, Brogi S, Calderone V. Improving Curcumin Bioavailability: Current Strategies and Future Perspectives. *Pharmaceutics.* 2021 Oct 17;13(10):1715. doi: 10.3390/pharmaceutics13101715. PMID: 34684008; PMCID: PMC8540263.

Tanvir, E.M., Hossen, M.S., Hossain, M.F., Afroz, R., Gan, S.H., Khalil, M.I. and Karim, N., 2017. Antioxidant properties of popular turmeric (Curcuma longa) varieties from Bangladesh. *Journal of Food Quality*, *2017*.

Teng, H., Chen, S., Fan, K., Wang, Q., Xu, B., Chen, D., Zhao, F. and Wang, T., 2023. Dexamethasone Liposomes Alleviate Osteoarthritis in miR-204/-211-Deficient Mice by Repolarizing Synovial Macrophages to M2 Phenotypes. *Molecular Pharmaceutics*, *20*(8), pp.3843-3853.

Testa, G., Giardina, S.M.C., Culmone, A., Vescio, A., Turchetta, M., Cannavò, S. and Pavone, V., 2021. Intra-articular injections in knee osteoarthritis: A review of literature. *Journal of Functional Morphology and Kinesiology*, *6*(1), p.15.

Theocharis, A.D., Skandalis, S.S., Gialeli, C. and Karamanos, N.K., 2016. Extracellular matrix structure. *Advanced Drug Delivery Reviews*, *97*, pp.4-27.

Towheed, T., Maxwell, L., Anastassiades, T.P., Shea, B., Houpt, J.B., Welch, V., Hochberg, M.C. and Wells, G.A., 2005. Glucosamine therapy for treating osteoarthritis. *Cochrane Database of Systematic Reviews*, (2).

Tran, P.H., Xiang, D., Tran, T.T., Yin, W., Zhang, Y., Kong, L., Chen, K., Sun, M., Li, Y., Hou, Y. and Zhu, Y., 2020. Exosomes and nanoengineering: a match made for precision therapeutics. *Advanced Materials*, *32*(18), p.1904040.

Tsubosaka, M., Kihara, S., Hayashi, S., Nagata, J., Kuwahara, T., Fujita, M., Kikuchi, K., Takashima, Y., Kamenaga, T., Kuroda, Y. and Takeuchi, K., 2020. Gelatin hydrogels with eicosapentaenoic acid can prevent osteoarthritis progression in vivo in a mouse model. *Journal of Orthopaedic Research*®, 38(10), pp.2157-2169.

Vedadghavami, A., Zhang, C. and Bajpayee, A.G., 2020. Overcoming negatively charged tissue barriers: Drug delivery using cationic peptides and proteins. *Nano Today*, *34*, p.100898.

Venkatesh, S., Saha, J., Pass, S. and Byrne, M.E., 2008. Transport and structural analysis of molecular imprinted hydrogels for controlled drug delivery. *European Journal of Pharmaceutics and Biopharmaceutics*, *69*(3), pp.852-860.

Walve, J.R., Bakliwal, S.R., Rane, B.R. and Pawar, S.P., 2011. Transfersomes: a surrogated carrier for transdermal drug delivery system.

Wang, E.C. and Wang, A.Z., 2014. Nanoparticles and their applications in cell and molecular biology. *Integrative Biology*, *6*(1), pp.9-26.

Wang, X., Zhao, H., Liu, Z., Wang, Y., Lin, D., Chen, L., Dai, J., Lin, K. and Shen, S.G., 2021. Polydopamine nanoparticles as dual-task platform for osteoarthritis therapy: A scavenger for

reactive oxygen species and regulator for cellular powerhouses. *Chemical Engineering Journal*, *417*, p.129284.

Wei, P., Song, R., Chen, C., Li, Z., Zhu, Z. and Li, S., 2019. A pH-responsive molecularly imprinted hydrogel for dexamethasone release. *Journal of Inorganic and Organometallic Polymers and Materials*, *29*, pp.659-666.

Wei, Y., Yan, L., Luo, L., Gui, T., Jang, B., Amirshaghaghi, A., You, T., Tsourkas, A., Qin, L. and Cheng, Z., 2021. Phospholipase A2 inhibitor–loaded micellar nanoparticles attenuate inflammation and mitigate osteoarthritis progression. *Science Advances*, *7*(15), p.eabe6374.

Wen, J., Li, H., Dai, H., Hua, S., Long, X., Li, H., Ivanovski, S. and Xu, C., 2023. Intra-articular nanoparticles based therapies for osteoarthritis and rheumatoid arthritis management. *Materials Today Bio*, *19*, p.100597.

Wilczewska, A.Z., Niemirowicz, K., Markiewicz, K.H. and Car, H., 2012. Nanoparticles as drug delivery systems. *Pharmacological Reports*, *64*(5), pp.1020-1037.

Xiong, F., Qin, Z., Chen, H., Lan, Q., Wang, Z., Lan, N., Yang, Y., Zheng, L., Zhao, J. and Kai, D., 2020. pH-responsive and hyaluronic acid-functionalized metal–organic frameworks for therapy of osteoarthritis. *Journal of Nanobiotechnology*, 18(1), pp.1-14.

Xu, X., Liang, Y., Li, X., Ouyang, K., Wang, M., Cao, T., Li, W., Liu, J., Xiong, J., Li, B. and Xia, J., 2021. Exosome-mediated delivery of kartogenin for chondrogenesis of synovial fluid-derived mesenchymal stem cells and cartilage regeneration. *Biomaterials*, *269*, p.120539.

Yang, J.C., Lim, S.J., Cho, C.H., Hazarika, D., Park, J.P. and Park, J., 2023. Determination of tumor necrosis factor-α in serum using extended-gate field-effect transistor-based chemosensors with molecularly imprinted polymer-coated gold dendrites. *Sensors and Actuators B: Chemical*, *390*, p.133982.

Yazici, Y., McAlindon, T.E., Fleischmann, R., Gibofsky, A., Lane, N.E., Kivitz, A.J., Skrepnik, N., Armas, E., Swearingen, C.J., DiFrancesco, A. and Tambiah, J.R.S., 2017. A novel Wnt pathway inhibitor, SM04690, for the treatment of moderate to severe osteoarthritis of the knee: results of a 24-week, randomized, controlled, phase 1 study. *Osteoarthritis and Cartilage*, *25*(10), pp.1598-1606.

Yellin, R.A., Hudák, A., Letoha, T. and Green, B.S., 2023. Tumor necrosis factor alpha (TNFα)-binding imprinted polymers. A non-systemic therapeutic approach for inflammatory bowel diseases. *European Journal of Medicinal Chemistry Reports*, *8*, p.100106.

Yuan, Z., Jiang, D., Yang, M., Tao, J., Hu, X., Yang, X. and Zeng, Y., 2024. Emerging roles of macrophage polarization in osteoarthritis: Mechanisms and therapeutic strategies. *Orthopaedic Surgery*, *16*(3), pp.532-550.

Zahedi, P., Fallah-Darrehchi, M., Nadoushan, S.A., Aeinehvand, R., Bagheri, L. and Najafi, M., 2017. Morphological, thermal and drug release studies of poly (methacrylic acid)-based molecularly imprinted polymer nanoparticles immobilized in electrospun poly (ε-caprolactone) nanofibers as dexamethasone delivery system. *Korean Journal of Chemical Engineering*, *34*, pp.2110-2118.

Zito, G., Siciliano, G., Seifalinezhad, A., Miranda, B., Lanzio, V., Schwartzberg, A., Gigli, G., Turco, A., Rendina, I., Mocella, V. and Primiceri, E., 2024. Molecularly Imprinted Polymer Sensor Empowered by Bound States in the Continuum for Selective Trace-Detection of TGF-beta. *Advanced Science*, p.2401843.

Zhang, D., Liu, D., Zhang, J., Fong, C. and Yang, M., 2014. Gold nanoparticles stimulate differentiation and mineralization of primary osteoblasts through the ERK/MAPK signaling pathway. *Materials Science and Engineering: C*, *42*, pp.70-77.

Zhang, J., Rong, Y., Luo, C. and Cui, W., 2020. Bone marrow mesenchymal stem cell-derived exosomes prevent osteoarthritis by regulating synovial macrophage polarization. *Aging (Albany NY)*, *12*(24), p.25138.

Zielińska, A., Carreiró, F., Oliveira, A.M., Neves, A., Pires, B., Venkatesh, D.N., Durazzo, A., Lucarini, M., Eder, P., Silva, A.M. and Santini, A., 2020. Polymeric nanoparticles: production, characterization, toxicology and ecotoxicology. *Molecules*, *25*(16), p.3731.

Zhu, X., Chan, Y.T., Yung, P.S., Tuan, R.S. and Jiang, Y., 2021. Subchondral bone remodeling: a therapeutic target for osteoarthritis. *Frontiers in Cell and Developmental biology*, *8*, p.607764.

CHAPTER THREE

The Design and Development of a Dexamethasone-Tranfersome-PF-127/HA Stimuli-responsive Hydrogel for Intra-articular Therapy in Osteoarthritis

3.1. Introduction

IA administration has gained prominence over systemic administration for various reasons. Such treatment is site-specific, minimizing systemic exposure, therefore significantly reducing the off-target effects of drugs. This approach ensures rapid drug action and improved residence time within the joint compared to systemically administered drugs (Jones *et al*., 2019). However, IA treatment face formidable obstacles due to the hostile environment of the joint where therapeutics are often lost to systemic circulation upon injection because of drainage via the venules and lymphatic vessels in the synovial membrane (Evans *et al*., 2014). The short residence time consequently mandates an increased frequency of injections, which is, however, not cost-effective (Jones *et al.*, 2019; Rhon *et al*., 2022). Moreover, the number of IA injections is restricted to minimize the risk of infection (Ayhan *et al*., 2014; Jung *et al*., 2020).

With advancements in nanotechnology, NP-based therapy offers a promising platform to address obstacles associated with current IA treatment therapies. NPs are nanoconstructs with an overall dimension of under 100 nm (Murthy, 2007). NPs can protect encapsulated IA-administrated drugs from degradation; help stabilize the incorporated drugs, and attain controlled and sustained drug release, leading to increased retention times. This strategy could also improve the side effect profile of the administered OA treatment regimens (Wen *et al,* 2023).

Concurrently, hydrogels - 3D cross-linked polymer matrices - possess unique abilities including their ability to mimic the structure of the ECM and respond to external stimuli, making them an appealing platform for OA therapeutic interventions (González-Díaz and Varghese, 2016; El-Husseiny *et al*., 2023). Additionally, hydrogels can imbibe and retain large volumes of biological fluids (Geckil *et al*., 2010). When combined with drug-loaded NPs, hydrogels have the potential to alleviate OA by replenishing joint fluid and acting as lubricants to reduce bone-to-bone friction. The reduction in joint friction, in turn, relieves pain while the drug-loaded NP-hydrogel system offers a sustained drug release achieving enhanced therapeutic effects (Wang *et al*., 2022; Zhao *et al.*, 2022).

Responsiveness to the stimuli, particularly the thermo-responsiveness of hydrogels, is a crucial property in OA therapy as it may aid the course for targeted delivery. In this study, we exploited the thermo-responsive properties of PF-127 in combination with HMW HA. PF-127, a biocompatible surfactant polyol, is readily water soluble in low temperatures and can undergo gelation at temperatures close to physiological conditions (Kushan and Senses, 2021; García-Couce *et al*., 2022). PF-127 has been extensively utilized for controlled drug release mainly due to its low immunogenicity and minimal toxicity. However, it has poor mechanical strength and a typically short drug-release profile (Chung *et al*., 2009; Li *et al.,* 2023). Nevertheless, these setbacks have been combated by combining PF-127 with complimentary polymers such as HA and chitosan (García-Couce *et al*.,2022).

HA, an endogenous glycosaminoglycan, is responsible for lubrication in the joint, reducing bone-to-bone friction, alleviating pain and inflammation (Gupta *et al*., 2019). Notably, there is a decline in concentrations of HA in OA joints compared to healthy joints (Liu et al., 2021). Agents such as corticosteroids and HA are indicated in OA for inflammation and viscosuplementation, respectively. Building on this background, this study aimed to address the shortcomings of current OA treatments. Specific lipid-based nanocarriers, tNPs, were employed to encapsulate a glucocorticoid drug, DEX, into a stimuli-responsive PF-127/HA hydrogel for IA administration in OA treatment.

The tNPs are ultra-deformable lipid-based nano-vesicular systems that consist of phospholipids and EAs, resulting in at least one inner aqueous compartment (Rai *et al*., 2017; Opatha *et al*., 2020). Hydrophobic drugs are lodged within the lipid bilayer while hydrophilic drugs are entrapped within the aqueous compartment (Fernández-García *et al*., 2020). The flexibility of tNPs is crucial to their ability to temporarily distort and intricately permeate through the ECM without compromising the integrity of its cargo. This allows them to reach their targets unblemished, thus effectively assisting with controlled and targeted drug delivery (Rajan *et al*, 2011). The degree of deformability in tNPs is dependent on the ratio of EA to lipid mixture. EAs are amphiphilic molecules known to compromise lipophilic and hydrophilic moieties; they help with increasing solubility and entrapping a wide range of drugs. EAs bring about membrane ultra-flexibility by acting as membrane destabilizing factors (Opatha *et al*., 2020). Co-surfactants have been previously used as EAs.

In this study, soya phosphatidylcholine was used as the primary phospholipid, while sodium deoxycholate and polysorbate 80 were selected as EAs. These co-surfactants are water-soluble. Water-soluble surfactants prevent tNP agglomeration by forming a perseverative layer on the

surface of tNPs, thereby stabilizing the formulation (Khan *et al.,* 2021). The presence of the hydrophilic head group may reduce the high interfacial tension between the tNPs, thus resulting in consistent PDIs resulting in the vesicles (Misono, 2019). Additionally, high surfactant concentrations have been associated with a small polydispersity index (PDI). A small PDI is indicative of a consistent size distribution resulting in a homogenous formulation.

EAs affect vesicle deformability, size, and entrapment efficiency (Moawad and Salem, 2017). Interestingly, at concentrations exceeding 15%, EAs induce micelle formation rather than tNPs and often become toxic at concentrations over 25% (Jain *et al*., 2003; (Rai *et al*., 2017; Opatha *et al*., 2020). An optimal balance of ratio is important for the formulation of tNPs desired for this study. polysorbate 80 and sodium deoxycholate have high hydrophilic lipophilic balance (HLB), 15 and 16 respectively (Kassem and Ahmed, 2019; Surini *et al.*, 2020). This means that they are more hydrophilic and, therefore, tend to stabilize oil-in-water (O/W) formulations Zheng *et al.*, 2015). NPs formulated using higher HLB values have been shown to produce larger particle sizes (Housaindokht and Pour, 2012; Nowroozi *et al*., 2018). Since polysorbate 80 and sodium deoxycholate have a relatively high HLB, particles are expected to enhance the entrapment of hydrophilic drugs (Bnyan *et al*., 2018).

Phospholipids play a crucial role as a primary vesicle-forming components. Phosphatidylcholine was selected as the phospholipid due to well-established safety profile and cost-effectiveness, which is excellent for the feasibility of future large-scale production of the tNPs (Opatha *et al*., 2020). Previous research has also proven the effectiveness of phosphatidylcholine in exhibiting excellent encapsulation capacities and fostering controlled drug release and has shown to act as a lubricant, important for reducing bone-to-bone friction in OA (Moqejwa *et al.,* 2022; Uwaezuoke *et al.,* 2022). EAs contribute to the flexibility and elasticity of tNPs by destabilizing the membrane, resulting in enhanced permeation (Opatha *et al*., 2020). DDAB was used to improve the surface charge of the particles, which would lead to dispersion stability as a result of repulsive forces between the tNPs (Silva *et al*., 2019). Cholesterol was added to reinforce the structure of the lipid bilayer of the tNPs, ensuring improved stability of the formulation (Nakhaei *et al.,* 2021).

3.2. Methods and Materials

3.2.1. Materials

Phosphatidylcholine (≥99% (TLC), cholesterol, dimethyl dioctadecyl ammonium bromide (DDAB), polysorbate 80, PF-127, DEX, HA (MW: 850 kDa) were all purchased from Merck (Pty Ltd., South Africa). Bovine serum albumin (BSA), Dulbecco's Modified Eagle's Medium

(DMEM), fetal bovine serum (FBS), penicillin and streptomycin solution, Dulbecco phosphate-buffered saline (DPBS, pH 7.4) were all procured from Thermo Fisher Scientific (Waltham, MA, USA). The 3-(4,5-dimethyl-2-thiazolyl)-2,5-diphenyltetrazolium bromide (MTT reagent) and solubilizing agent (acid-isopropanol; 0.04 N HCl in isopropanol), Kit (MTT Cell Proliferation Kit I, Roche, Basel, Switzerland) were all purchased from Sigma-Aldrich (St. Louise, MO, USA). High-performance liquid chromatography (HPLC)-grade methanol and chloroform and dimethylsulfoxide (DMSO) methanol were purchased from Merck (Pty Ltd., South Africa). The IL-4 instant ELISA KIT was purchased from Thermo Fisher Scientific (Waltham, MA, USA) and RAW 264.7 macrophages were procured from Separation Scientific Pty Ltd (Johannesburg, SA). All chemicals used were of analytical reagent grade and directly used without prior modification. Double-deionised water was used for all preparations.

3.2.2. Methods

3.2.2.1. Preparation of tNPs by Thin Film Hydration

The lipid phase was prepared with a blend of phosphatidylcholine, polysorbate 80, cholesterol and DDAB (Figure 3.1). The blend was dissolved into a mixture of solvents, chloroform, and methanol, followed by a transfer into a round-bottomed flask. The organic solvents were subsequently removed in vacuo using a rotary evaporator at 60°C, which is above the transition temperature of 55 °C. This step was carried out until a thin film formed along the interior walls of the round-bottomed flask. The round bottom flask was then left overnight to dry out and allow any residual solvents to evaporate. To rehydrate the lipid film and facilitate vesicle formation, 10 mg of DEX was dissolved in 10 mL of deionized water and added to the film. As expected, this hydration collapsed the film, forming the vesicles. The resultant suspension underwent sonication on ice using a probe sonicator (Sonics Vibra cell, Newtown, CT, USA) for 10 minutes at 0 pulse and 40% amplitude to reduce and homogenize the size of tNPs (Thabet *et al*., 2022). For the blank-tNPs, the same procedure was followed without the entrapment of DEX.

Table 2. Summary of components of tNPs as well as their functions

Raw Materials	Examples	Functions
Lipids	• Soy phosphatidylcholine • Cholesterol	Vesicle forming component
Surfactant	• Polysorbate 80	Increase flexibility and permeability of tNPs
Alcohol	• Methanol	Solvent for dissolving raw materials

	•	Chloroform	
Medium	•	Distilled Water	Hydration medium
Quaternary lipid	•	DDAB	Cationic lipid for surface charge

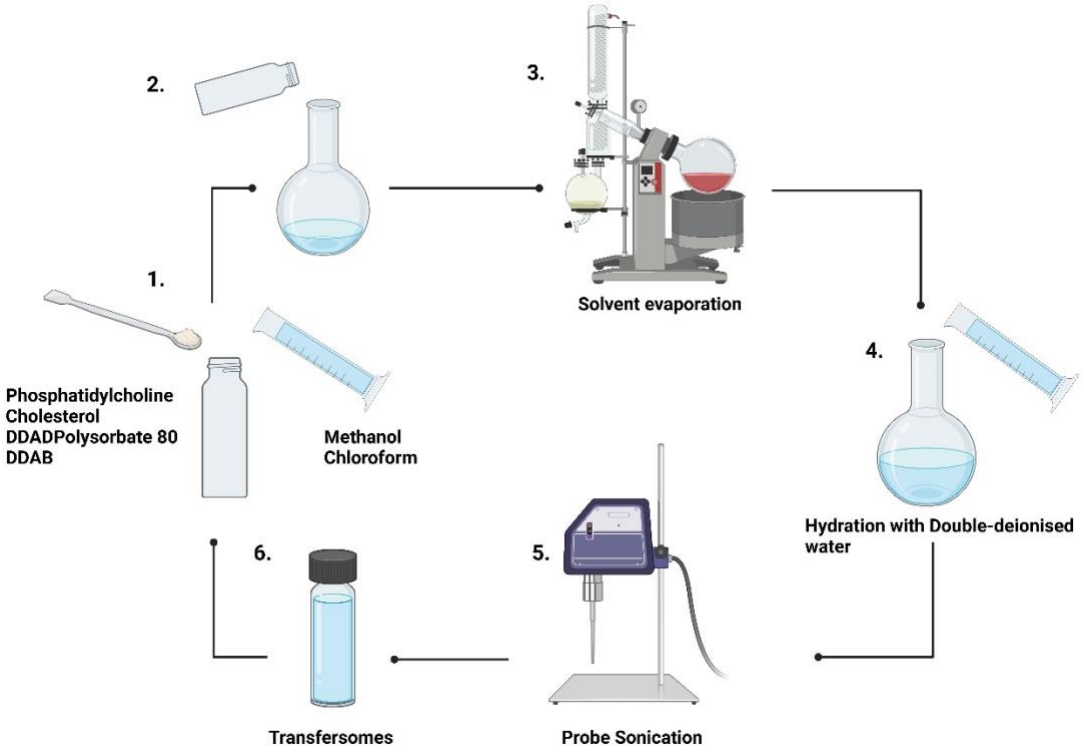


Figure 3.1. Schematic representation of Thin Film Hydration method employed for the preparation of DEX-loaded tNPs.

3.2.2.2. Determination of particle size, morphology, and zeta potential of the tNPs

The size, polydispersity index (PDI), and zeta potential of the tNPs were determined using dynamic light scattering (DLS) on the ZetaSizer NanoZS (Malvern Instruments (Pty) Ltd., Worcestershire, UK). The measurements were conducted using a 2:8 dilution of the transfersomal suspension solution with phosphate-buffered saline (PBS) at a pH of 7.4 (Tawfeek *et al*., 2020). The diluted sample was transferred into a quartz cuvette to measure the size and PDI, whereby a folded capillary cell was also used to quantify the zeta potential of the sample (Tawfeek *et al*., 2020). The readings were conducted in triplicates and the mean values were noted.

The scanning electron microscope (SEM) was used to determine morphology and confirm the size of the tNPs. A sufficient amount of the diluted suspension solution of the tNPs was dropped on to cover an aluminum stub and allowed to air dry completely for a few hours while avoiding any disturbances and contamination before being coated with gold-palladium and viewed using the SEM (Jeol JSM-120, Tokyo, Japan). As an additional measure, transmission electron microscopy (TEM) was also used to confirm the morphology and the size of the tNPs. The diluted sample in suspension was dropped onto a carbon-coated copper grid. A 2% (v/v) uranyl acetate negative stain solution was added to the 3 mM forman-coated copper grid of 300 mesh for 90 seconds and allowed to dry overnight to be visualized using the TEM (FEI Tecnai T12, FEI Company, Hillsboro, OR, USA) (Tawfeek *et al*., 2020)

3.2.2.3. Wave Scan (Lambda Max) and Standard Curve of DEX

Before any UV-Vis assays involving DEX were conducted, a wave scan was conducted to detect the lambda max (λ max) of DEX on the instrument, which is the wavelength at which DEX has its strongest photon absorption. Subsequently, and prior to the determination of the entrapment efficiency and drug release profiles, a standard curve of DEX was determined. The standard curve was used to obtain a linear equation y = mx + c to further calculate DEX concentrations. A series of concentrations of DEX were prepared from a 100 µg/ml Stock solution, and absorbances were determined using UV-Vis.

3.2.2.4. Drug Loading and Dug Entrapment Efficiency.

The percent entrapment efficiency (%EE) is the amount of drug entrapped in the formulation (Opatha *et al*., 2020). The indirect approach was used to determine drug EE. This was conducted by separating the free drug from the drug-loaded vesicles and using equation **(2)** to determine the %EE. This was achieved using Amicon® Ultra4 centrifugal filter tubes (Millipore Corp., USA) with a molecular weight cut-off (MWCO) of 10 kDa (Chen *et al*., 2016). An amount of 2 mL (n=3) was sampled from the suspension into the upper chamber of the mini-column tube and then centrifuged at 2500 rpm for 45 minutes. After centrifugation, the supernatant was collected, and the drug content was determined through UV-Vis analysis at 245 nm. Ultimately, the %EE was calculated using equation (1) below (Garms *et al*., 2021), and the drug loading was calculated using equation 2:

$$\textbf{EE=}\ \frac{Total\ amount\ of\ the\ drug\ added - Amount\ of\ the\ free\ drug}{Total\ amount\ of\ the\ drug\ added} \times 100 \qquad \textbf{(1)}$$

$$\mathrm{DL} = \frac{Weight\ of\ Dex\ in\ nanonaprticles}{weight\ of\ Nanoparticles} \times 100 \qquad \textbf{(2)}$$

3.2.2.5. Degree of deformability

This test was conducted to determine the flexibility of the tNPs (Amnuaiki *et al.*, 2018). The transfersomal dispersion was extruded through the polycarbonate filter membrane (Sigma Chemicals, UK) having a pore diameter of 0.1 µm, and the extruded vesicles were measured using DLS. The diameters before and after extrusion were compared and the deformability index was calculated using the equation (3) below (Amnuaiki *et al.*, 2018):

$$\mathrm{D} = J \times \left(\frac{Rv}{Rp}\right) \quad \textbf{(3)}$$

where D = deformability index: J= amount of sample extruded Rv = vesicle size after extrusion Rp = pore size of filter.

3.2.2.6. Physiochemical characterizations of tNPs

3.2.2.6.1 Thermogravimetric Analysis (TGA)

Freshly synthesized tNPs were frozen and subsequently lyophilized (Nowak and Jakubczyk, 2020). To evaluate the thermal degradation properties of the DEX, blank-tNPs, and DEX-loaded tNPs, TGA (PerkinElmer, TGA 4000, Llantrisant, Wales, UK) was employed (Saadatkhah *et al.*, 2020). Approximately 15 mg of the sample was placed in a crucible and kept for 1 minute at 30 °C after which it was heated from 30 °C to 900 °C at 10°C/minute increments and further held for a minute at 900 °C.

3.2.2.6.2 Fourier Transform Infrared (FTIR) spectroscopy

FTIR spectroscopy was performed using the Perkin Elmer Spectrum 2000 ATR-FTIR spectrometer fitted with a single reflection (PerkinElmer 100, Llantrisant, Wales, UK). Similar quantities of the DEX, blank-tNPs, and DEX-loaded tNPs were placed on the diamond stage, and analysis was performed within a range of 650-4000 cm^{-1}.

3.2.2.6.3 X-ray diffraction (XRD)

The XRD assay was performed to analyze the structural properties (crystalline or amorphous) of DEX, blank-tNPs, and DEX-loaded tNPs using powder X-ray diffractometer (PANalytical 3 kW X'pert Powder, Cambridge, UK). Samples were scanned from 2 h to 6 h with an operating voltage

of 40 kV and a current of 30 mA. A Cu-Ka radiation source was used, with a scanning rate of (2Ɵ /min) and a temperature ramp of 5 °C/min were used.

3.2.2.7. Determination of the Physical Stability of DEX-loaded tNPs

DEX-loaded tNPs formulations were placed both at ambient temperature and at 4 ˚C over a period of 3 months, after which the particle size, PDI, zeta potential, and visual inspections were conducted. Ambient temperatures were used because they are typical short-term storage conditions, while 4 ˚C is used to simulate long-term storage conditions (Opatha *et al*., 2020). Thus, observations of any physical changes, such as colour and sedimentation formation, were noted from the visual assessment.

3.2.2.8. In Vitro Drug Release

A cellulose dialysis membrane was prepared according to the manufacturer's manual instructions to activate its pores. A fresh batch of tNPs was prepared, and aliquots of the DEX-loaded samples, blank-tNPs, and free DEX were then dispatched into respective dialysis tubes and placed in receivers with PBS pH 7.4 as the release media. The receivers were placed into a gently shaking (20-25 rpm) incubator at 37°C. Samples were withdrawn from the receivers at predetermined intervals (0.5 hr, 1 hr, 2 hrs, 4 hrs, 6 hrs, 8 hrs, 10 hrs, 12 hrs, 24 hrs, 48 hrs and 72 hrs) and immediately replaced with the same amount of fresh buffer pre-equilibrated at 37°C. The samples (n=3) were ultimately assayed using UV-Vis at 245 nm (Omolo *et al*., 2021).

3.2.2.9. PF-127/HA Hydrogel Synthesis

The cold method was used to synthesize the hydrogel whereby appropriate amounts of PF-127 were progressively added into deionized water with continual stirring at an equilibrated and regulated temperature of 4˚C to form 17% of PF-127 (w/v) (Schmolka, 1972). Then, appropriate amounts of HA were added to the PF-127 solution to form 1% (w/v) and kept overnight at 4 °C until a clear solution was obtained to allow full hydration of the polymers (Hsieh *et al*., 2020). Finally, the suspension of tNPs was added to the PF-127/HA hydrogel and mixed to form a homogenous mixture. Following the successful synthesis of the hydrogel, further characterizations were conducted.

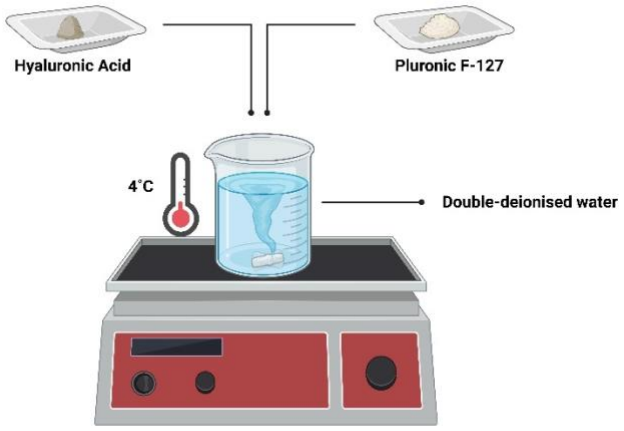


Figure 3.2. Schematic representation of the cold method employed for the preparation of PF-127/HA hydrogel.

3.2.2.10. Brunauer–Emmett–Teller (BET) Analysis for Hydrogel Pore Analysis

The composite's surface area was measured using the BET surface adsorption method (Sinha *et al.*, 2019). In brief, the freeze-dried samples were prepared and loaded into the glass tube, de-gassed, and immersed into a liquid nitrogen bath. The liquid nitrogen was used as an adsorbate during the analysis (Brame and Giggs, 2016).

3.2.2.11. Determination of the Gelation Time of DEX-tNPs-PF-127/HA Hydrogel

Aliquots of the composite were put in glass vials and placed into a water bath at 37 °C to determine the gelation time. After set time intervals of 30 seconds the vials were inverted to determine the gelation time and to verify the sol-gel transition (Panyamao *et al*., 2020; Giliomee *et al*., 2021).

3.2.2.12. Syringeability of DEX-tNP-P127/HA Hydrogel

Syringeability is defined as the amount of force that needs to be exerted to inject the sample solution (Wang *et al.*, 2018). The syringeability measurement was attained using a TA-XT Plus texture analyzer (Stable Micro Systems, Surrey, UK) set in compression mode at room temperature. A 3 mL syringe, containing 1 mL of a freshly prepared sample of the hydrogel composite was set up on the instrument adapter. The sample was extruded through the syringe with a 22-gauge needle applying a test speed of 1 mm/s, and the maximum value was analyzed from the resulting texture analysis profile (Panyamao *et al*., 2020).

3.2.2.13. In Vitro Drug Release Using a Knee Joint Simulator

3.2.2.13.1. Construction of Knee Simulator for In Vitro Drug Release Studies

Conventional drug release methods like simple dissolution or vertical Franz diffusion cells apparatus do not necessarily provide an environment that mimics the joint (Larsen *et al*., 2009). On the other hand, the knee simulator (Figure 4.3) can be used to mimic knee movements whereby 1 million simulator cycles = 12hr = 1 year of adult walking, running, and folding (Wimmer *et al*., 2015). The joint simulator, designed and developed to mimic a particular joint's movement, operation, and conditions, can also be used to simulate *in vivo* drug release (Liu *et al*., 2019). The knee simulator used in this study was developed in collaboration with Marathwada Mitra Mandal's College of Pharmacy, Pune, India very closely to ISO 14243 and ASTM F1223 guidelines, excluding load and some dimensional specifications. The main aim of the simulator was to perform *in vitro* drug release studies for the injectable formulation developed for knee arthritis conditions. The materials used in the device design are medical-grade high-density polyethylene (HDPE) and polyacrylic. The moving HDPE semicircular part has a radius of 24 mm and thickness of 25 mm, representing 1 binary large object (LOB) of a knee joint of the femur bone. The semicircular cut fixed HDPE part has a radius of 25 mm and a thickness of 25 mm, representing the cavity of the Tibia bone for 1 LOB of a knee joint of the femur bone. On the simulator, the semicircular cut DHPE part is fixed on a support base made up of HDPE. The fixed HDPE part has screw points on both sides to fix transparent acrylic parts forming a watertight chamber representing the knee synovial cavity. The moving semicircular HDPE part fits exactly into the cavity generated using fixed HDPE, acrylic sheets, and spacer parts. The moving semicircular HDPE part is connected to a stepper motor moving at 45^0 flexion angles on both sides (total 90^0 maximum adjustable in accordance with the ASTM F2083 – 21 Standard Specification for Knee Replacement Prosthesis) from the center using a specially designed polypropylene part. The stepper motor is connected to the controller, which is connected to the DC power source to complete the setup of the Knee simulator. The watertight compartment with a moving HDPE part can accommodate 10 ml of synovial fluid-like media (SFM). The whole Knee simulator with SFM and drug formulation can be placed in an incubator to maintain the temperature of the whole system at 37 ^{0}C. For this setup, the stepper motor is programmed for 1Hz frequency, representing 1 gait cycle during the experiment (Wimmer *et al*., 2015).

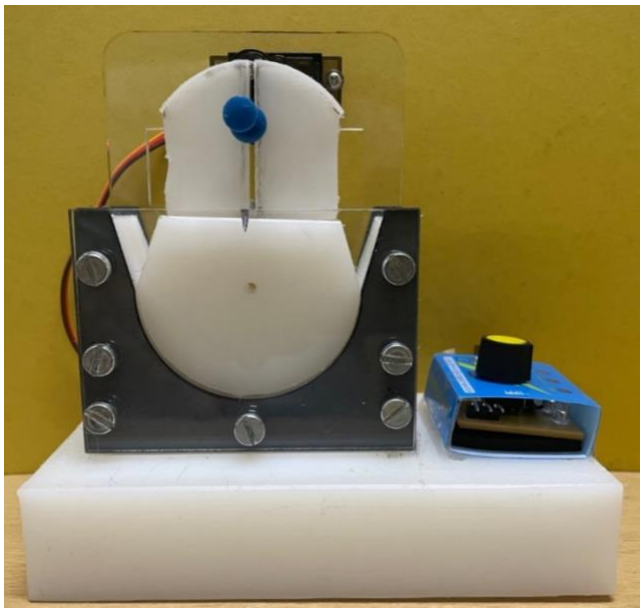


Figure 3.3. Knee simulator setup developed for the in vitro drug release studies (Indian Design Registration no 375583-001).

The SFM was prepared by dissolving BSA, phosphatidylcholine, and HA into PBS and equilibrated to a pH of 7.4 (Krishna and Sankar, 2023). This medium was used as a release medium and loaded into the joint cavity of a knee joint simulator. An aliquot of the hydrogel composite was injected into the joint cavity, and the medium was allowed to mix. Samples were withdrawn at predetermined intervals (0.5h, 1h, 2h, and 4h, and replaced with fresh SFM equilibrated at 37 °C. Samples were evaluated using UV-Vis at a wavelength of 245 nm to determine the amount of drug that was released at the set intervals (Al-Owaidi *et al.,* 2021).

Similarly, *in vitro* release studies for the hydrogel were conducted using the same method. Physiochemical characterizations for the DEX-loaded tNPs and blank-tNPs were conducted as described above in Section 2.4. Also, those for hydrogels (Blank-tNPs-PF-127/HA and DEX-tNPs-PF-127/HA) were performed as detailed in Section 3.2.2.

3.2.2.14. Rheological Characterization of the DEX-tNPs-PF-127/HA Hydrogel

An AR 2000 Rheometer (TA instruments, USA) was used to evaluate the rheological properties of tNPs-PF-127/HA hydrogel. The samples were sandwiched between two parallel metal plates with a 40 mm radius and a spacing gap of 1 mm (Giliomee *et al.*, 2021). Once the samples were applied to the stage, they were given 5 minutes to conform to the environment (temperature and

relief from the stress applied), and a 35 mm silicon cone was used to cover the sample in order to keep the environmental conditions around the sample constant. The linear viscoelastic (LVE) region was attained by conducting stress sweep tests with a stress of 0.10% to 1000% at a constant frequency of 1 Hz and 37 °C (Panyamao *et al*., 2020). The LVE was then used to carry out the frequency sweep with a frequency ranging between 0.1-100 Hz. The results were analyzed as a function of the storage modulus (G′) and loss modulus (G″), two important parameters that make up the complex modulus (G*). Since G' represents elasticity, a higher G' indicates a more elastic behavior. On the other hand, G'' quantifies viscosity; therefore, the higher the G", the more viscous the sample is (Wang *et al*., 2018).

3.2.2.15. Molecular Modeling of the DEX-tNP Complex

Using the Maestro Materials Science platform of Schrödinger software (version 2023-2), the molecular interactions of DEX and the tNPs were assessed (Rants'o *et al*., 2022). Mimicking the *in vitro* study, the tNP was computationally designed from four components including phosphatidylcholine, cholesterol, polysorbate 80, and DDAB. The 3D chemical structures of the first three components were obtained from Mol-Insticts chemical database (Samigulina and Samigulina., 2020) (IDs: CT1089733823, CT1001897301, and CT1080213202, respectively) while that of DDAB was downloaded from PubChem (Govender *et al*., 2023; Rants'o *et al*., 2022). These were all treated as monomers and subjected to the Polymer Builder tool to form a polymer. In the Polymer Builder, the co-polymeric system was randomized in a 1:1 ratio of the monomers and a system minimized under the OPLS4 force field. Lastly, the system was optimized for Desmond calculations and allowed to form an amorphous cell at a density of 0.5 g/cm^3 (Govender *et al*., 2023).

Next, the final polymer was modeled under the Nanoparticle Builder as a sphere to generate a tNP (Lolicato *et al*., 2017). However, to form a drug-loaded tNP and simulate associated interactions, the resulting tNP was submitted to the Disordered System Builder and ran for simulation with DEX as a substrate. The disorder options included having the DEX-tNP in an SPC-buffered water model that mimicked the physiological environment by adding sodium and chloride ions to a concentration of 0.15M. The final tNP was then assessed for successful drug loading and drug-tNP intermolecular interactions (Govender *et al*., 2023; Gartner and Jayaraman, 2019).

3.2.2.16. Cytocompatibility Studies

3.2.2.16.1. Cell Culture

The 264.7 RAW macrophage cells were grown in growth media of DMEM supplemented with 10% (*v*/*v*) FBS and 1% (v/v) antibiotics (penicillin, and streptomycin) in a 95 % humidified incubator (NUAIRE, Radobio, China) at 37 °C with 5% CO_2. The culture medium was refreshed daily until the desired cell confluency of ≈ 90% was reached.

3.2.2.16.2. Cell Viability and Proliferation Assay of 264.7 RAW Macrophage Cells

The impact of DEX, Blank-tNPs, DEX-tNPs, Blank-tNPs-PF-127/HA hydrogel, and DEX-tNPs PF-127/HA hydrogel composites on the viability of RAW 264.7 macrophage cells was evaluated using the MTT Cell Proliferation Kit I assay (Roche, Basel, Switzerland). This analysis was conducted after 24 hours of incubation in the absence of lipopolysaccharide activation. The MTT assay is based on the ability of metabolically active cells to reduce MTT, a yellow tetrazolium salt, into insoluble formazan crystals (Ghasemi et al., 2021). These formazan crystals were then dissolved in isopropanol and quantified spectrophotometrically at 595 nm (Ngema *et al*., 2022).

For the assay, RAW 264.7 cells were seeded in a 96-well plate at a density of 5 × 10^3 cells per well. Each well was filled with 90 µL of cell suspension and incubated at 37°C in a 5% CO2 atmosphere for 24 hours to allow for adequate cellular adherence. Following this incubation period, cells were treated in triplicate with 10 µL of DEX, Blank-tNPs, DEX-tNPs, Blank-tNPs-PF-127/HA hydrogel, and DEX-tNPs-PF-127/HA hydrogel composites at concentrations of 50 µg/mL, 25 µg/mL, 12.5 µg/mL, and 6.25 µg/mL. A final concentration of 4% (v/v) DMSO was used as the negative control, whereas untreated cells served as the positive control.

After 48 hours of treatment, 10 µL of 5 mg/mL MTT solution was added to each well, and the cells were further incubated at 37°C with 5% CO2 for an additional 4 hours. The formazan crystals formed within viable cells were dissolved using 100 µL of a solubilizing agent (acid-isopropanol; 0.04 N HCl in isopropanol). Absorbance measurements were recorded using a TECAN GENios multireader (TECAN Group Ltd., Männedorf, Switzerland) equipped with Magellan v7.0 software, set at 595 nm. The mean absorbance readings (± standard deviation) were computed and used to determine cell viability (%) using Equation (4).

Cell viability $= \frac{Atreatment - Aneg.control}{Apos.control - Aneg.control} \times 100$ (where, *A* = absorbance). **(4)**

3.2.2.16.3. IL-4 Quantification from RAW 26.4 Macrophage Cells After Various Treatments.

The RAW 264.7 macrophage cells were seeded in a 96-well plate and incubated for 24 h for cells to adhere to the base. The cells were then treated in triplicates with 50 mg/mL of either DEX, Blank-tNPs, DEX-tNPs, Blank-tNPs-PF-127/HA hydrogel or DEX-tNPs-PF-127/HA hydrogel composites for a further 24 hours. Post-treatment, 50 µL of cell culture supernatant was collected and subsequently added to the ELISA plate, covered with an adhesive film, and incubated at room temperature for 3 hours. The ELISA plate wells were emptied and gently washed with 400 µL of wash buffer (PBS, 1% Tween-20) where in each cycle, the wash buffer was kept in the wells for 15 seconds. The 3,3′,5,5′-Tetramethylbenzidine (TMB) substrate buffer (100 µL) was added to the wells and further incubated for 10 minutes at room temperature, avoiding direct light. The reaction was stopped by adding 100 µL of stop solution (1M phosphoric acid) with the development of a strong dark blue colour from the highest concentration (250 pg/mL). The absorbances were read and measured using a microplate reader at 450 nm as the primary wavelength and 620 nm as the reference wavelength.

3.3. RESULTS

tNPs

3.3.1. Wave Scan (Lambda Max) and Standard Curve of DEX

The working optimal UV wavelength was detected to be 245 nm. The value corresponded to the value reported in the current literature (Watson *et al*., 2005; Al-Owaidi *et al*., 2021). The calibration curve is shown in the figure below (Figure 3.5). The linear equation was $y = 0.0253x + 0.006$ with a correlation coefficient (r^2) of 1, which indicates good linearity.

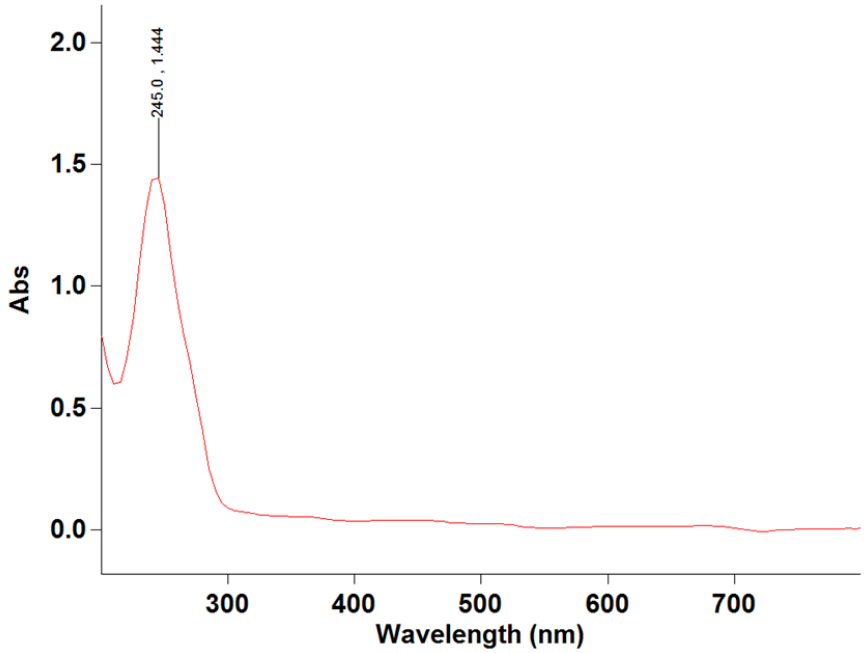


Figure 3.4. Wave scan showing lambda max of DEX.

The standard curve (figure 3.2.) presented shows that an increase in the concentration value is followed by an increase in the absorbance value. The curve was used to quantify concentrations of DEX using equation 5:

$$y = 0{,}0253x + 0{,}006 \quad \textbf{(5)}$$

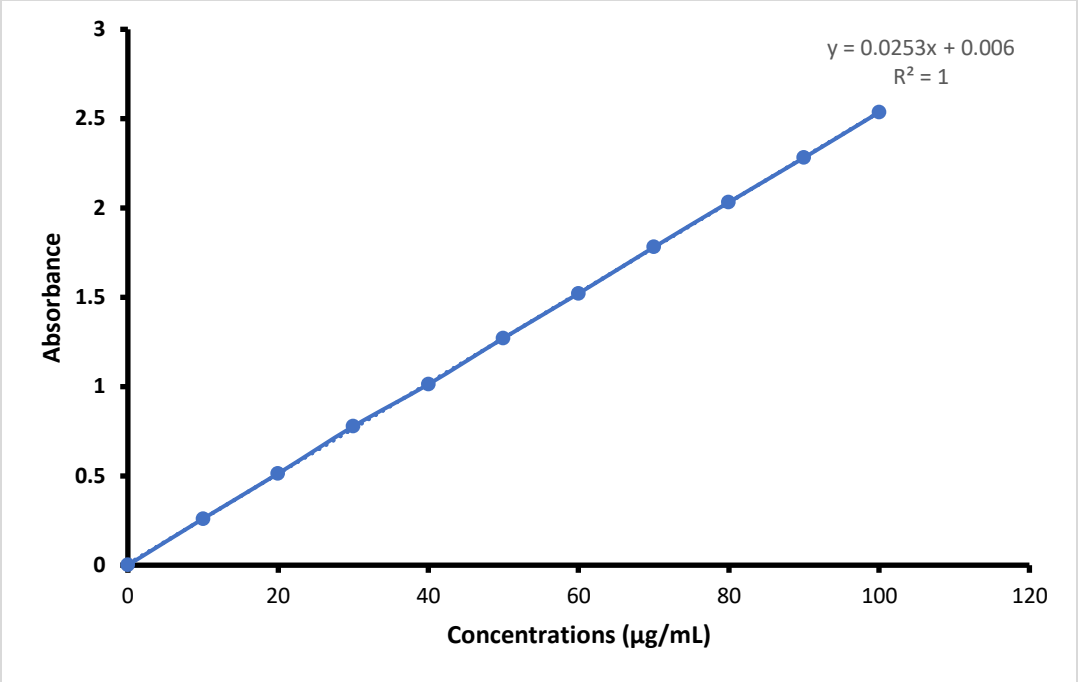


Figure 3.5. Calibration curve for DEX quantification: the curve illustrates the relationship between DEX concentration and absorbance.

3.3.2. **Size and Morphology of tNPs**

A DLS study was used to determine the vesicle size, distribution, and surface charge. An increase in size from 60.93 nm to 76.43 nm upon loading of DEX into tNPs synthesized with polysorbate 80, accompanied by a decrease in the zeta potential (from 15.8 mV to 10.58 mV), was observed. DEX is negatively charged, thus resulting in the decrease in zeta potential of the tNPs. Coincidently, the PDI decreased upon loading DEX into the tNPs, exhibiting a decline from 0.191 to 0.183 (Table 4.1). The results from DLS showed that tNPs synthesized using sodium deoxycholate were in the favourable range (74.62 ± 0.528 nm) and had an excellent polydispersity index; however, they possessed an inferior entrapment efficiency (48.93 ± 0.45%). The PDI of 0.183 ± 0.003 suggests that the particles had a relatively uniform size. Their zeta potential (3.98 ± 0.382 mV) was also close to neutral, suggesting the possibility of low stability and agglomeration of the particles. For these reasons, the particles were not characterized further. On the other hand, the synthesized tNPs using polysorbate 80 had pristine size (76.43 ± 0.48346) and an entrapment efficiency of 98 ± 0.31. Similarly to the sodium deoxycholate tNPs, polysorbate 80 tNPs had an excellent PDI of 0.183 ± 0.008. The polysorbate 80 tNPs showed desired characteristics and were therefore assessed and characterized further.

The size and morphology of tNPs played an integral role in the application of tNPs as a drug delivery system. The nanosized and spherical morphology of tNPs observed in Figure 3.6 ensured an enhanced ability to permeate biological barriers, the capability of drug encapsulation, and the potential for sustained drug release – all which are objectives in this study.

Table 3.2. DLS characterization of the generated tNPs.

Co-surfactant	**EE (%)**	**Size (nm)**	**PDI**	**Zeta Potential (Mv)**
Blank	-	60.93 ± 0.370	0.191 ± 0.002	15.8 ± 1.129
Sodium Deoxycholate	48.93 ± 0.45	74.62 ± 0.528	0.183 ± 0.003	3.98 ± 0.382
Polysorbate 80	98 ± 0.31	76.43 ± 0.48346	0.183 ± 0.008	10.58 ± 0.706

The overall morphology of the tNPs was visualized using SEM (Figure 3.6), which showed that the particles were spherical and homogenously dispersed (Figure 3.6a-3.6b), supporting the data presented by the PDI (0.183 ± 0.008) (Table 3.1). To confirm this observation, TEM imagery was obtained which confirmed the successful synthesis of the tNPs by illustrating the size and morphology (Figure 3.6 c).

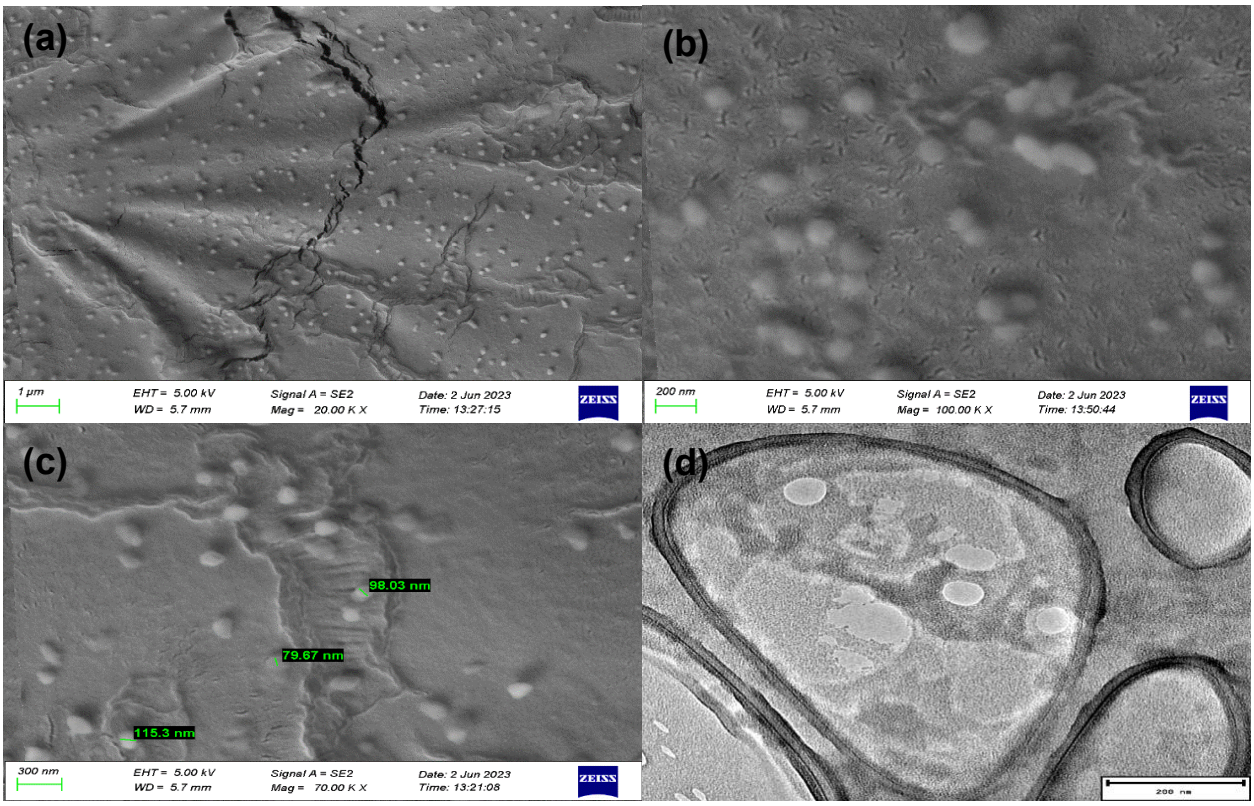


Figure 3.6. Morphology of the tNPs shown by SEM at a scale of 1 µm (a), 200 nm (b) and 200 nm annotated with sizes (c) as well as TEM (200 nm) (d).

Physiochemical Characterizations of tNPs

3.3.3. Degree of Deformability

Upon 10 extrusion passes from a mini extruder, the size of DEX-loaded tNPs decreased from 75 nm to 64 nm. Notably, the PDI was also reduced from 0.183 to 0.134. The vesicles had a degree of deformability of 660 µL and a size reduction of 16%.

3.3.4. FTIR: Analysis of Identification of Structural Characteristics and Functional Groups of the tNPs

The FTIR analysis was conducted to obtain insights into molecular interactions between the excipients and the drug. The outcomes illustrated in Figure 3.7 represent the FTIR profiles for DEX, blank-tNPs, and DEX-loaded tNPs. The spectra of both the blank and DEX-loaded tNPs exhibited indistinguishable patterns with identical bands identified for functional moieties at equal intensities and wavenumbers (Figure 3.7). For both samples, we observed a signal at 3375.35 cm^{-1} indicative of the hydroxyl (O-H) functional group and another at 1736.88 $cm^{-1,}$, a quality of the carbonyl (C=O) group present in the transferosome structure. We also observed two peaks at 2853.47cm^{-1} and 2923.14 cm^{-1}, which belong to the Methylene (CH_2) functional group and a pick at 1243.65 $cm^{-1,}$ which is ascribed to a phosphoryl group (P=O) on the tNPs. Notably, none of the distinctive bands associated with DEX are detectable in the FTIR spectrum of the DEX-loaded tNPs suggesting successful encapsulation of DEX into the tNPs.

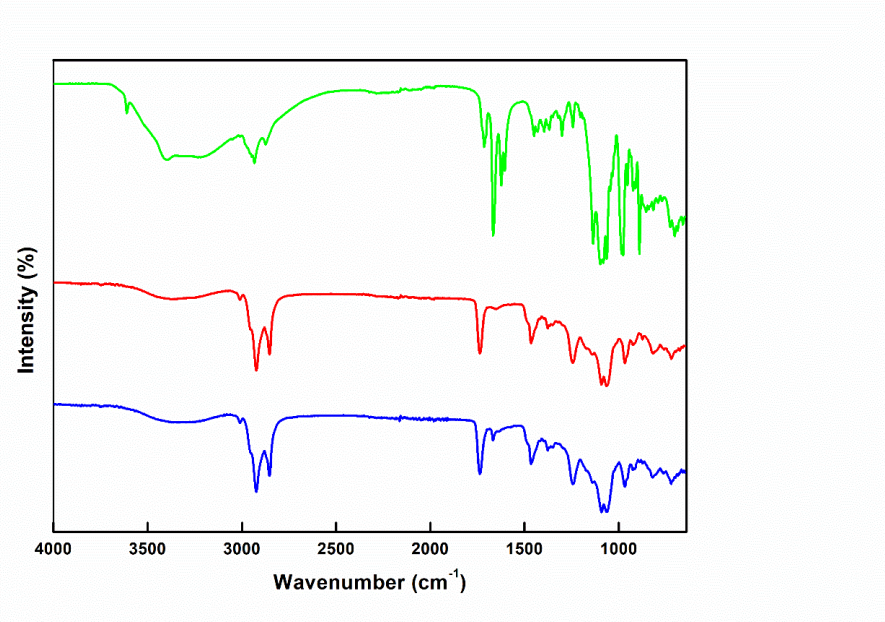


Figure 3.7. FTIR spectra of DEX (green), Blank tNPs (red) and DEX-loaded tNPs(blue).

3.3.5. TGA: Thermal Stability and Decomposition of tNPs

The thermograms (Figure 3.8) were derived from the TGA conducted on DEX, blank-tNPs, and DEX-loaded tNPs. The TGA was employed to evaluate the thermal stability of the tNPs and DEX by continuously monitoring their weight changes while subjected to heating at a constant rate. The thermogram of DEX-loaded tNPs exhibited DEX's thermal degradation characteristics. Conversely, the blank-tNPs do not exhibit the thermal degradation characteristics of DEX as anticipated.

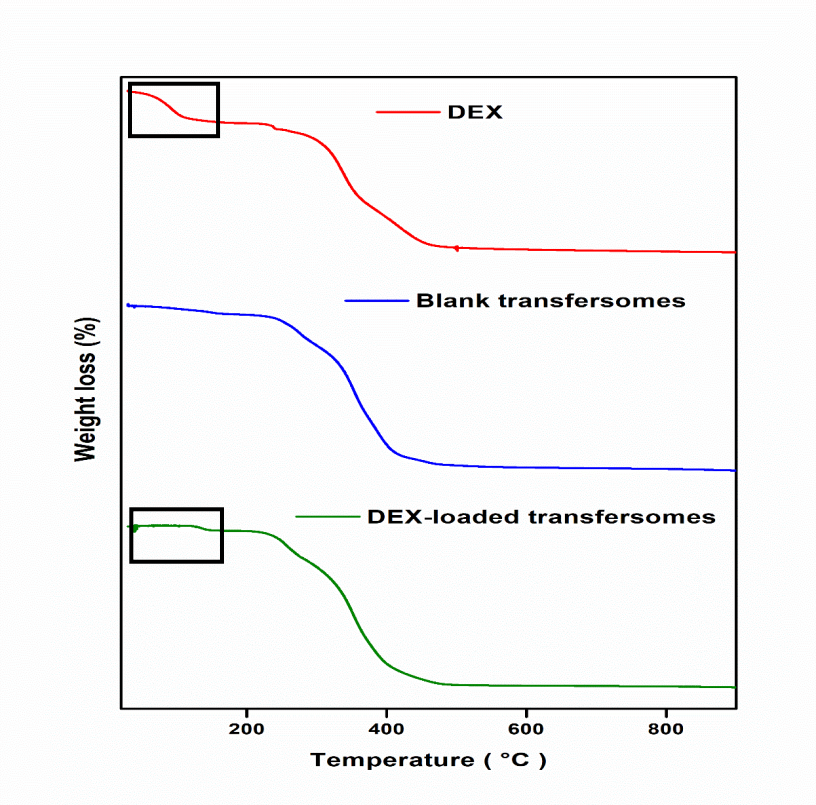


Figure 4.8. TGA thermogram of DEX, blank-tNPs, and DEX-loaded tNPs.

3.3.6. XRD: Analysis of the Crystallographic Structure of the tNPs

XRD diffractogram (Figure 3.9) of pure DEX shows multiple sharp and intense peaks, while the diffractogram of both the DEX-loaded and blank-tNPs showed single broad peaks at the same angles (20° and 40°). This propounded that DEX is crystalline while both the blank and loaded tNPs were amorphous which further supported the successful encapsulation of DEX into the tNPs.

.

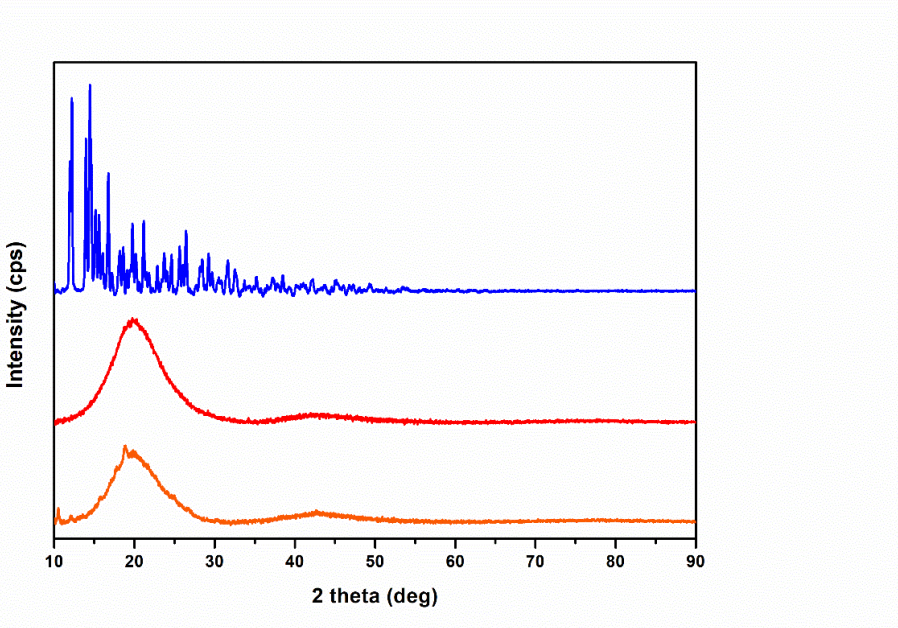


Figure 3.9. XRD diffractograms of DEX (blue), Blank-tNPs (red), and DEX-loaded tNPs (orange).

3.3.7. Physical Stability of DEX-Loaded tNPs

Physical stability studies were conducted over 3 months to assess the structural integrity of the formulations (Table 4.4). The size, PDI, and zeta potential of the particles showed changes at both 4°C and 25°C, where an increase in PDI was observed with longer storage time, while on the other hand, the zeta potential was slightly reduced. The size stayed relatively consistent over 3 months in both storage conditions. However, there were no physical changes (sedimentation and turbidity) observed in the formulation.

Table 3.3. Effect of storage conditions on DEX-loaded tNPs over three months at 4°C and 25°C.

	4°C			25°C		
Days	**Size (nm)**	**PDI**	**Zeta Potential (mV)**	**Size (nm)**	**PDI**	**Zeta Potential (mV)**
1	73.43 ± 0.405	0.180 ± 0.006	10,1 ± 0.523	73.43 ± 0.4046	0.180 ± 0.006	10,1 ± 0.523
14	73.19 ± 0.570	0.182 ± 0.002	9,84 ± 0.509	73.19 ± 0.57042	0.182 ± 0.002	9.84 ± 0.509
21	72.70 ± 0.379	0.184 ±0.004	9,90 ± 0.0442	74.12 ± 0.6521	0.187 ± 0.006	8.58 ± 0.410

30	73.14 ± 0.105	0.184 ± 0.004	9.38 ± 1.17	73.60 ± 0,549	0.185 ± 0.007	8.96 ± 0,628
60	73.33 ± 0.650	0.184 ± 0.004	10.6 ± 0.252	73.90 ± 0.5983	0.186 ± 0.004	8.87 ± 1.123
90	75.14 ± 0.364	0.185 ± 0.009	8.26 ± 0.863	74.57 ± 0.364	0.194 ± 0.002	6.27 ± 0.297

3.3.8. *In Vitro* DEX Release from tNPs

The cumulative drug release profiles of DEX in its free form and from the tNPs were determined using the cellulose membrane dialysis bag at pH 7.4. This study was conducted to quantify the amount of DEX released from the tNPs in comparison to the free drug over time. The release profiles showed that the free DEX had a burst release and a complete release within 10 hrs (Figure 3.10). Conversely, the release of DEX from the DEX-loaded tNPs showed a burst release of approximately 60% within 10 hrs, with the release being more gradual than the free form. Approximately 90% of DEX was released within 72 hrs with the remainder of DEX completely released after this time frame from the tNPs.

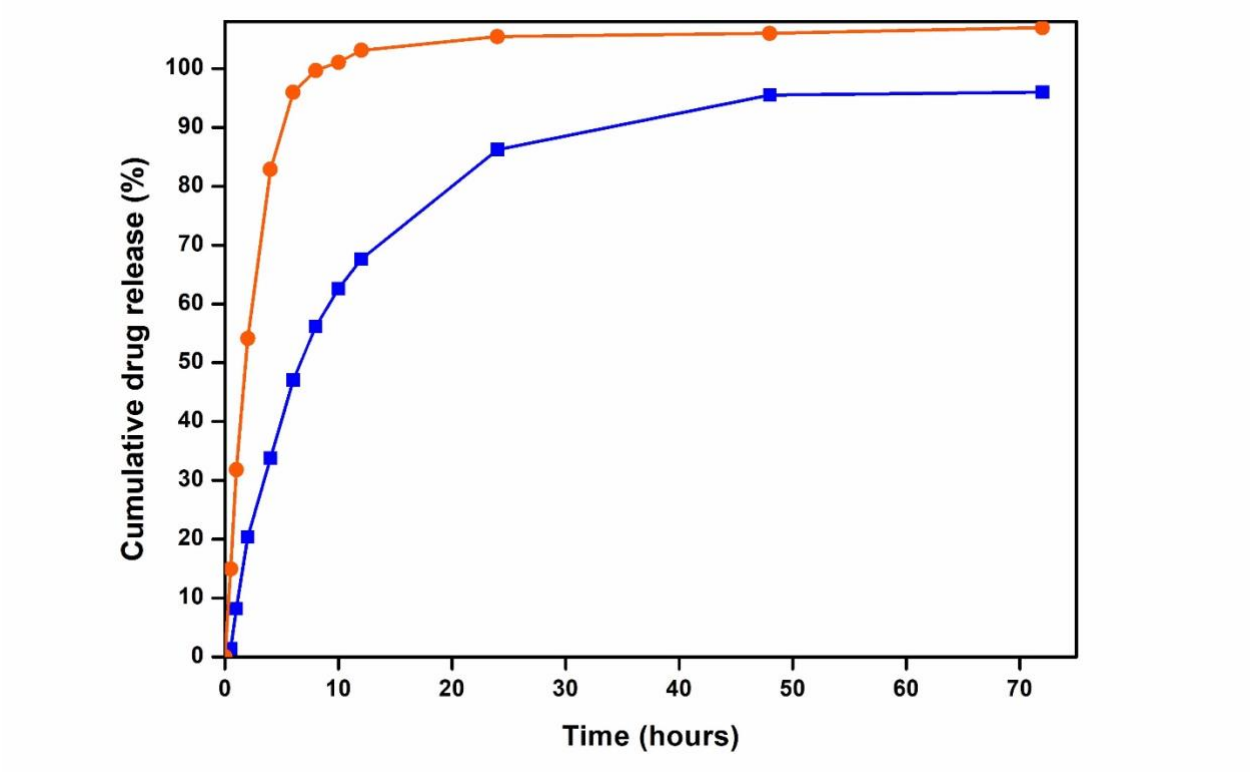


Figure 3.10. DEX-release profiles from tNPs (blue) versus free drug (orange).

Preparation and Characterization of DEX-tNPs-PF-127/HA Stimuli-Responsive Hydrogel (Composite)

3.3.9. BET Surface Area Analysis Measurements of DEX-tNPs-PF-127/HA Hydrogel

The BET-generated surface area and porosities of the hydrogel composite indicated that the pore sizes of the hydrogel decreased upon loading of DEX-tNPs (Table 3.5).

Table 3.4. BET measurement results of the hydrogel composite.

Pore Size	**Blank-tNPs-PF-127/HA (nm)**	**DEX-tNPs-PF-127/HA (nm)**
Adsorption average pore width (4V/A by BET)	7.7538	3.96020
BJH Adsorption average pore diameter (4V/A)	26.7007	19.3421
BJH Desorption average pore diameter (4V/A)	31.4027	2.16320

The SEM images showed that the morphology of the synthesized blank-tNPs-PF-127/HA and DEX-tNPs-PF-127/HA Stimuli-responsive hydrogels and confirmed the porous nature of the structure (Figure 3.11).

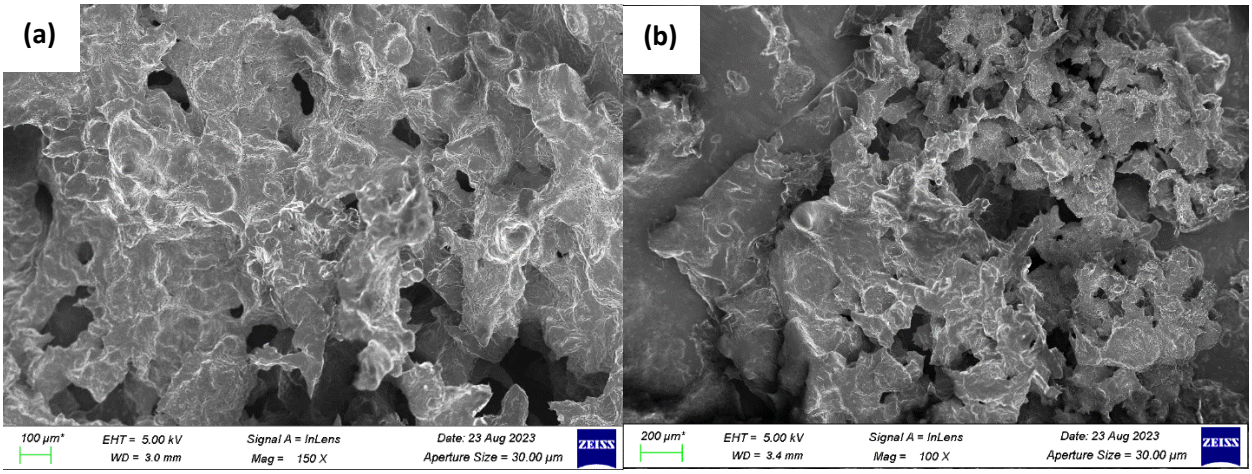


Figure 3.11. Morphological characterization of the (a) Blank-tNPs-PF-127/HA and (b) DEX-tNPs-PF-127/HA Stimuli-responsive hydrogels.

Physiochemical Characterization of DEX-tNPs-PF-127/HA Hydrogels

3.3.10. FTIR: Analysis of Identification of Structural Characteristics and Functional Groups of tNPs-PF127/HA Hydrogels

The FTIR analysis was conducted to obtain insights into molecular interactions between HA, PF-127, as well as blank-tNPs-PF-127/HA and DEX-tNPs-PF-127/HA hydrogels (Figure 3.12). The FTIR spectra of both the blank-tNPs-PF-127/HA and DEX-tNPs-PF-127/HA hydrogels exhibited identical patterns with the same bands identified for functional groups at the same intensities and wavenumbers as that of PF-127, suggesting that HA did not alter the chemical structure of PF-127 (Figure 3.12). The FTIR spectra of the blank-tNPs-PF-127/HA and DEX-tNPs-PF-127/HA hydrogels showed the presence of the majority of characteristics of PF-127, the main constituent of the hydrogel with bands at approximately 2881.93; 1979; 1466.69, 1373.01 cm^{-1} (Dmitrenko *et al*., 2019). On the other hand, the bands at approximately 1620 and 1373.01 cm^{-1} were characteristic of HA (Al-Sibani *et al.*, 2018; Güngör *et al.*, 2019). Notably, none of the distinctive bands associated with the tNPs (Figure 3.7) are detectable in the FTIR spectrum of the DEX-tNPs-PF-127/HA (Figure 3.12 - green). This suggested successful encapsulation of DEX-loaded tNPs within the bipolymeric hydrogel matrix (Figure 3.12).

.

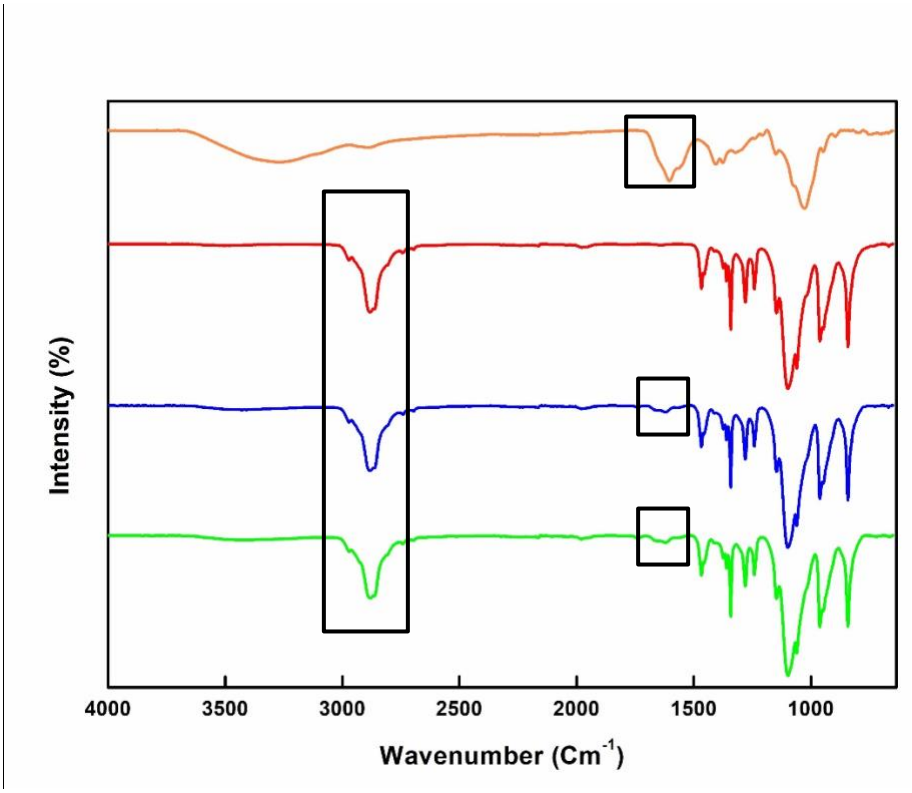


Figure 3.12. FTIR spectra of HA (orange), PF-127 (red), blank-tNPs-PF-127/HA hydrogel (blue) and DEX-tNPs-PF-127/HA hydrogel (green).

The molecular interaction between HA and PF-127 is driven primarily by hydrogen bonding (Figure 3.13). The carboxyl and hydroxyl groups interact through hydrogen bonding resulting in a thermoresponsive hydrogel with improved viscoelasticity, and controlled gelation behaviour. Figure 3.13 shows our proposed molecular interaction between HA and PF-127 to form the PF-127/HA hydrogel.

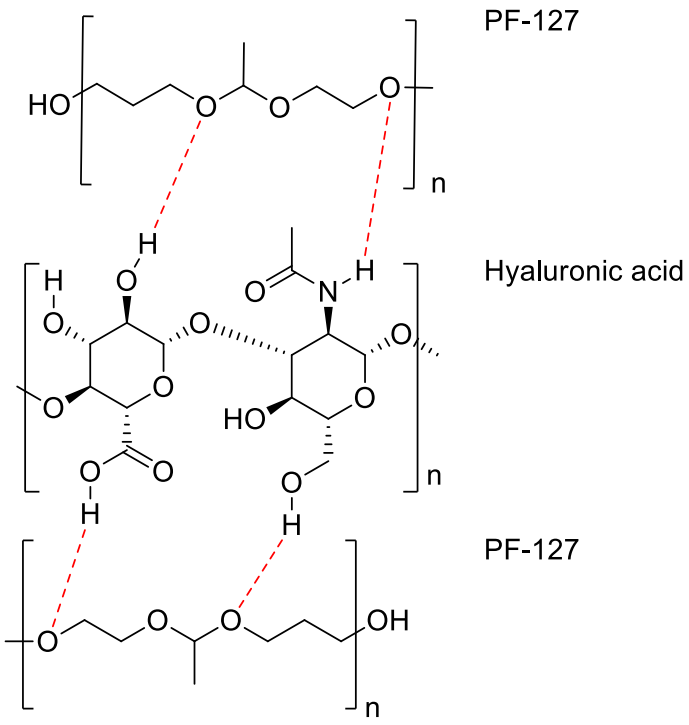


Figure 3.13. Proposed molecular interactions between PF-127 and HA.

3.3.11. XRD: Analysis of the Crystallographic Structure of the tNPs-PF-127/HA Hydrogels

The XRD diffractogram of HA showed a broad singular peak while the blank and DEX-tNPs-loaded hydrogels displayed similar diffractograms (Figure 3.14). Interestingly, the peaks of the DEX-tNPs-PF-127/HA and blank-tNPs-PF-127/HA hydrogels were at the same position as that of PF-127 (19.3° and 23.4°) but with a significantly lower intensity.

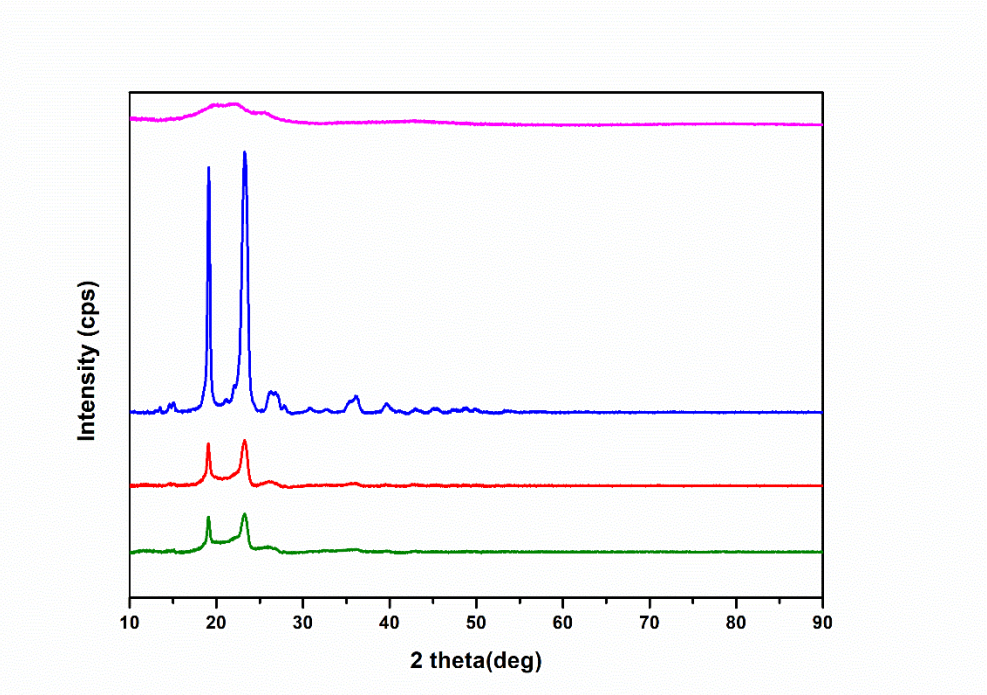


Figure 3.14. XRD diffractograms of HA (pink), PF-127 (blue), blank-tNPs-PF-127/HA hydrogel (red) and DEX-tNPs-PF-127/HA hydrogel (green).

3.3.12. TGA: Thermal Stability and Decomposition for tNPs-PF-127/HA Hydrogels

TGA was conducted to evaluate the thermal degradation properties of the tNPs-P127/HA hydrogels (Saadatkhah *et al.*, 2020); the thermograms of the loaded and blank hydrogel exhibited thermal degradation traits of both PF-127 and HA which were indicative of their respective presence within the formulation (Figure 3.15). The HA groups were not as prevalent in these spectra because only 1% (w/v) was used which was too low to be significantly observed.

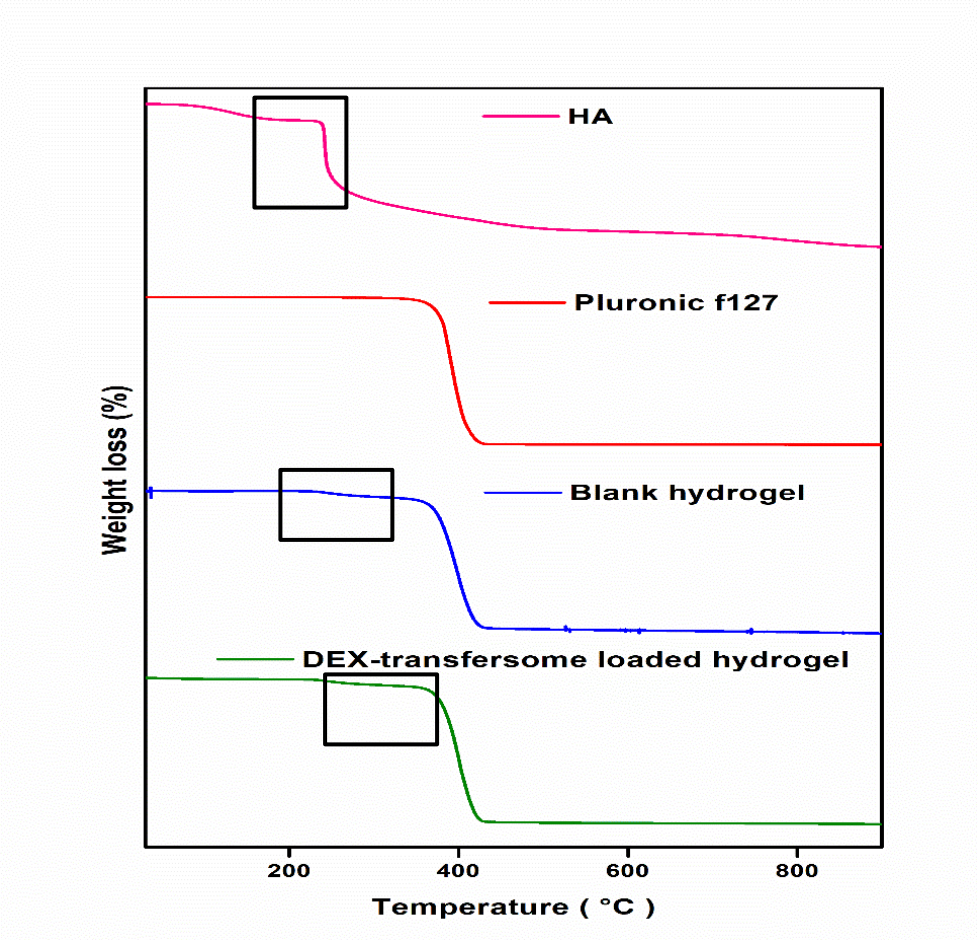


Figure 3.15. TGA thermograms of HA, PF-127, blank hydrogel and loaded hydrogel.

3.3.13. Gelation Time and Syringeability Evaluation of the DEX-tNPs-PF-127/HA Hydrogel

The *in situ* hydrogel behaved like a solution with relatively low viscosity at room temperature and a physically crosslinked gel upon incubation at 37°C (Figure 3.16). It took the hydrogel approximately 150-200 seconds to form a gel and a sol–gel transition was obtained using from the tube inversion test to verify the gelation (Figure 4.16a). Moreover, the syringeability test profile attained from the TA showed that hydrogel required a maximum force of 24 N to extrude from a standard 22-gauge needle (Figure 3.16b).

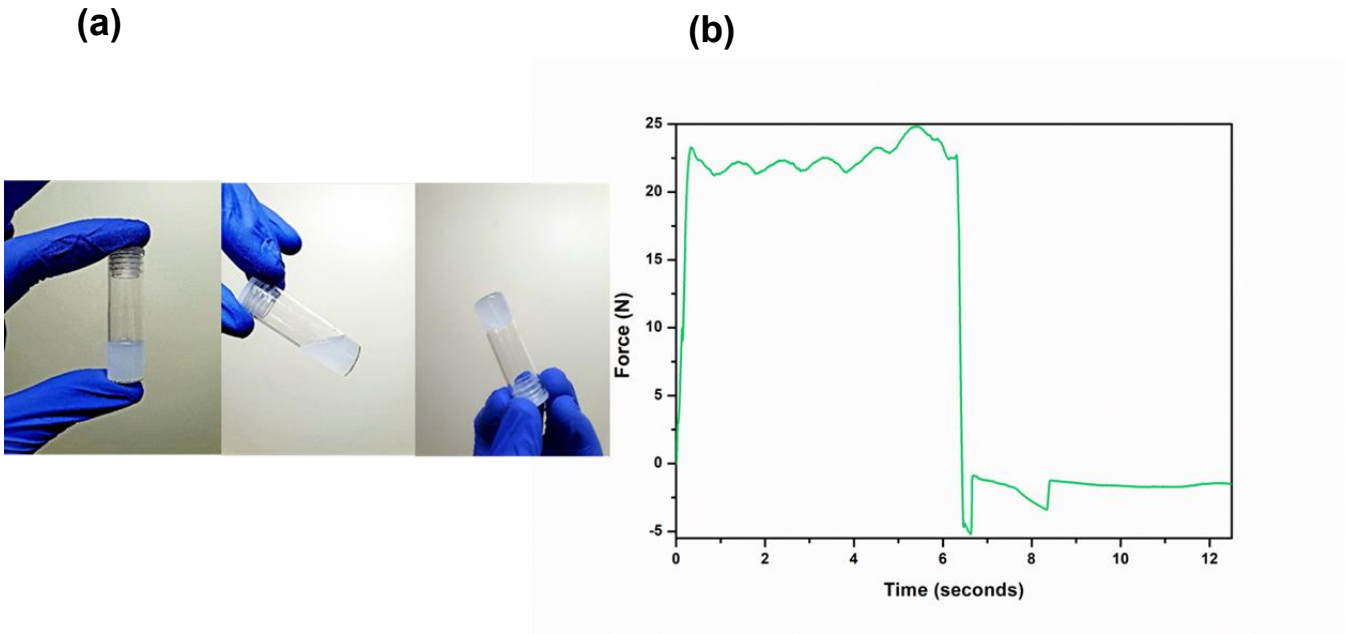


Figure 3.16. The inverted tube method depicts the sol-gel transition (a) of the composite and syringeability profile of the hydrogel (b).

3.3.14. *In Vitro* DEX Release Profile from PF-127/HA Hydrogel

The cumulative drug release profiles of DEX from the tNPs incorporated into the PF-127/HA hydrogel from a cellulose membrane dialysis bag at pH 7.4 were determined. The release profile showed an initial burst release during the first week (62.5 %) and a more gradual and sustained release for the following 6 weeks, with minimal DEX getting released from weeks 5 to 8 (Figure 3.17).

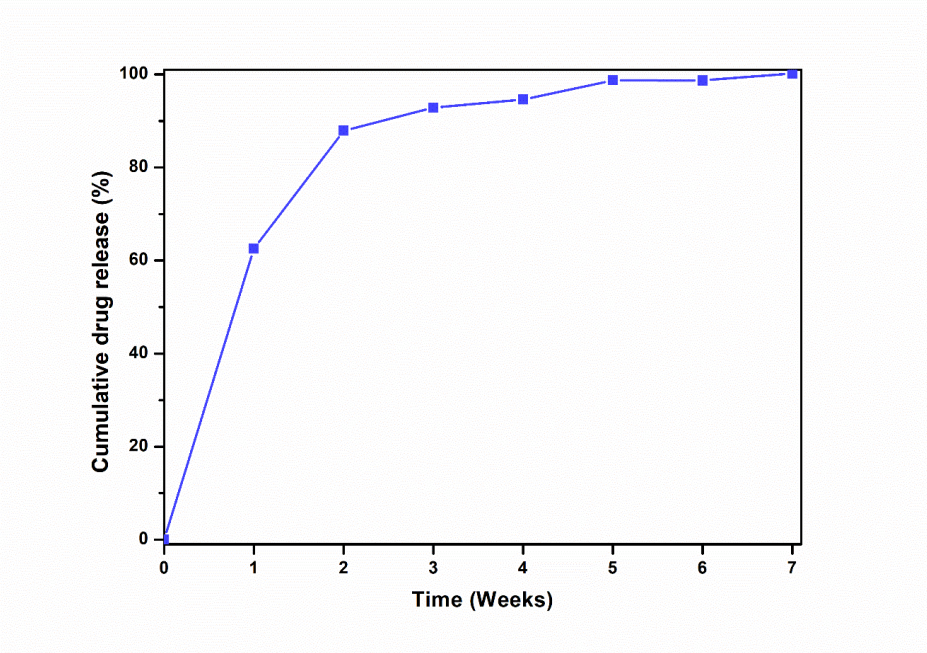


Figure 3.17. *In vitro* release profile of DEX from the tNPs incorporated into PF-127/HA hydrogel at pH 7.4.

3.3.15. *In Vitro* Drug Release Using a Knee Joint Simulator

Mimicking the *in vivo* environment, the knee simulator was used to determine the drug release during normal knee movements. The obtained release profile showed a burst release of 48% within the first 30 minutes, followed by a more steady and sustained release for a further three and a half hrs. (Figure 3.18). According to Indian Design Patent Registration no 375583-00, this would mean that within the first week (30-minute simulator cycles), there was a burst release followed by a sustained release, summing up to a release of 2 months (Wimmer *et al.,* 2015).

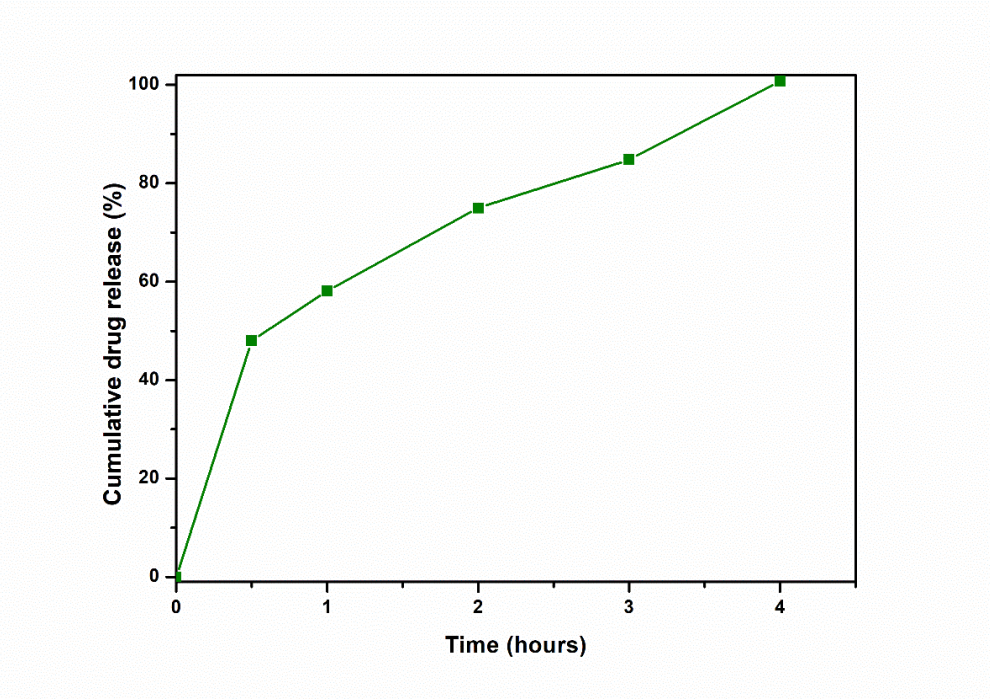


Figure 3.18. The DEX-release profile was obtained using the knee joint simulator.

3.3.16. Rheological Characterization of DEX-tNP-PF-127/HA Hydrogels

To study the dynamic rheological properties of the generated DEX-tNPs loaded hydrogel, the temperature ramp, stress sweep, frequency sweep, yield stress, and thixotropy tests were conducted. The temperature ramp is an indicator of the gelation point of the hydrogel (Goudoulas and Germann, 2017). The temperature ramp showed that the loss modulus (G'') was initially greater than the storage modulus (G') at lower temperatures until a crossover at 30 °C (Figure 3.19a). The viscosity of the hydrogel increased with the increase in temperature from 1627,83 mPas at room temperature to 9295,78 mPas at the gelation temperature (30 °C) and 901754,63 mPas at body temperature (37°C). The stress-sweep test was conducted to evaluate the LVE region, enabling the frequency sweep test to be conducted within the moduli recorded for the LVE. The LVE region was identified as a plateau at 9175 Pa (Figure 3.19b) and additionally, the LVE regions for the hydrogel ranged between 0.1 Pa and 100Pa. Furthermore, the frequency sweep was conducted at 0.1 and 10 Hz within the LVE. The frequency sweep test showed that G' was greater than G'' as well as a crossover point between G' and G'' at higher frequencies (Figure 4.19c).

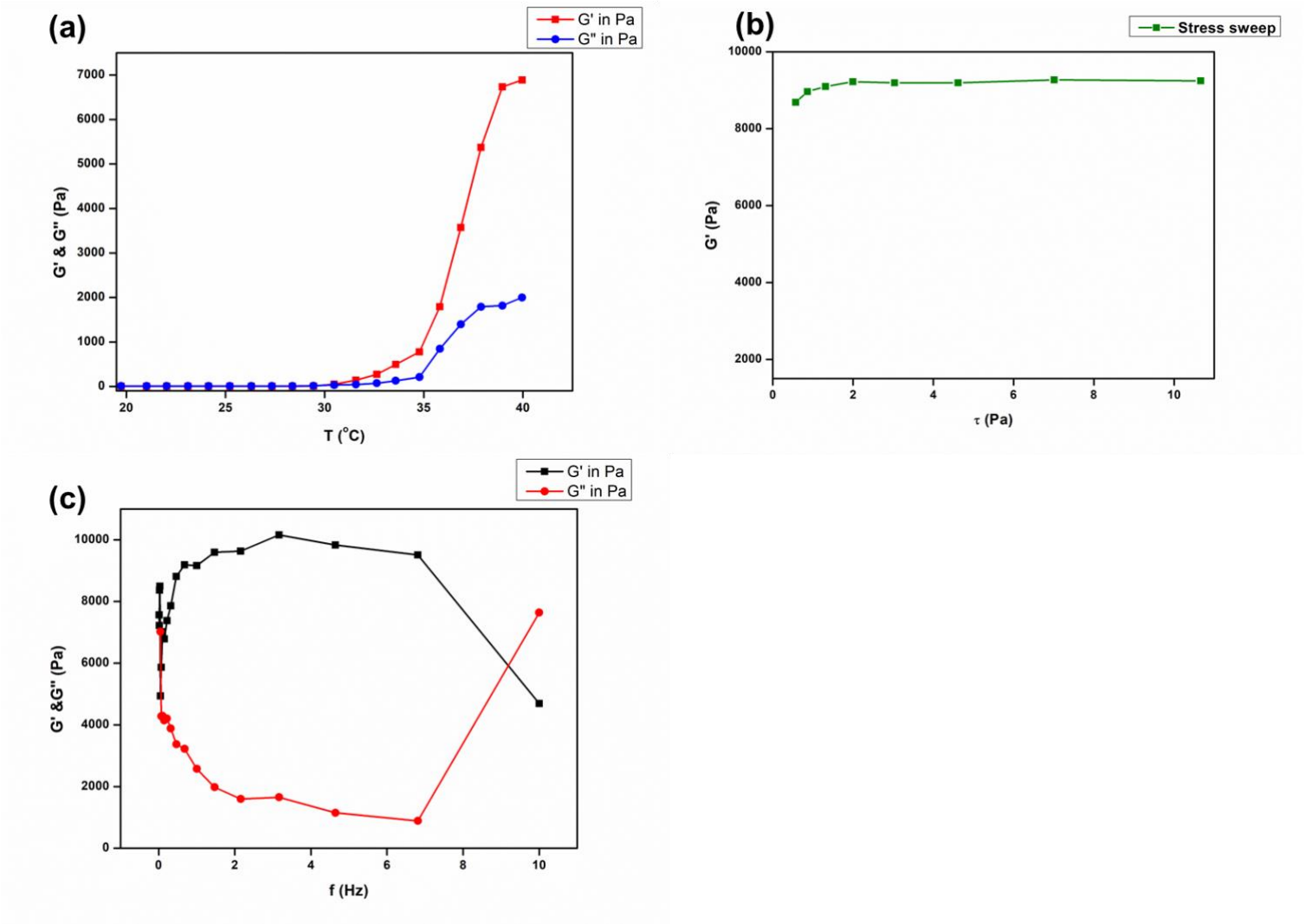


Figure 3.19. Rheograms presenting the temperature ramp (a), stress sweep (b), and frequency sweep (c) of the DEX-tNPs-PF-127/HA hydrogel.

On the other hand, yield stress is defined as the minimum amount of stress required to induce the flow of a polymer solution (Mouser *et al.,* 2016). The yield stress of the hydrogel was 108.8 Pa (Figure 3.20a). A hysteresis loop was obtained from the thixotropy test, and the area of the loop was used to determine the thixotropy. The area under the curve was calculated as 38170 Pa·s (Figure 3.20b).

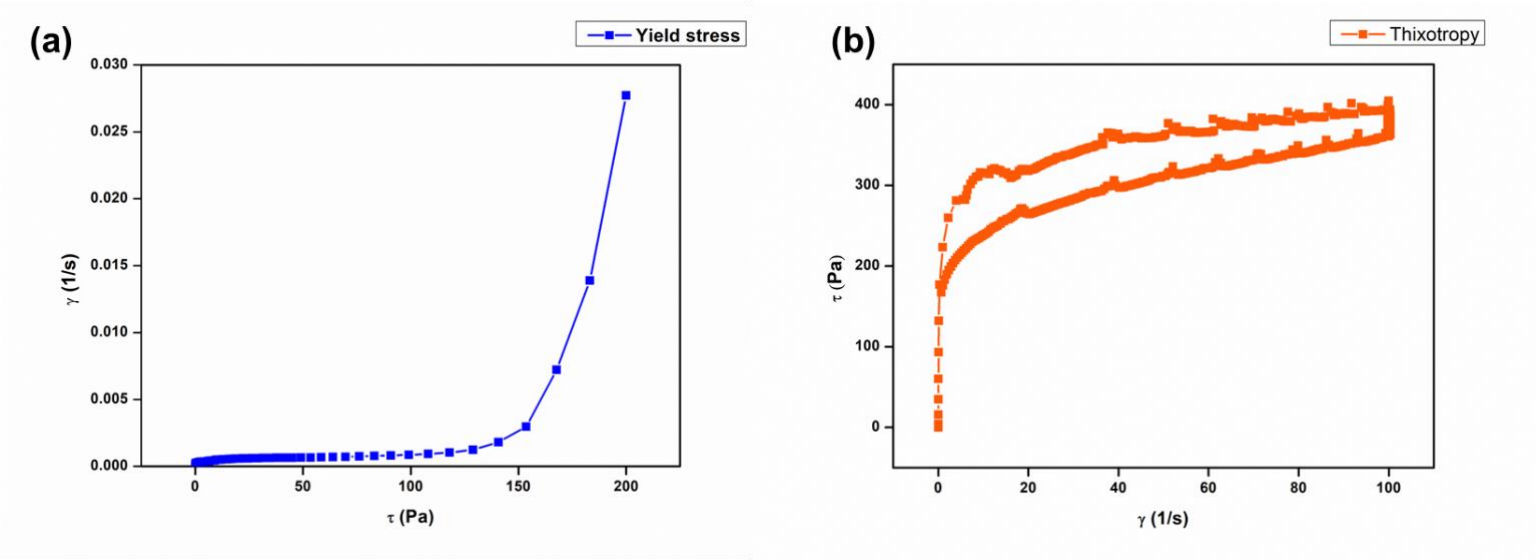


Figure 3.20. Rheograms presenting the yield stress (a) and thixotropy (b) of the DEX-tNPs-PF-127/HA hydrogel.

3.3.17. *In Silico* Analysis, the DEX-tNP Complex

The DEX-tNP complex was successfully built using the molecular modeling technique. This started from the initial building of a polymer from four components of the tNP: phosphatidylcholine, cholesterol, polysorbate 80, and DDAB. The polymer was transformed into a tNP through the Nanoparticle Builder tool after which the DEX loading and its interaction with the tNP was simulated through the Disordered System platform. Modeling of the DEX-tNPs complex in the physiological solvent system (Figure 3.21a) showed successful DEX loading in the centroid of the tNPs (Figure 3.21b). As expected, it was observed that due to being quaternary ammonium compounds, both phosphatidylcholine and DDAB introduced and maintained a cationic charge in the transfersomal system. Furthermore, a detailed analysis of the DEX-tNP interactions revealed that DEX mainly interacted with phosphatidylcholine through nonpolar interactions and with at least one hydrogen bond (Figure 3.21c). This suggested a well-balanced interaction between DEX and the tNP that is usually regarded as optimum for controlled drug release (Govender *et al*., 2023).

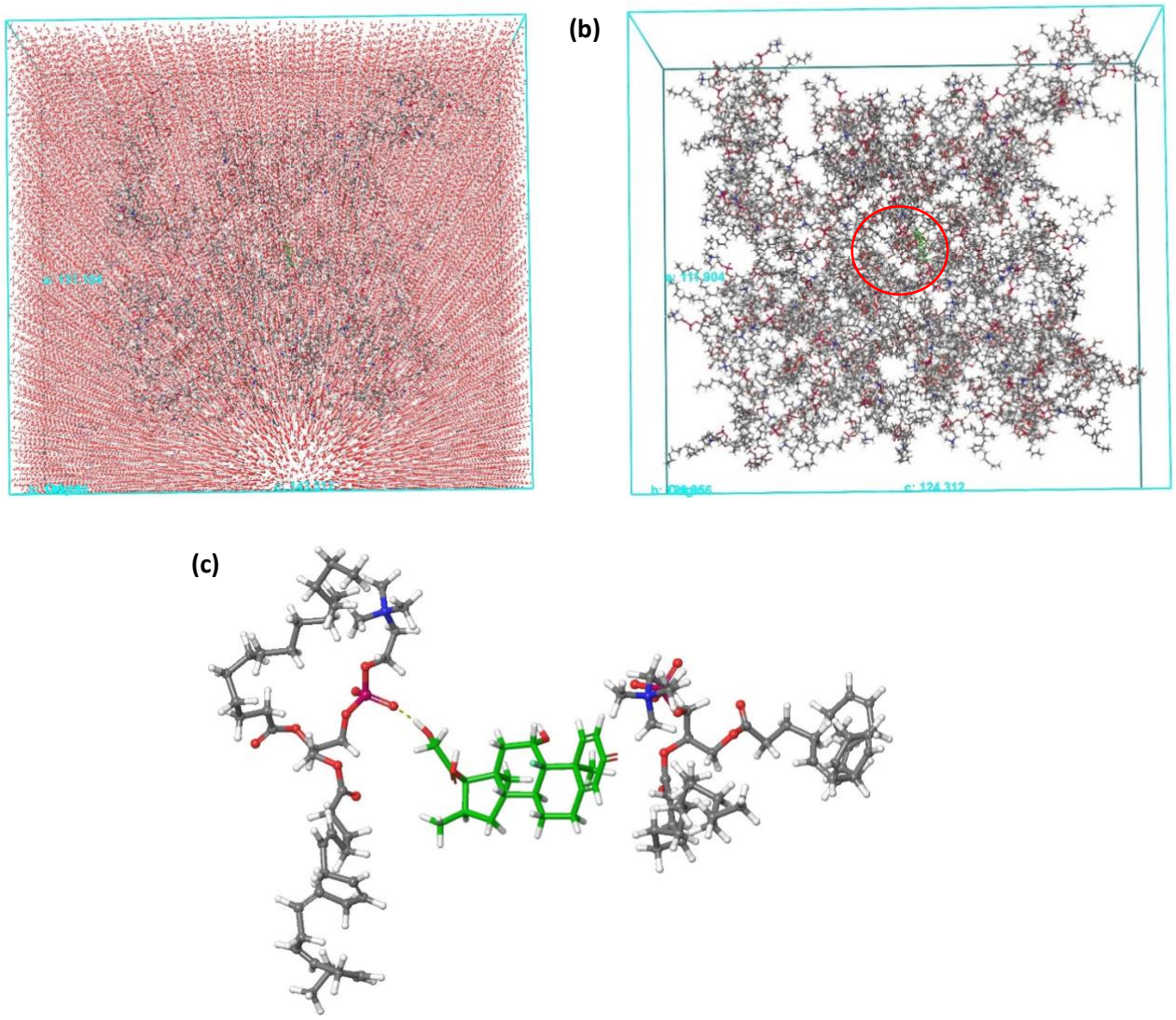


Figure 3.21. The *in silico* simulation of DEX-tNP complex. A) shows the DEX-tNP complex in the buffered water model. B) shows the successful DEX-loading in the tNP and, C) displays the established molecular interactions between DEX and transfersomal constituents (only two monomers closest to DEX selected).

3.3.18. Cytocompatibility Studies

The microphotographs of 264.7 RAW macrophages (Figure 3.22) show the cells actively growing with a slightly elongated morphology, possibly undergoing phagocytosis vs. a more rounded shape and less spread out 72 hours post-treatment.

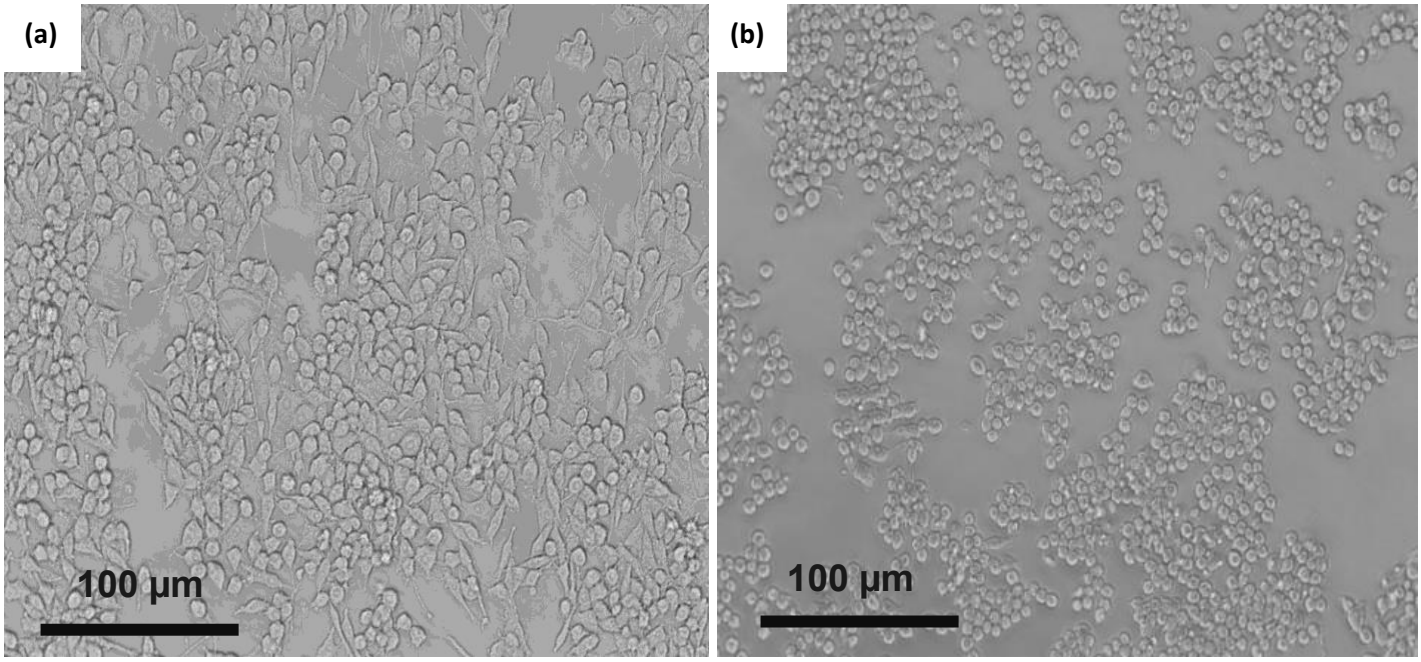


Figure 3.22. Micrographs of 264.7 RAW macrophage cells before treatment at 20× for (a) 264.7 RAW macrophage cells post 72 hours of treatment

The cytotoxic effects of DEX, Blank-tNPs, DEX-loaded tNPs, Blank-tNPs-PF-127/HA hydrogel, and DEX-tNPs-PF-127/HA hydrogel composites on the viability of RAW 264.7 were evaluated using MTT assay. The results are presented as a percentage of cell viability. The relative metabolic activity of RAW 264.7 cells exposed to varying doses of the various treatments (50 µg/mL, 25 µg/mL, 12.5 µg/mL, and 6.25 µg/mL) demonstrated that all concentrations of all treatments exhibited no cytotoxic effect on cell viability in RAW 264.7 cells (Figure 3.23). At the highest concentration, all treatments maintained relatively high cell viability, with the Blank-tNPs hydrogel showing the highest at 107.14%. At lower concentrations, both hydrogel treatments continued to show elevated viability compared to other treatments, particularly the Blank-tNPs hydrogel. Therefore, all concentrations of the various treatments would be used for subsequent experiments to ensure effective and sustained compound activity over the treatment period.

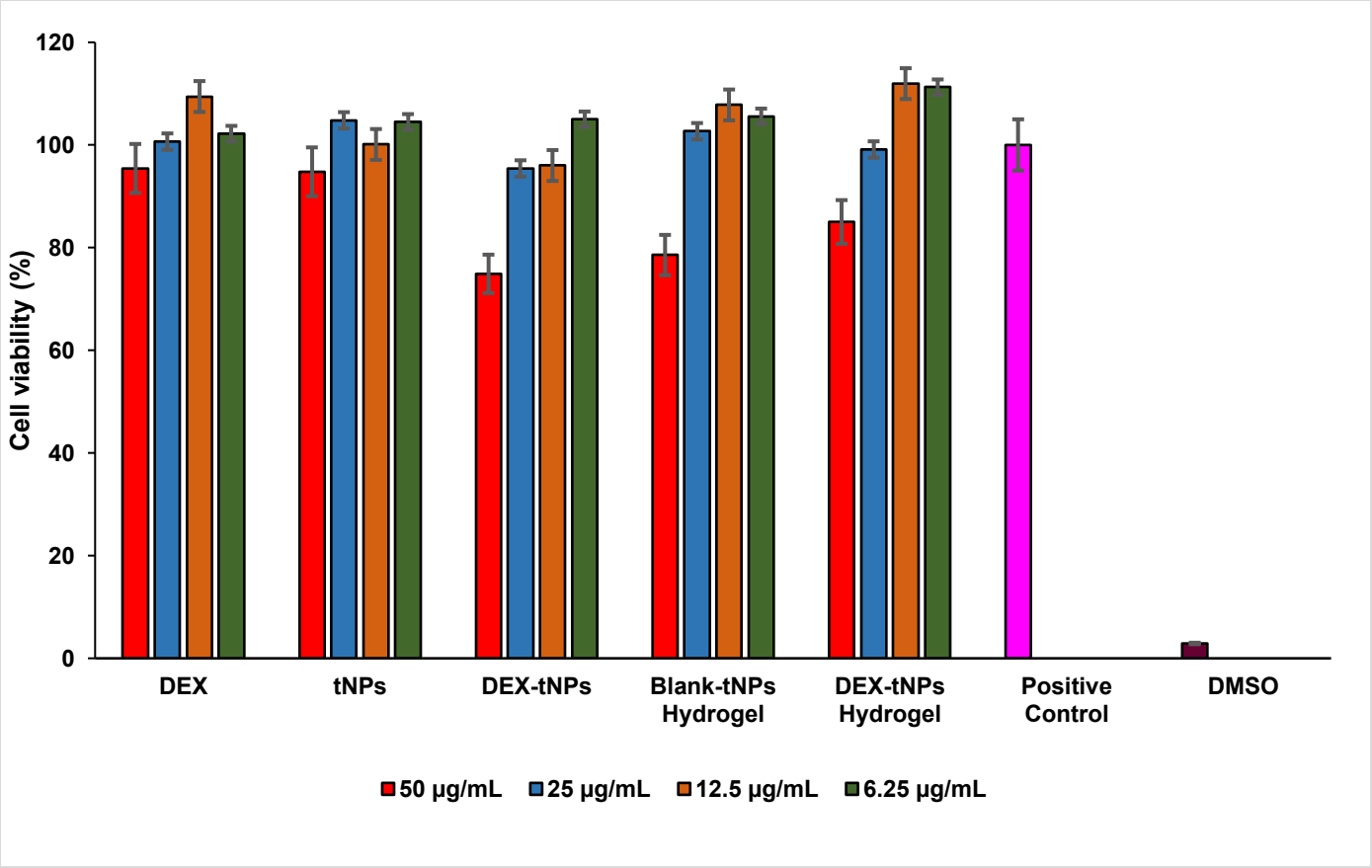


Figure 3.23. Cell proliferation and viability of murine RAW 264.7 macrophages exposed to DEX, Blank-tNPs, DEX-tNPs, Blank-tNPs hydrogel, and DEX-tNPs hydrogel composites for 72 hours.

IL-4 Quantification from RAW 26.4 Macrophage Cells After Treatment.

The study evaluated the effects of various treatments on the secretion of IL-4 by Raw 264.7 macrophages. An increase in IL-4 would suggest that the treatment administered exerts an anti-inflammatory response on the RAW 264.7 macrophages. The negative control group did not receive any treatment. The quantified IL-4 concentrations (pg/mL) for each treatment group are presented in Figure 3.25. The DEX treatment group resulted in an IL-4 concentration of 78.27±26.35 pg/mL, while the blank-tNPs treated group produced 107.85 ± 23.17 pg/mL. The DEX-loaded-tNPs showed a reduced IL-4 level of 63.37± 60.37pg/mL compared to the blank-tNPs. However, the change was insignificant. The Blank-tNPs-PF-127/HA hydrogel treatment showed the highest IL-4 concentration at 135.51±17.61 pg/mL. The DEX-tNPs-PF-127/HA hydrogel treatment resulted in lower levels of IL-4 (107±43.89 pg/mL) compared to their hydrogel counterpart. The negative control group showed a negative value of -38.55±10.19 pg/mL, indicating that the levels in the samples were below the quantitation limit, thus no IL-4 production.

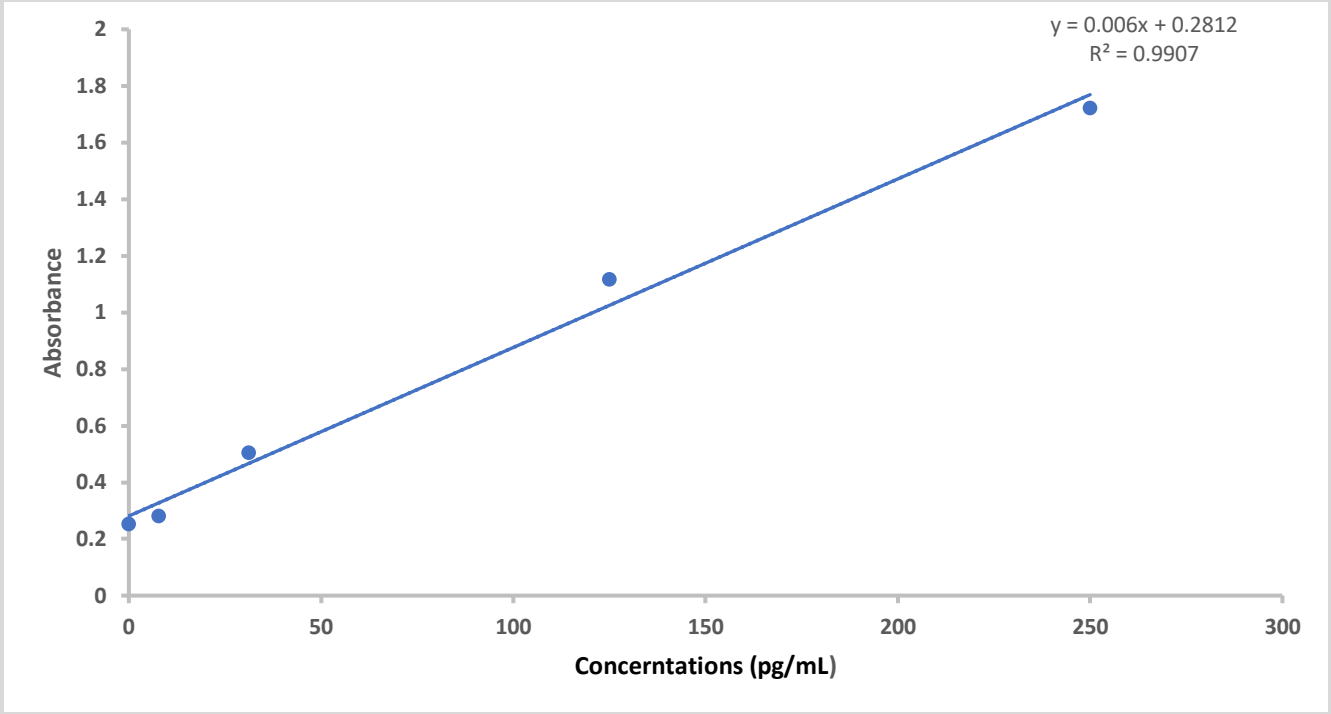


Figure 4.24. Standard curve representative for mouse IL-4 Instant ELISA KIT.

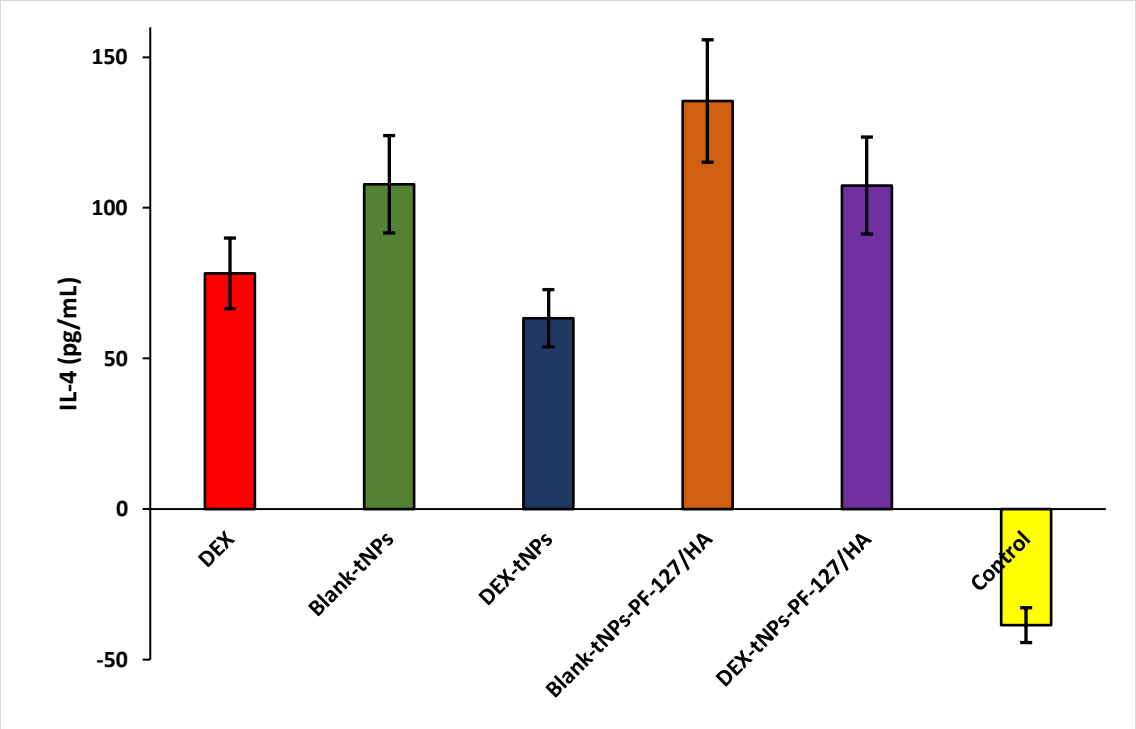


Figure 4.25. Quantification of IL-4 secretion by raw macrophages post-treatment with various formulations after 24 hours of incubation (Control:Blank/negative control).

4. Discussion

Relevant literature was reviewed involving recent developments in research undertaken for IA drug delivery in OA (Chapter 2). It was shown that nanotechnology, in a multitude of modalities, has been effective in enhancing the treatment of OA. Furthermore, hydrogels were demonstrated to potentiate the efficiency of nanosystems in IA drug delivery treatment of OA. Of the hydrogels reviewed, the thermo-responsive hydrogels were better suited for IA administration.

In this study, we designed and developed a DEX-tNPs-P127/HA stimuli-responsive hydrogel suitable for IA delivery in OA. An optimal DEX-loaded tNPs formulation was subjected to studies including morphology analysis, physicochemical characterizations, *in vitro* DEX release and stability of the formulation. A stimuli-responsive P127/HA hydrogel was prepared, and the optimal DEX-loaded tNPs formulation was incorporated to form the DEX-tNPs-P127/HA hydrogel composite.

Using the Maestro Materials Science platform of Schrödinger software, the Nanoparticle Builder and Polymer Builder tools were utilized to model potential molecular interactions between tNPs and DEX. A polymer composed of phosphatidylcholine, cholesterol, polysorbate 80, and DDAB was constructed and transformed into a tNP, followed by DEX loading simulations via the Disordered System platform. The modeling confirmed successful DEX loading at the tNP centroid, with phosphatidylcholine and DDAB maintaining a cationic charge due to their quaternary ammonium nature. Detailed analysis revealed that DEX primarily interacted with phosphatidylcholine through nonpolar interactions and at least one hydrogen bond, suggesting a well-balanced interaction ideal for controlled drug release (Govender *et al*., 2023). This confirmation supported the synthesis of tNPs and subsequent DEX loading.

The tNPs were successfully synthesized employing the thin layer film hydration method. Subsequently, SEM and TEM analysis confirmed nanosized and spherical morphology of tNPs, which ideal for drug encapsulation and biomedical application. DLS analysis revealed that the size of the tNPs increased when the DEX was loaded from an average hydrodynamic size of 60.93 nm to 76.43 nm with a PDI values less than 0.5 units (Table 3.2). Since the size of the tNPs is originally below 100 nm, they are in a desirable range to be delivered and to maneuver through the ECM of cartilage in OA drug delivery (Rothenfluh *et al*., 2008; Sophia *et al.,* 2009; DiDomenico *et al*., 2018). The size difference of the blank vs the loaded tNPs was an indication that the anionic drug had been successfully incorporated into the cationic tNPs, while both sets of tNPs had a good particle size distribution with PDI values remaining below 0.5, indicating a highly

monodispersed system conducive to uniform drug distribution (Hoseini *et al*., 22023). Interestingly, the PDI of the DEX-loaded tNPs (0.183 ± 0.008) was lower than that of the blank particles (0.191 ± 0.002), depicting that the drug had a stabilizing effect on the tNPs, possibly reducing agglomeration of the tNPs (Opatha *et al*., 2020). Unlike conventional lipid nano-carriers, tNPs consist of hydrophilic and hydrophobic moieties, which means that DEX (a hydrophilic drug) was encapsulated in the aqueous core compartment of the tNPs (Opatha *et al.*, 2020; Buga *et al*., 2021). Furthermore, the zeta potential of the blank-tNPs (15.8 mV) decreased after encapsulation of the drug (10.58 mV). Since DEX has an anionic charge, the decrease in the surface charge of the tNPs also showed that the drug was successfully entrapped. The tNPs maintained their cationic charge with an overall surface charge of 10.58 mV. Cationic NPs can traverse cellular membranes more easily compared to their anionic counterparts. This is because cationic NPs induce the development of a disintegrated surface unity in the bilayer and hydrophilic pores, allowing them to penetrate the cell membrane readily (Lin *et al*., 2010). The EE of the tNPs was found to be supreme, entrapping a staggering 98 ± 0.31% of the loaded DEX further substantiating the suitability of the tNPs for drug delivery. Essentially, this correlates with previous studies depicting that tNPs generally have an excellent EE capacity (Gupta *et al.,* 2012; Khan *et al*., 2021; Prashanthini *et al.,* 2023). The tNPs vesicles were also flexible, showing a 16% decrease in diameter, which is concurrent with the literature on the flexibility of tNPs (Modi. and Bharadia, 2012). This is attributed to the presence of EAs, which bring about membrane ultra-flexibility by acting as membrane destabilizing factors. Due to their deformability, the tNPs have the capacity to adapt to the narrow spaces within the OA joint, enhancing drug penetration and distribution.

Upon the preparation of the PF-127/HA hydrogel, a suspension of DEX-loaded tNPs was loaded into the hydrogel solution. The observed reduced pore size of the hydrogel upon the integration of the DEX-loaded tNPs suggested a successful incorporation of the tNPs within the network, filling up the pores and thus a formation of DEX-tNPs-P127/HA hydrogel (Table 3.4) (Kong *et al*., 2020; Zhang *et al*., 2021). The decrease in the pore sizes suggests that the release of the drug from the tNPs happens as the hydrogel network degrades. This suggests that the degradation of the hydrogel network was a drug release rate-limiting step from the PF-127/HA hydrogel network (Tsubosaka *et al*., 2020). SEM micrographs (Figure 3.11) confirmed the porous structure of the hydrogel matrix. The porous nature of the matrix is important because it allows a high volume of the DEX-loaded tNPs to get diffused through and retained, therefore enhancing the drug-loading capacity and improving the rate of drug release (Lee and Hwang, 2023).

The FTIR broadband on both DEX loaded and blank tNPs at 3375.35 cm-1 was assigned to stretching vibration of O-H bonds, indicating the presence of hydroxyl groups in both cholesterol and phosphatidylcholine (Figure 3.7). The two narrow peaks observed at 2923.14 cm^{-1} and 2853.47 cm^{-1} were ascribed to the stretching vibration of CH_2 groups. Interestingly, Polysorbate 80, cholesterol, phosphatidylcholine, and DDAB all contain these hydrocarbon chains within their structures (Pereira and Mallya, 2015; Javed *et al.*, 2018; Bide *et al.*, 2021). The intense, narrow band at 1736.88 cm^{-1} was attributed to the C=O (carbonyl) stretching vibration from phosphatidylcholine which has ester linkages within its structure (Kanno *et al*., 2007). None of the distinctive characteristic bands associated with DEX are detectable in the FTIR spectrum of the DEX-loaded tNPs. This observation indicates that there was no unwanted interaction between DEX and excipients in the formation of the tNPs. This finding thereby confirms the compatibility of the reagents in the formulation and that no new chemical bonds were formed when loading the DEX into tNPs (Uwaezuoke *et al.,* 2022). The absence of DEX-specific bands also validated the successful encapsulation of DEX into the tNPs (Wagh and Apar, 2014).

Nevertheless, the FTIR spectra of the DEX-tNPs-PF-127/HA and blank-tNPs-PF-127/HA hydrogels showed the presence of the majority of characteristics of PF-127, the main constituent of the hydrogel with bands at approximately 2881.93; 1979; 1466.69, 1373.01 cm^{-1} (Figure 3.12) (Dmitrenko *et al*., 2019). On the other hand, the bands at approximately 1620 and 1373.01 cm^{-1} were characteristic of HA (Al-Sibani *et al.*, 2018; Güngör *et al.*, 2019). On the other hand, the medium band at 2881.93 cm^{-1} corresponds to the presence of C-H stretching vibration. The weak band at 1979 cm^{-1} can be attributed to a stretching C-H bond (Moqejwa *et al*., 2022). The only band indictive of HA at 1620 cm^{-1} is an illustration of the presence of a stretching C=O bond (Al-Sibani *et al.,* 2018). Lastly, the 1466.69 cm^{-1} shows a bending CH_2 bond, while 1373.01 cm^{-1} corresponds with the presence of a CH_3 (methyl group) in the system (Nikafshar *et al*., 2017). The absence of the bands of the tNPs and pure DEX (Figure 3.7) proved that the particles were embedded into the hydrogel matrices (Wagh and Apar, 2014).

XRD diffractograms (Figure 4.9) of pure DEX showed multiple sharp and intense peaks, indicating that the structure was highly crystalline, while both the DEX-loaded and blank tNPs could be classified as amorphous, displaying diffraction peaks (2θ) at 20° and 40° (Karava *et al.,* 2020). The absence of structural characteristics of DEX meant that there was a conversion from crystalline to amorphous structure which was indicative of successful encapsulation of DEX into the nanosystem. Short-term stability studies revealed a decrease in zeta potential and an increase in PDI, meaning that the DEX-loaded tNPs were slightly destabilized at 25°C compared to 4°C.

This suggested that 4°C was more ideal than the 25°C storage condition. The formulations had no colour changes or phase separation (sedimentation) throughout the study period (Table 3.3). This showed that the DEX-loaded tNPs were stable for 3 months. On the other hand, the diffractograms of PF-127 and HA (Figure 3.14) suggested that they were crystalline and amorphous, respectively. HA presented an undefined hump, while PF-127 had 2 clearly defined peaks at 19° and 23.4°. Since the blank-tNPs-PF-127/HA and DEX-tNPs-PF-127/HA hydrogels displayed no variation in diffractograms, this further proposed that the drug was successfully loaded into the nanosystem (Karava *et al*., 2020). Interestingly, the peaks of the loaded hydrogels were at the same position as that of PF-127 but with a significantly lower intensity meaning that PF-127 had decreased crystallinity, possibly from the presence of amorphous HA (Figure 3.14) (Islam *et al.,* 2021). However, hydrogen bonds can decrease the peak intensity of diffractograms. This effect arises because hydrogen bonding influences the crystal structure and the degree of crystallinity of the material. The presence of hydrogen bonds often diminishes the peak intensity and sharpness in XRD diffractograms, reflecting a decrease in crystallinity or an increase in structural disorder. Based on the proposed interactions of HA and PF-127 (Figure 3.13), the lower intensities might support our proposed interactions in Figure 3.13.

The thermogram (Figure 3.8) of the DEX-loaded tNPs showed their first degradation after approximately 120°C, which is indicative of the presence of DEX in the system, which also degraded at around 100°C (Pérez-González *et al.*, 2021). After 350 °C, the DEX-loaded tNPs underwent a major decomposition (98% of its mass) which was attributed to the decomposition of the main component of tNPs, phosphatidylcholine (Kumar *et al*., 2018). The presence of DEX degradation characteristics showed that the drug was indeed present in the formulation. On the other hand, the blank-tNPs had a slightly different degradation profile, with the first point of degradation being after 200 °C and no characteristics of DEX degradation. The degradation of DEX in the tNPs was minimal compared to that of pristine DEX illustrating that the tNPs enhanced the thermal stability of DEX. However, similar to the loaded formulation, the blank formulation also lost 98% of its mass after 350 °C since they both consist of phosphatidylcholine (Kumar *et al*., 2018). TGA thermograms of the hydrogels showed an initial weight loss at 220 °C which was ascribed to loss of H_2O molecules (Guillot *et al.*, 2023); the same trait could be observed on the thermogram of HA (Figure 3.15). Notably, while DEX-loaded tNPs exhibited major weight loss at approximately 220 °C (Figure 3.8), they were stable up to 380 °C when incorporated into the hydrogel. This is a trait that could also be observed on the thermogram of the blank-tNPs-PF/HA hydrogel and PF-127, the main constituent of the hydrogel. This suggested that the hydrogel was stable up to 380 °C which concurred with available literature (Nguyen *et al*., 2019).

The drug release study demonstrated that free DEX was completely released within 10 h, whereas DEX-tNPs exhibited sustained release for up to 72 h (Figure 3.10). The burst release observed from the profile of the tNPs can possibly be attributed to the encapsulated DEX molecules that were close to the inner surface of the tNPs (Kim *et al.*, 2021). Notably, when incorporated into the hydrogel matrix, drug release conducted using the dialysis method was extended to approximately six weeks (Figure 3.17), indicating significant improvement in controlled IA drug delivery. The knee joint simulator model, which better mimics physiological conditions, suggested an *in vitro* drug release duration of nearly two months (Figure 3.18). This translates to a reduced frequency of IA injections (approximately three per year), improving patient compliance while minimizing the risk of infection associated with frequent IA administration. The gelation time (150-200 seconds) of the DEX-tNPs-PF-127/HA hydrogel was suitable for IA applications, allowing sufficient handling time while ensuring rapid sol-gel transition upon administration. The hydrogel required an extrusion force of 24 N through a 22-gauge needle (Figure 3.16b), well within the acceptable limit for IA injections (≤30 N) (El Kechai *et al.*, 2015).

Figure 3.19a showed that G''>G,' indicating that the DEX-tNPs-PF-127/HA hydrogel was a solution at lower temperatures, and the cross-over between G' and G" showed that the solution transitioned to form a gel at 30 °C (Goudoulas and Germann, 2017)**.** The crossover point where G'=G'' symbolizes a balance between storage and loss modulus (Ramli *et al.*, 2022). The LVE region of the DEX-tNPs-PF-127/HA hydrogel was identified at 9175 Pa between 0.1 Pa and 100 Pa (Figure 3.19b) of the applied stress suggesting that the hydrogel network could withstand a threshold of 100 Pa stress before deformation (Panyamao *et al*., 2020). The G' in the frequency sweep was greater than the G'', indicating the viscoelastic and gel-like behavior of the hydrogel at 37°C (Figure 3.19c). The yield stress (108 Pa) was relatively low (Di Giuseppe *et al*., 2015), meaning that the hydrogel flowed at relative ease, making it ideal for IA injections through the needle, and once injected, the gel could adapt to the contours of the joint (Figure 3.20a) (Weston *et al*., 2017). Moreover, hydrogels with yield stress greater or equal to 25 Pa are considered more stable and more robust (Jons *et al*., 2022). The attained yield stress would potentially allow the even distribution of hydrogel solution in the OA joint. The hydrogel exhibited shear-thinning properties suggesting that it assumed a non-Newtonian fluid character as its viscosity was affected by shear rate (Amoo and Fagbenle, 2020) (Figure 3.20b). Self-healing properties of the hydrogel were observed through the inversely proportional relationship between viscosity and shear rate, with self-healing occurring at static conditions. The shear-thinning of the hydrogel supported the yield stress and syringeability results suggesting a reduced injection force for

administration. More importantly, this also suggested that the hydrogel had the potential to recover its structure within the joint following its injection.

The molecular modeling-based simulation of DEX- tNP complex correlated with the *in vitro* data whereby the generated tNP showed a cationic charge introduced by phosphatidylcholine and DDAB (Figure 3.21). This was in agreement with the literature that identified DDAB as an ingredient used to optimize the surface charge of tNPs (Silva *et al*., 2019). Furthermore, DEX was shown to interact mainly with phosphatidylcholine, which was previously suggested to achieve excellent encapsulation and enhance controlled drug release from the tNPs (Moqejwa *et al.,* 2022; Uwaezuoke *et al.,* 2022). Additionally, DEX interacted with phosphatidylcholine through balanced polar and nonpolar interactions that are required to achieve controlled drug release (Govender *et al*., 2023). Therefore, these supported the notion that DEX was successfully loaded into the tNP and could be easily released in a controlled manner.

The MTT assay is commonly employed to assess cellular proliferation, as the MTT reagent is reduced by metabolically active cells, excluding the non-viable portion of the cell population from the measurement. The results indicate that all treatments were non-toxic to RAW 264.7 macrophages at the tested concentrations (Figure 3.23). Notably, hydrogels and DEX-tNPs hydrogels consistently enhanced cell viability, suggesting a possible protective or proliferative effect. The DEX-tNPs showed the most significant increase in cell viability at the lowest concentration, which might be due to enhanced drug delivery and sustained release properties.

The primary objective of IL-4 Quantification from RAW 26.4 macrophage cells after treatment was to assess the effects of the various treatments on the secretion of IL-4 by the RAW 264.7 cells (Figure 3.25). IL-4 plays a vital role in preventing the progression of OA; thus, its levels can be used to predict the therapeutic effect of various treatments in OA (Wojdasiewicz *et al.*, 2014). The comparative analysis of the results showed notable differences in the section of IL-4 among the different treatment groups, which was used to provide valuable insights into their respective anti-inflammatory potentials. Results from the IL4-quantification suggest that the Blank-tNPs-PF-127/HA hydrogel had the best effect on the secretion of IL-4. The results suggest that all treatments can increase levels of IL-4 production compared to the control group. This means that all treatment groups can potentially induce an anti-inflammatory response. Blank-tNPs-PF-127/HA hydrogel (135.51 pg/mL) had the highest IL-4 production, suggesting that it elicited the most anti-inflammatory response. This is possible because of the presence of HMW HA in the formulation, which has been proven to induce the M2 anti-inflammatory macrophage phenotype (Shahbazi *et al*., 2018). DEX, a well-known anti-inflammatory agent, had the second highest

response, supporting its established role in the regulation of inflammation. Interestingly, both the Blank-tNPs and the DEX-loaded tNPs elicited a relatively high response compared to the control group, albeit the DEX-tNPs had slightly lower production. This surprising outcome suggests that the encapsulation of DEX into the tNPs possibly attenuates inflammation modulation of DEX. The same behaviour can be observed in the reduced production of IL-4 by DEX-tNPs-PF-127/HA hydrogel compared to Blank-tNPs-PF-127/HA loaded hydrogel, suggesting that the DEX-loaded tNPs reduced the system's anti-inflammatory activity. Further investigations are warranted to elucidate the underlying mechanisms. More importantly, the results suggest that the Blank tNPs and the Blank-tNPs-PF-127/HA hydrogel, irrespective of DEX encapsulation, may have potential as novel anti-inflammatory agents.

5. References

Adebajo, A., 2012. Non-steroidal anti-inflammatory drugs for the treatment of pain and immobility-associated osteoarthritis: consensus guidance for primary care. *BMC Family Practice*, *13*(1), pp.1-7

Allen, K.D. and Golightly, Y.M., 2015. Epidemiology of osteoarthritis: state of the evidence. *Current Opinion in Rheumatology*, *27*(3), p.276.

Al-Owaidi, M.F., Alkhafaji, S.L. and Mahood, A.M., 2021. Quantitative determination of dexamethasone sodium phosphate in bulk and pharmaceuticals at suitable pH values using the spectrophotometric method. *Journal of Advanced Pharmaceutical Technology & Research*, *12*(4), p.378.

Al-Sibani, M., Al-Harrasi, A. and Neubert, R.H.H., 2018. Characterization of linear and chemically cross-linked hyaluronic acid using various analytical techniques including FTIR, ESI-MS, H1 NMR, and SEM. *J. Biochem. Anal. Stud*, 3, pp.1-8.

Amoo, L.M. and Fagbenle, R.L., 2020. Overview of non-Newtonian boundary layer flows and heat transfer. In *Applications of Heat, Mass and Fluid Boundary Layers* (pp. 413-435). Woodhead Publishing.

Ayhan, E., Kesmezacar, H. and Akgun, I., 2014. Intraarticular injections (corticosteroid, hyaluronic acid, platelet rich plasma) for the knee osteoarthritis. *World Journal of Orthopedics*, *5*(3), p.351.

Baker, M., Brook, B.S. and Owen, M.R., 2017. Mathematical modelling of cytokines, MMPs and fibronectin fragments in osteoarthritic cartilage. *Journal of Mathematical Biology*, 75, pp.985-1024.

Brame, J.A. and Griggs, C.S., 2016. Surface area analysis using the Brunauer-Emmett-Teller (BET) method: scientific operation procedure series: SOP-C. https://erdc-library.erdc.dren.mil/jspui/handle/11681/20339. [accessed on 10 September 2022].

Bnyan, R., Khan, I., Ehtezazi, T., Saleem, I., Gordon, S., O'Neill, F. and Roberts, M., 2018. Surfactant effects on lipid-based vesicles properties. *Journal of Pharmaceutical Sciences*, *107*(5), pp.1237-1246.

Buga, I., Uzoma, J.I., Reindel, K., Rashid, K., Diep, T., McCartan, P. and Zhao, F., 2021. Physical and chemical stability of dexamethasone sodium phosphate in intravenous admixtures used to prevent chemotherapy-induced nausea and vomiting. *Hospital Pharmacy*, 56(4), pp.215-220.

Celik, M.Ö., Labuz, D., Keye, J., Glauben, R. and Machelska, H., 2020. IL-4 induces M2 macrophages to produce sustained analgesia via opioids. *JCI Insight*, *5*(4).

Chen, Y., Liu, J., Angelov, B., Drechsler, M., Garamus, V.M., Willumeit-Römer, R. and Zou, A., 2016. Baicalin loaded in folate-PEG modified liposomes for enhanced stability and tumor targeting. *Colloids and Surfaces B: Biointerfaces*, *140*, pp.74-82.

Chung, T.W., Lin, S.Y., Liu, D.Z., Tyan, Y.C. and Yang, J.S., 2009. Sustained release of 5-FU from Poloxamer gels interpenetrated by crosslinking chitosan network. *International Journal of Pharmaceutics*, 382(1-2), pp.39-44.

DiDomenico, C.D., Lintz, M. and Bonassar, L.J., 2018. Molecular transport in articular cartilage—what have we learned from the past 50 years?. *Nature Reviews Rheumatology*, *14*(7), pp.393-403.

Di Giuseppe, E., Corbi, F., Funiciello, F., Massmeyer, A., Santimano, T.N., Rosenau, M. and Davaille, A., 2015. Characterization of Carbopol® hydrogel rheology for experimental tectonics and geodynamics. *Tectonophysics*, 642, pp.29-45.

Dmitrenko, M.E., Penkova, A.V., Atta, R.R., Zolotarev, A.A., Plisko, T.V., Mazur, A.S., Solovyev, N.D. and Ermakov, S.S., 2019. The development and study of novel membrane materials based on polyphenylene isophthalamide-Pluronic F127 composite. *Materials & Design*, 165, p.107596.

D'Souza, S., 2014. A Review ofIn VitroDrug Release Test Methods for Nano-Sized Dosage Forms. *Advances in Pharmaceutics*, *2014*, pp.1-12.

El-Husseiny, H.M., Mady, E.A., El-Dakroury, W.A., Doghish, A.S. and Tanaka, R., 2023. Stimuli-responsive hydrogels: Smart state of-the-art platforms for cardiac tissue engineering. *Frontiers in Bioengineering and Biotechnology*, *11*.

El Kechai, N., Bochot, A., Huang, N., Nguyen, Y., Ferrary, E. and Agnely, F., 2015. Effect of liposomes on rheological and syringeability properties of hyaluronic acid hydrogels intended for local injection of drugs. *International Journal of Pharmaceutics*, 487(1-2), pp.187-196.

Fernández-García, R., Lalatsa, A., Statts, L., Bolás-Fernández, F., Ballesteros, M.P. and Serrano, D.R., 2020. Transferosomes as nanocarriers for drugs across the skin: Quality by design from lab to industrial scale. *International Journal of Pharmaceutics*, *573*, p.118817.

Fuentes-Iglesias, A., Garcia-Outeiral, V., Pardavila, J.A., Wang, J., Fidalgo, M. and Guallar, D., 2020. An optimized immunoprecipitation protocol for assessing protein-RNA interactions *in vitro*. *STAR protocols*, 1(2), p.100093.

García-Couce, J., Tomás, M., Fuentes, G., Que, I., Almirall, A. and Cruz, L.J., 2022. Chitosan/Pluronic F127 thermosensitive hydrogel as an injectable dexamethasone delivery carrier. *Gels*, 8(1), p.44.

Garms, B.C., Poli, H., Baggley, D., Han, F.Y., Whittaker, A.K., Anitha, A. and Grøndahl, L., 2021. Evaluating the effect of synthesis, isolation, and characterisation variables on reported particle size and dispersity of drug loaded PLGA nanoparticles. *Materials Advances*, *2*(17), pp.5657-5671.

Giliomee, J., du Toit, L.C., Kumar, P., Klumperman, B. and Choonara, Y.E., 2021. Evaluation of Composition Effects on the Physicochemical and Biological Properties of Polypeptide-Based Hydrogels for Potential Application in Wound Healing. *Polymers*, *13*(11), p.1828.

Gartner III, T.E. and Jayaraman, A., 2019. Modeling and simulations of polymers: a roadmap. *Macromolecules*, *52*(3), pp.755-786.

González-Díaz, E.C. and Varghese, S., 2016. Hydrogels as extracellular matrix analogs. *Gels*, 2(3), p.20.

Goudoulas, T.B. and Germann, N., 2017. Phase transition kinetics and rheology of gelatin-alginate mixtures. *Food Hydrocolloids*, 66, pp.49-60.

Govender, M., Rants'o, T.A. and Choonara, Y.E., 2023. A Micro-In-Macro Gastroretentive System for the Delivery of Narrow-Absorption Window Drugs. *Polymers*, *15*(6), p.1385.

Grässel, S. and Muschter, D., 2020. Recent advances in the treatment of osteoarthritis. *F1000Research, 9.*

Geckil, H., Xu, F., Zhang, X., Moon, S. and Demirci, U., 2010. Engineering hydrogels as extracellular matrix mimics. *Nanomedicine*, 5(3), pp.469-484.

Gupta, A., Aggarwal, G., Singla, S. and Arora, R., 2012. Transfersomes: a novel vesicular carrier for enhanced transdermal delivery of sertraline: development, characterization, and performance evaluation. *Scientia Pharmaceutica*, 80(4), pp.1061-1080.

Housaindokht, M.R. and Pour, A.N., 2012. Study the effect of HLB of surfactant on particle size distribution of hematite nanoparticles prepared via the reverse microemulsion. *Solid State Sciences*, *14*(5), pp.622-625.

Hoseini, B., Jaafari, M.R., Golabpour, A., Momtazi-Borojeni, A.A., Karimi, M. and Eslami, S., 2023. Application of ensemble machine learning approach to assess the factors affecting size and polydispersity index of liposomal nanoparticles. *Scientific Reports*, *13*(1), p.18012.

Hsieh, H.Y., Lin, W.Y., Lee, A.L., Li, Y.C., Chen, Y.J., Chen, K.C. and Young, T.H., 2020. Hyaluronic acid on the urokinase sustained release with a hydrogel system composed of poloxamer 407: HA/P407 hydrogel system for drug delivery. *Plos One*, *15*(3), p.e0227784.

Islam, N., Irfan, M., Zahoor, A.F., Iqbal, M.S., Syed, H.K., Khan, I.U., Rasul, A., Khan, S.U.D., Alqahtani, A.M., Ikram, M. and Abdul Qayyum, M., 2021. Improved bioavailability of ebastine through development of transfersomal oral films. *Pharmaceutics*, *13*(8), p.1315.

Javed, H., Islam, A., Chauhan, A., Kumar, S. and Kumar, S., 2018. Efficacy of engineered GO Amberlite XAD-16 picolylamine sorbent for the trace determination of Pb (II) and Cu (II) in fishes by solid phase extraction column coupled with inductively coupled plasma optical emission spectrometry. *Scientific Reports*, *8*(1), p.17560.

Jain, S., Jain, P., Umamaheshwari, R.B. and Jain, N.K., 2003. Transfersomes—a novel vesicular carrier for enhanced transdermal delivery: development, characterization, and performance evaluation. *Drug Development and Industrial Pharmacy*, *29*(9), pp.1013-1026.

Jiang, T., Kan, H.M., Rajpura, K., Carbone, E.J., Li, Y. and Lo, K.W.H., 2018. Development of targeted nanoscale drug delivery system for osteoarthritic cartilage tissue. *Journal of Nanoscience and Nanotechnology,* 18(4), pp.2310-2317.

Jons, C.K., Grosskopf, A.K., Baillet, J., Yan, J., Klich, J.H., Saouaf, O.M. and Appel, E.A., 2022. Yield-Stress and Creep Control Depot Formation and Persistence of Injectable Hydrogels Following Subcutaneous Administration. *Advanced Functional Materials*, *32*(40), p.2203402.

Jones, I.A., Togashi, R., Wilson, M.L., Heckmann, N. and Vangsness Jr, C.T., 2019. Intra-articular treatment options for knee osteoarthritis. *Nature Reviews Rheumatology*, 15(2), pp.77-90.

Jung, J.H., Kim, S.E., Kim, H.J., Park, K., Song, G.G. and Choi, S.J., 2020. A comparative pilot study of oral diacerein and locally treated diacerein-loaded nanoparticles in a model of osteoarthritis. *International journal of pharmaceutics*, *581*, p.119249.

Kanno, K., Wu, M.K., Scapa, E.F., Roderick, S.L. and Cohen, D.E., 2007. Structure and function of phosphatidylcholine transfer protein (PC-TP)/StarD2. *Biochimica et Biophysica Acta (BBA)-Molecular and Cell Biology of Lipids*, *1771*(6), pp.654-662.

Karava, A., Lazaridou, M., Nanaki, S., Michailidou, G., Christodoulou, E., Kostoglou, M., Iatrou, H. and Bikiaris, D.N., 2020. Chitosan derivatives with mucoadhesive and antimicrobial properties for simultaneous nanoencapsulation and extended ocular release formulations of dexamethasone and chloramphenicol drugs. *Pharmaceutics*, *12*(6), p.594.

Kassem, M.G., Ahmed, A.M.M., Abdel-Rahman, H.H. and Moustafa, A.H., 2019. Use of Span 80 and Tween 80 for blending gasoline and alcohol in spark ignition engines. *Energy Reports*, *5*, pp.221-230.

Khan, I., Needham, R., Yousaf, S., Houacine, C., Islam, Y., Bnyan, R., Sadozai, S.K., Elrayess, M.A. and Elhissi, A., 2021. Impact of phospholipids, surfactants and cholesterol selection on the performance of transfersomes vesicles using medical nebulizers for pulmonary drug delivery. *Journal of Drug Delivery Science and Technology*, 66, p.102822.

Kong, Y., Hou, Z., Zhou, L., Zhang, P., Ouyang, Y., Wang, P., Chen, Y. and Luo, X., 2020. Injectable self-healing hydrogels containing CuS nanoparticles with abilities of hemostasis, antibacterial activity, and promoting wound healing. *ACS Biomaterials Science & Engineering*, *7*(1), pp.335-349.

Krishna, D.V. and Sankar, M.R., 2023. Bioinspired artificial synovial fluid for in vitro frictional behavior of bovine articular cartilage and auxiliary biomaterials. *Journal of Molecular Liquids*, 388, p.122836.

Kumar, P., Singh, S.K., Handa, V. and Kathuria, H., 2018. Oleic acid nanovesicles of minoxidil for enhanced follicular delivery. *Medicines*, *5*(3), p.103.

Kushan, E. and Senses, E., 2021. Thermoresponsive and injectable composite hydrogels of cellulose nanocrystals and pluronic F127. *ACS applied bio materials*, 4(4), pp.3507-3517.

Larsen, C., Larsen, S.W., Jensen, H., Yaghmur, A. and Østergaard, J., 2009. Role of in vitro release models in formulation development and quality control of parenteral depots. *Expert Opinion on drug Delivery*, *6*(12), pp.1283-1295.

Lee, C.S. and Hwang, H.S., 2023. Starch-based hydrogels as a drug delivery system in biomedical applications. *Gels*, *9*(12), p.951.

Leifer, V.P., Katz, J.N. and Losina, E., 2022. The burden of OA-health services and economics. *Osteoarthritis and Cartilage*, 30(1), pp.10-16.

Li, S., Yang, C., Li, J., Zhang, C., Zhu, L., Song, Y., Guo, Y., Wang, R., Gan, D., Shi, J. and Ma, P., 2023. Progress in Pluronic F127 Derivatives for Application in Wound Healing and Repair. *International Journal of Nanomedicine*, pp.4485-4505.Lin, J., Zhang, H., Chen, Z. and Zheng, Y., 2010. Penetration of lipid membranes by gold nanoparticles: insights into cellular uptake, cytotoxicity, and their relationship. *ACS Nano*, *4*(9), pp.5421-5429.

Liu, K., Zhang, D. and Wang, W., 2021. Nanoparticle-Based Drug Delivery System—A Target Strategy for Osteoarthritis Treatment. *Journal of Nanomaterials*, 2021.

Liu, A., Ingham, E., Fisher, J. and Jennings, L.M., 2019. Development of a pre-clinical experimental simulation model of the natural porcine knee with appropriate ligamentous constraints. *PloS One*, *14*(5), p.e0216872.

Lolicato, F., Akola, J., Martinez-Searaa, H. and Vattulainen, I., 2017. Nanoparticle builder: New software for preparing nanoparticles for molecular dynamics simulations. *European Biophysics Journal*, *46*(1 Supplement), pp.S222-S222.

Mancipe Castro, L.M., Sequeira, A., García, A.J. and Guldberg, R.E., 2020. Articular cartilage- and synoviocyte-binding poly (ethylene glycol) nanocomposite microgels as intra-articular drug delivery vehicles for the treatment of osteoarthritis. *ACS Biomaterials Science & Engineering*, 6(9), pp.5084-5095.

Manju, S. and Sreenivasan, K., 2011. Conjugation of curcumin onto hyaluronic acid enhances its aqueous solubility and stability. *Journal of Colloid and Interface Science*, *359*(1), pp.318-325.

Misono, T., 2019. Interfacial tension between water and oil. *Measurement Techniques and Practices of Colloid and Interface Phenomena*, pp.39-44.

Moawad, F.A., Ali, A.A. and Salem, H.F., 2017. Nanotransfersomes-loaded thermosensitive in situ gel as a rectal delivery system of tizanidine HCl: preparation, in vitro and in vivo performance. *Drug Delivery*, *24*(1), pp.252-260.

Modi, C.D. and Bharadia, P.D., 2012. Transfersomes: new dominants for transdermal drug delivery. *Am J Pharm Tech Res*, 2(3), pp.71-91.

Molnar, V., Matišić, V., Kodvanj, I., Bjelica, R., Jeleč, Ž., Hudetz, D., Rod, E., Čukelj, F., Vrdoljak, T., Vidović, D. and Starešinić, M., 2021. Cytokines and chemokines involved in osteoarthritis pathogenesis. *International Journal of Molecular Sciences*, 22(17), p.9208.

Mora, J.C., Przkora, R. and Cruz-Almeida, Y., 2018. Knee osteoarthritis: pathophysiology and current treatment modalities. *Journal of Pain Research*, pp.2189-2196.

Mouser, V.H., Melchels, F.P., Visser, J., Dhert, W.J., Gawlitta, D. and Malda, J., 2016. Yield stress determines bioprintability of hydrogels based on gelatin-methacryloyl and gellan gum for cartilage bioprinting. *Biofabricatio*n, 8(3), p.035003.

Moqejwa, Thope, Thashree Marimuthu, Pierre PD Kondiah, and Yahya E. Choonara. "Development of stable nano-sized transfersomes as a rectal colloid for enhanced delivery of cannabidiol." *Pharmaceutics* 14, no. 4 (2022): 703.

Murthy, S.K., 2007. Nanoparticles in modern medicine: state of the art and future challenges. *International Journal of Nanomedicine* , 2(2), pp.129-141.

Nakhaei, P., Margiana, R., Bokov, D.O., Abdelbasset, W.K., Jadidi Kouhbanani, M.A., Varma, R.S., Marofi, F., Jarahian, M. and Beheshtkhoo, N., 2021. Liposomes: structure, biomedical applications, and stability parameters with emphasis on cholesterol. *Frontiers in Bioengineering and Biotechnology,* 9, p.705886.

Nikafshar, S., Zabihi, O., Moradi, Y., Ahmadi, M., Amiri, S. and Naebe, M., 2017. Catalyzed synthesis and characterization of a novel lignin-based curing agent for the curing of high-performance epoxy resin. *Polymers*, *9*(7), p.266.

Nguyen, D.T., Dinh, V.T., Dang, L.H., Nguyen, D.N., Giang, B.L., Nguyen, C.T., Nguyen, T.B.T., Thu, L.V. and Tran, N.Q., 2019. Dual interactions of amphiphilic gelatin copolymer and nanocurcumin improving the delivery efficiency of the nanogels. *Polymers*, *11*(5), p.814.

Nowak, D. and Jakubczyk, E., 2020. The freeze-drying of foods—The characteristic of the process course and the effect of its parameters on the physical properties of food materials. *Foods*, *9*(10), p.1488.

Nowroozi, F., Almasi, A., Javidi, J., Haeri, A. and Dadashzadeh, S., 2018. Effect of surfactant type, cholesterol content and various downsizing methods on the particle size of niosomes. *Iranian Journal of Pharmaceutical Research: IJPR*, *17*(Suppl2), p.1.

Omolo, C.A., Megrab, N.A., Kalhapure, R.S., Agrawal, N., Jadhav, M., Mocktar, C., Rambharose, S., Maduray, K., Nkambule, B. and Govender, T., 2021. Liposomes with pH responsive 'on and off'switches for targeted and intracellular delivery of antibiotics. *Journal of Liposome Research*, *31*(1), pp.45-63.

Opatha, S.A.T., Titapiwatanakun, V. and Chutoprapat, R., 2020. Transfersomes: A promising nanoencapsulation technique for transdermal drug delivery. *Pharmaceutics*, *12*(9), p.855.

Palazzo, C., Nguyen, C., Lefevre-Colau, M.M., Rannou, F. and Poiraudeau, S., 2016. Risk factors and burden of osteoarthritis. *Annals of Physical and Rehabilitation Medicine*, 59(3), pp.134-138.

Panyamao, P., Ruksiriwanich, W., Sirisa-Ard, P. and Charumanee, S., 2020. Injectable thermosensitive chitosan/pullulan-based hydrogels with improved mechanical properties and swelling capacity. *Polymers*, *12*(11), p.2514.

Pereira, A. and Mallya, R., 2015. Formulation and evaluation of a photoprotectant cream containing Phyllanthus emblica extract-phospholipid complex. *Journal of Pharmacognosy and Phytochemistry,* 4(2), pp.232-240.

Pérez-González, G.L., Villarreal-Gómez, L.J., Olivas-Sarabia, A., Valdez, R. and Cornejo-Bravo, J.M., 2021. Development, characterization, and in vitro assessment of multilayer mucoadhesive system containing dexamethasone sodium phosphate. *International Journal of Polymeric Materials and Polymeric Biomaterials,* 70(18), pp.1316-1328.

Prashanthini, V.P., Sivaraman, S., Kathirvelu, P., Shanmugasundaram, J., Subramanian, V., Ramesh, S.S., Karthikeyan, E. and Cheriyan, B.V., 2023. Transferosomal gel for transdermal delivery of insulin: Formulation development and ex vivo permeation study. *Intelligent Pharmacy*.

Ramli, H., Zainal, N.F.A., Hess, M. and Chan, C.H., 2022. Basic principle and good practices of rheology for polymers for teachers and beginners. *Chemistry Teacher International*, *4*(4), pp.307-326.

Rants'o, T.A., Van der Westhuizen, C.J. and van Zyl, R.L., 2022. Optimization of covalent docking for organophosphates interaction with Anopheles acetylcholinesterase. *Journal of Molecular Graphics and Modelling*, *110*, p.108054.

Rothenfluh, D.A., Bermudez, H., O'Neil, C.P. and Hubbell, J.A., 2008. Biofunctional polymer nanoparticles for intra-articular targeting and retention in cartilage. *Nature Materials*, *7*(3), pp.248-254.

Saadatkhah, N., Carillo Garcia, A., Ackermann, S., Leclerc, P., Latifi, M., Samih, S., Patience, G.S. and Chaouki, J., 2020. Experimental methods in chemical engineering: Thermogravimetric analysis—TGA. *The Canadian Journal of Chemical Engineering*, 98(1), pp.34-43.

Samigulina, G. and Samigulina, Z., 2020. Ontological model of multi-agent Smart-system for predicting drug properties based on modified algorithms of artificial immune systems. *Theoretical Biology and Medical Modelling*, 17(1), p.12.

Schmolka, I.R., 1972. Artificial skin I. Preparation and properties of pluronic F-127 gels for treatment of burns. *Journal of Biomedical Materials Research*, 6(6), pp.571-582.

Shahbazi, M.A., Sedighi, M., Bauleth-Ramos, T., Kant, K., Correia, A., Poursina, N., Sarmento, B., Hirvonen, J. and Santos, H.A., 2018. Targeted reinforcement of macrophage reprogramming toward M2 polarization by IL-4-loaded hyaluronic acid particles. *Acs Omega*, *3*(12), pp.18444-18455.

Silva, A.M., Martins-Gomes, C., Coutinho, T.E., Fangueiro, J.F., Sanchez-Lopez, E., Pashirova, T.N., Andreani, T. and Souto, E.B., 2019. Soft cationic nanoparticles for drug delivery: Production and cytotoxicity of solid lipid nanoparticles (SLNs). *Applied Sciences*, 9(20), p.4438.

Sinha, P., Datar, A., Jeong, C., Deng, X., Chung, Y.G. and Lin, L.C., 2019. Surface area determination of porous materials using the Brunauer–Emmett–Teller (BET) method: limitations and improvements. *The Journal of Physical Chemistry C*, *123*(33), pp.20195-20209.

Song, P., Cui, Z. and Hu, L., 2022. Applications and prospects of intra-articular drug delivery system in arthritis therapeutics. *Journal of Controlled Release*, 352, pp.946-960.

Sophia Fox, A.J., Bedi, A. and Rodeo, S.A., 2009. The basic science of articular cartilage: structure, composition, and function. *Sports Health*, *1*(6), pp.461-468.

Steinmetz, J.D., Culbreth, G.T., Haile, L.M., Rafferty, Q., Lo, J., Fukutaki, K.G., Cruz, J.A., Smith, A.E., Vollset, S.E., Brooks, P.M. and Cross, M., 2023. Global, regional, and national burden of

osteoarthritis, 1990–2020 and projections to 2050: a systematic analysis for the Global Burden of Disease Study 2021. *The Lancet Rheumatology*, 5(9), pp.e508-e522.

Surini, S., Leonyza, A. and Suh, C.W., 2020. Formulation and in vitro penetration study of recombinant human epidermal growth factor-loaded transfersomal emulgel. *Advanced Pharmaceutical Bulletin*, *10*(4), p.586.

Taruc-Uy, R.L. and Lynch, S.A., 2013. Diagnosis and treatment of osteoarthritis. *Primary Care: Clinics in Office Practice*, *40*(4), pp.821-836.

Tawfeek, H.M., Abdellatif, A.A., Abdel-Aleem, J.A., Hassan, Y.A. and Fathalla, D., 2020. Transfersomal gel nanocarriers for enhancement the permeation of lornoxicam. *Journal of Drug Delivery Science and Technology*, *56*, p.101540.

Testa, G., Giardina, S.M.C., Culmone, A., Vescio, A., Turchetta, M., Cannavò, S. and Pavone, V., 2021. Intra-articular injections in knee osteoarthritis: A review of literature. *Journal of Functional Morphology and Kinesiology*, *6*(1), p.15.

Thabet, Y., Elsabahy, M. and Eissa, N.G., 2022. Methods for preparation of niosomes: A focus on thin-film hydration method. *Methods*, *199*, pp.9-15.

Tsubosaka, M., Kihara, S., Hayashi, S., Nagata, J., Kuwahara, T., Fujita, M., Kikuchi, K., Takashima, Y., Kamenaga, T., Kuroda, Y. and Takeuchi, K., 2020. Gelatin hydrogels with eicosapentaenoic acid can prevent osteoarthritis progression in vivo in a mouse model. *Journal of Orthopaedic Research®*, *38*(10), pp.2157-2169.

Uwaezuoke, O., Du Toit, L.C., Kumar, P., Ally, N. and Choonara, Y.E., 2022. Linoleic Acid-Based Transferosomes for Topical Ocular Delivery of Cyclosporine A. *Pharmaceutics,* 14(8), p.1695.

von Kaeppler, E.P., Wang, Q., Raghu, H., Bloom, M.S., Wong, H. and Robinson, W.H., 2021. Interleukin 4 promotes anti-inflammatory macrophages that clear cartilage debris and inhibits osteoclast development to protect against osteoarthritis. *Clinical Immunology*, *229*, p.108784.

Wang, Q., Sun, C., Xu, B., Tu, J. and Shen, Y., 2018. Synthesis, physicochemical properties and ocular pharmacokinetics of thermosensitive in situ hydrogels for ganciclovir in cytomegalovirus retinitis treatment. *Drug Delivery*, *25*(1), pp.59-69.

Wagh, V.D. and Apar, D.U., 2014. Cyclosporine a loaded PLGA nanoparticles for dry eye disease: in vitro characterization studies. *Journal of Nanotechnology*, *2014*.

Wang, S., Qiu, Y., Qu, L., Wang, Q. and Zhou, Q., 2022. Hydrogels for treatment of different degrees of osteoarthritis. *Frontiers in Bioengineering and Biotechnology*, *10*, p.858656.

Watson, D.G., Lin, M., Morton, A., Cable, C.G. and McArthur, D.A., 2005. Compatibility and stability of dexamethasone sodium phosphate and ketamine hydrochloride subcutaneous infusions in polypropylene syringes. *Journal of Pain and Symptom Management*, *30*(1), pp.80-86.

Weston, J.S., Harwell, J.H. and Grady, B.P., 2017. Rheological characterization of yield stress gels formed via electrostatic heteroaggregation of metal oxide nanoparticles. *Soft Matter*, *13*(38), pp.6743-6755.

Wimmer, M.A., Nechtow, W., Schwenke, T. and Moisio, K.C., 2015. Knee flexion and daily activities in patients following total knee replacement: a comparison with ISO standard 14243. *BioMed Research International*, *2015*.

Wojdasiewicz, P., Poniatowski, Ł.A. and Szukiewicz, D., 2014. The role of inflammatory and anti-inflammatory cytokines in the pathogenesis of osteoarthritis. *Mediators of inflammation*, *2014*(1), p.561459.

Zhang, M., Qiao, X., Han, W., Jiang, T., Liu, F. and Zhao, X., 2021. Alginate-chitosan oligosaccharide-ZnO composite hydrogel for accelerating wound healing. *Carbohydrate Polymers*, *266*, p.118100.

Zhao, T., Wei, Z., Zhu, W. and Weng, X., 2022. Recent developments and current applications of hydrogels in osteoarthritis. *Bioengineering*, *9*(4), p.132.

Zheng, Y., Zheng, M., Ma, Z., Xin, B., Guo, R. and Xu, X., 2015. Sugar fatty acid esters. In *Polar Lipids* (pp. 215-243). Elsevier.

CHAPTER FOUR

Conclusions, Limitations, and Future Recommendations

5.1. Conclusions

This study explored and demonstrated the extensive development of an innovative and efficacious formulation for sustained IA drug delivery. The formulated DEX-loaded tNPs possessed a rosy size of 76.43 ± 0.48346 nm, suggesting that once administrated, the particles would be able to maneuver through the densely packed ECM. The size corroborated SEM imagery that further depicted a uniform, spherical morphology showing that the tNPs were not agglomerated. Furthermore, the uniformity of the tNPs was further shown by the PDI of 0.183 ± 0.008, and the zeta potential of 10.58 ± 0.706 mV further indicated that the tNPs would be stable and not agglomerate This data correlates with the physical stability test showing that the nano-formulation could be stored for as long as 3 months without being compromised. The drug of choice, DEX, an anti-inflammatory corticosteroid, was successfully encapsulated within the tNPs at an efficiency of 98 ± 0.31%, and the tNPs had a drug loading of 7.14 ± 0.58%, indicating a highly efficient entrapment with minimal DEX wastage with a moderate drug loading capacity. The drug release of DEX-loaded tNPs showed a vast improvement compared to the free DEX, releasing DEX for 72 hrs, more than 62 hrs longer than free DEX. Therefore, the tNPs did indeed provide sustained release of DEX.

The thermo-responsive hydrogel, comprising of HA and PF-127, was successfully synthesized using the cold method. DEX-loaded tNPs were integrated into the hydrogel matrix. The hydrogel had a sol-gel transition at 30°C; with an increase in temperature, the hydrogel illustrated increased viscosity, this implied that the formulation could be easily transported and should be administrated at lower temperatures than at 30°C. The increase in viscosity can potentially help increase the residence time of drugs and lubrication in the joints. The DEX-tNPs-PF-127/HA delivery system showed a sustained release of 7 weeks, which supported literature that, indeed, hydrogels can greatly improve the efficiency of nanosystems. Interestingly, *in vitro* DEX release using a knee joint simulator, which provided a more accurate reading, showcased 2 months of DEX release from the DEX-tNPs-PF-127/HA hydrogel. This DEX release profile means that the administration of this treatment would mandate fewer IA injections, thus increasing patient compliance and decreasing the risk of injection site infections.

The DEX-tNPs-PF-127/HA hydrogel showed favourable physicochemical properties. Importantly, the rheological properties were remarkably well-suited making the drug delivery ideal for IA drug delivery in OA joints.

In summary, subject to further testing, such as *in vivo* studies, the developed DEX-Tranfersome-PF-127/HA hydrogel has the potential to be considered a viable option for IA treatment of OA. The formulation can alleviate the inflammatory effects of OA by reducing bone-to-bone friction while providing sustained release of an anti-inflammatory drug. This will overcome the challenge of the required highly frequent dosages of IA treatment. Instead of weekly administration, the DEX-Tranfersome-PF-127/HA hydrogel may only require quarterly administration. This has the potential to improve patient compliance while decreasing the risk of infection posed by frequent IA injections and will be cost-effective. Overall, results obtained from this study suggest that an advanced delivery system that provides a promising platform for sustained drug delivery in IA-based OA therapy was successfully synthesized, providing superior mechanical and therapeutic properties.

5.2. Limitations of the study

Due to difficulty procuring chondrocytes and synoviocytes, it was not possible to conduct biocompatibility of the DEX-Tranfersome-P127/HA hydrogel on these OA joint-related cell lines within the proposed timeline. However, targeting the pathogenesis of OA was a viable alternative. Thus, RAW macrophage cell line (RAW 264.7) was used for their convenience in studying inflammatory conditions like OA. The cytotoxicity studies were also conducted on this cell line.

5.3. Future Recommendations

Biocompatibility studies on chondrocytes and synoviocytes coupled with anti-inflammatory studies will provide much more insight. Quantifying pro-inflammatory cytokines, more anti-inflammatory cytokines, chemokines, matrix-degrading proteins such as MMPs, and ADAMTs will provide more valuable and comprehensive insight into the capability of the nanosystem. Furthermore, macrophage polymerization studies may provide further biological activity data in identifying the type of macrophages induced by the formulated nanosystem. Cellular uptake studies would also provide insight into the system's efficiency and uptake mechanisms utilized in chondrocytes. As promising and brilliant as this drug delivery system has been revealed, *in vivo* studies, including pharmacokinetic and pharmacodynamics studies, must be conducted to assess its translation into a clinical setting.

APPENDICES

1. SAYAS Annual Young Scientist Conference - Oral Presentation abstract

Stimuli-responsive transferosome-based bio-mimetic gels for intraarticular drug delivery in osteoarthritis

Atang Motaung, Yahya E. Choonara and Thankhoe A. Rants'o

Wits Advanced Drug Delivery Platform Research Unit, Department of Pharmacy and Pharmacology, Faculty of Health Sciences, School of Therapeutic Science, University of the Witwatersrand, 7 York Road, Parktown, Johannesburg 2193, South Africa

Introduction:

Osteoarthritis (OA) is one of the most prevalent joint diseases affecting millions globally. This disease is characterized by cartilage degeneration, leading to pain, inflammation, and stiffness in the affected joints. Current commercial treatment options for OA are mainly symptomatic and palliative. These include acetaminophen, NSAIDs, cyclooxygenase 2 (COX-2) inhibitors, opioids, and glucocorticoids. However, these are associated with limitations such as gastric ulceration, acute kidney injury (NSAIDs), increased risk of cardiovascular (COX-2) disease and the need for repeated intraarticular injection (glucocorticoids), which result in low patient compliance. However, to overcome some of these problems, stimuli-responsive drug delivery systems, such as hybrid systems comprising nanoparticles incorporated into hydrogels, offer a promising approach for treating OA. In this study, we investigated the use of dexamethasone-loaded transfersomes incorporated in a hydrogel to treat OA. Dexamethasone is a potent anti-inflammatory and immunosuppressive drug that has been used for the treatment of various inflammatory diseases, including OA.

Methods:

The transfersomes were synthesized using the thin film hydration method. Characterized for size, entrapment efficiency (%), morphology, Dexamethasone release kinetics from transfersomes and hydrogel, and physicochemical characteristics (Fourier transform infrared (FTIR), Thermogravimetric Analyzer (TGA), and X-Ray diffraction (XRD), rheology, syringeability (Texture analyser)

Results:

The transfersomes drug release kinetic profile displayed 100% DEX release after 72 hours, which improved to 7 weeks upon incorporation into the hydrogel matrix. The rheological analysis demonstrated that the hydrogel was thixotropic, with a high yield stress and compatible frequency and strain sweeps, making it suitable for the administration of osteoarthritis

Conclusions/Impact:

The results from the study suggest that this nano-system could be a promising platform for extended drug delivery in OA, providing mechanical and therapeutic properties

Acknowledgements:

This study was funded by National Research Foundation (NRF) of South Africa and HETERO Pharmaceuticals Drugs.

Presenters Bibliography

Atang Motaung is a master's candidate at the University of the Witwatersrand. He carries out research in fields of nanotechnology and drug delivery systems where he focuses on with potential to improve the treatment of osteoarthritis with intraarticular injectables.

2. Annual Conference of Pharmaceutical Sciences - Oral Presentation Abstract

Stimuli-responsive transfersome-based bio-mimetic gels for intra-articular drug delivery in osteoarthritis

Atang Motaung[1], Thankhoe Rants'o[1], Yahya Choonara[1]

[1] Wits Advanced Drug Delivery Platform Research Unit, Department of Pharmacy and Pharmacology, Faculty of Health Sciences, School of Therapeutic Science, University of the Witwatersrand, 7 York Road, Parktown, Johannesburg 2193, South Africa

E-mail-address: 1389970@students.wits.ac.za

Purpose: Osteoarthritis (OA) is one of the most prevalent joint diseases affecting millions of people globally. This disease is characterized by cartilage degeneration, leading to pain, inflammation, and stiffness in the affected joints. Current commercial treatment options for OA are mainly symptomatic and palliative. These include acetaminophen, NSAIDs, opioids, and glucocorticoids. However, these are associated with limitations such as gastric ulceration, acute kidney injury (classical NSAIDs), increased risk of cardiovascular (COX-2) disease and the need for repeated intra-articular injection (glucocorticoids) which apart from increasing the risk for exposure to infections, is not cost effective and, can result in low patient compliance. However, to overcome some of these problems, stimuli-responsive drug delivery systems, such as nanocomposites offer a promising approach for effective and sustainable treatment of OA. In this study, we investigated the use of dexamethasone-loaded transfersomes incorporated in a hydrogel to treat OA. Dexamethasone is a potent anti-inflammatory and immunosuppressive drug that has been used for the treatment of various inflammatory diseases, including OA.

Methods: The transfersomes were synthesized using the thin film hydration method. Characterized for size, entrapment efficiency (%), morphology (Scanning Electron Microscopy), Dexamethasone release kinetic profiles from transfersomes and hydrogel, and physicochemical characteristics (Fourier transform infrared (FTIR), Thermogravimetric Analyzer (TGA), and X-Ray diffraction (XRD), rheology, syringeability (Texture analyser).

Results: The transfersomes showed hydrodynamic particle size of 76.43 ± 0.48 nm and SEM images showed that the nanoparticles had a smooth and spherical morphology. The transfersomes drug release kinetic profile displayed complete DEX release after 72 hours, which interestingly improved to 7 weeks upon incorporation into the hydrogel matrix. The rheological analysis signified that the hydrogel was thixotropic, with a high yield stress and

compatible frequency and strain sweeps, making it suitable for the administration of osteoarthritis.

Conclusions: Results from this study suggest that a smart delivery system that provides a promising platform for sustained drug delivery in OA was successfully synthesized, providing mechanical and therapeutic properties. The delivery system has the potential to overcome limitations associated with conventional intraarticular drug delivery systems in OA.

3. Graphical abstract for chapter two

